ABSTRACT

Title of Document: AN INVESTIGATION OF VOID FRACTION FOR LOW GWP REFRIGERANTS

James Daniel Spencer, Master of Science, 2013

Directed By: Professor Reinhard Radermacher, Ph.D.
Department of Mechanical Engineering

An experimental facility was designed and fabricated to test the void fraction of fluids. Measurements of the void fraction for R134a, R290, and R1234yf were conducted for low mass flux conditions at air-conditioning evaporator temperatures. Test sections of round tube inner diameters 2.99 and 4.56 mm were tested. Flow visualization was performed on the 4.56 mm test section. Results of the flow visualization revealed similar flow regime transition characteristics among the three refrigerants. Void fraction trends for R134a and R290 were found to be similar, while the void fraction for R1234yf trended higher than R134a for most points. The experimental data was compared to predictions by twelve void fraction correlations. For R134a and R290, the Steiner correlation most accurately predicted the data. For R1234yf, the Baroczy correlation was found to most accurately predict the data.

AN INVESTIGATION OF VOID FRACTION FOR LOW GWP REFRIGERANTS

By

James Daniel Spencer

Thesis submitted to the Faculty of the Graduate School of the
University of Maryland, College Park, in partial fulfillment
of the requirements for the degree of
Master of Science
2013

Advisory Committee:
Professor Reinhard Radermacher, Chair
Assistant Professor Yunho Hwang
Assistant Professor Amir Riaz

Dedication

To Heather

Acknowledgements

As graduate research is hardly an individual venture, I would like to thank everyone who has guided me and provided support in the pursuit of my master's degree. First, I would like to thank our two outstanding lab managers, Jan Muehlbauer and Daniel Leighton, for teaching me the basics of experimental research in the beginning, providing support and advice throughout my graduate career, and often filling in the gaps of my knowledge in laboratory technique. I would also like to thank my colleagues in the heat pump lab, both past and present, who have provided help in the development of my project: Abdullah Alabdulkarem, Ali Alalili, Tao Cao, Magnus Eisele, Xiaojie Ling, Bracha Mandel, Sahil Popli, and Xing Xu. I would like to thank my advisors Dr. Reinhard Radermacher and Dr. Yunho Hwang for providing support and guidance on the direction of my research. I would also like to thank the Honeywell and Dupont corporations for their donation of a sample of R1234yf, which made some of the more interesting results of this investigation possible. Finally, I would like to thank my family, especially my fiancé, Heather, for supporting me in my pursuit of this life goal.

Table of Contents

List of Tables

List of Figures

List of Abbreviations

A – Area [m^2]

e – Mean Deviation

G – Mass Flux [kg/m^2s]

g – Gravitational Constant [9.81 m/s^2]

h – Specific Enthalpy [kJ/kg]

ID – Inner Diameter [m]

m – Mass [kg]

$\dot{m}$ – Mass Flow [kg/s]

P – Pressure [kPa]

$\dot{Q}$ – Heat [kW]

T – Temperature [°C]

u – Velocity [m/s]

V – Volume [m^3]

x – Homogenous Quality [--]

Greek Symbols

α – Void Fraction [--]

μ – Viscosity [Pa-s]

ρ – Density [kg/m^3]

σ – Surface Tension [N/m]

Subscripts

avg – average

boil – boiling point

crit – critical point

cs – cross sectional

ev – expansion volume

exp – experimental

fg – latent difference

G – vapor

htr - heater

L – liquid

m - mixture

pre – pre-heater

pred – predicted

post – post-heater

rand – random error

sys – systematic error

tot – total

ts – test section

Abbrevations

AHRI – Air-conditioning, Heating, and Refrigeration Institute

ASHRAE - American Society of Heating Refrigeration & Air-Conditioning Engineers

CFC – Chloroflourocarbon

EEV – Electronic Expansion Valve

EPA – Environmental Protection Agency

HCFC – Hydrochloroflourocarbon

HFC – Hydroflourocarbon

HGBP – Hot Gas Bypass

GWP – Global Warming Potential

ODP – Ozone Depletion Potential

QCV – Quick Closing Valves

VFD – Variable Frequency Drive

Dimensionless Numbers

Reynolds Number: $Re = \frac{\rho * u * D}{\mu}$

Weber Number: $We = \frac{\rho * u^2 * D}{\sigma}$

Chapter 1: Introduction

1.1: Project Motivation: An Introduction to Low GWP Refrigerants

Beginning after World War II and up until the 1980's, the primary classes of refrigerants utilized in vapor compression systems were Hydrochloroflourocarbons (HCFC's) and Chlorofluorocarbons (CFC's). These industrially synthesized refrigerants had mass market appeal due to their favorable heat transfer characteristics without the toxic effects of some of the earlier natural refrigerants. However, as the issue of environmental protection gained importance throughout the 1970's and 1980's, these classes of refrigerant fell out of favor as the chlorine in their structure greatly contributes to ozone depletion. In 1987, the Montreal Protocol, an internationally ratified treaty to combat ozone depletion, set a timeline for the phase out of CFC's and HCFC's. In response to this, Hydroflourocarbons (HFC's) were billed as environmentally responsible replacements due to their negligible Ozone Depletion Potential (OPD). R134a, or 1,1,1,2-Tetraluoroethane, was introduced into the market by Dupont in the 1990's and was marketed as an environmentally responsible replacement for the CFC, R12, which had been phased out by the treaty. Since its introduction, it has become one of the most widely utilized refrigerants, employed in stationary and automotive air-conditioning systems as well as in refrigeration systems. However, in recent years even HFC's, which were once considered environmentally friendly, are being scrutinized due to their high Global Warming Potential (GWP). Thus, these refrigerants are beginning to be phased by government and organizational policies.

This necessitates the investigation of new low GWP refrigerants to replace these environmentally harmful HFC's. The bulk of these new refrigerants can be classified into one of two categories: (1) new refrigerants synthesized in industry to have environmentally friendly properties, and (2) natural refrigerants, typically some form of hydrocarbon, which are considered environmentally friendly because they exist in nature. The current investigation considers two R134a replacements, one from each category. Table 1 lists select properties for each of these refrigerants.

Table 1: Select Properties for Refrigerants in the Current Investigation

	R134a	R290	R1234yf
Normal Boiling Point, T_{boil}	**-26.1°C**	**-42.1°C**	**-29.5°C**
Critical Temperature, T_{crit}	**101°C**	**96.7°C**	**94.7°C**
Critical Pressure, P_{crit}	**4.06MPa**	**4.25MPa**	**3.37MPa**
Density Ratio, ρ_L/ρ_G (7.2°C)	**68.94**	**40.71**	**51.74**
Viscosity Ratio, μ_L/μ_G (7.2°C)	**21.65**	**14.76**	**18.04**
Heat of Vaporization, h_{fg} (7.2°C)	**193.1 kJ/kg**	**364.1 kJ/kg**	**159.3 kJ/kg**
ASHRAE Safety Rating	**A1**	**A3**	**A2L**
ODP	**0**	**0**	**0**
GWP	**1430**	**3**	**4**

R1234yf, a refrigerant manufactured by Honeywell and DuPont, was developed to meet the European directive, 2006/40/EC, which phases out all refrigerants with a GWP greater than 150 in automotive applications. Due to its similar pressure and capacity characteristics, it can be considered as a "drop-in" replacement for R134a. This means it can be charged to systems built for R134a without a significant degradation in performance. However, when compared to R134a, the latent capacity is approximately 30% lower. It also has an ASHARAE flammability classification of 2L, meaning it is non-toxic yet mildly flammable.

R290, or propane, in contrast, has nearly twice the latent heat capacity of R134a at evaporator conditions for medium temperature applications and is low cost compared synthesized refrigerants, making it a viable replacement. However, though it is still classified as a medium-pressure refrigerant, its pressure characteristics are higher than R134a. This means it cannot serve as a drop-in replacement and would require new equipment for implementation. In addition, the refrigerant is highly flammable, with an ASHRAE flammability rating of 3.

A common characteristic of these two refrigerants, and in fact of many new and natural refrigerants, is that they are flammable. ASHRAE provides a guideline for rating of refrigerants [1] by their toxicity and flammability (Table 2).

Table 2: ASHRAE Safety Classifications [1]

	ASHRAE Safety Group	
Higher Flammability	A3	B3
Lower Flammability	A2	B2
	A2L	B2L
No Flame Propagation	A1	B1
	Lower Toxicity	**Higher Toxicity**

For most jurisdictions, the use of any refrigerant other than a class A1, non-flammable, non-toxic fluid in medium temperature air-conditioning applications is prohibited. However, as the list of acceptable A1 refrigerants dwindles due to increased environmental regulation, regulations surrounding the use of flammable refrigerants are being relaxed. In fact, many countries in Europe and Asia are beginning to allow mildly-flammable class 2L refrigerants depending on the charge and application. As recently as December 2011, the Environmental Protection

Agency (EPA) issued a Notice of Proposed Rulemaking in the U.S. Federal Register [2] which lists R290 as an acceptable replacement for R12, R22, and R502 in small scale refrigeration applications. As regulations regarding the use of flammable refrigerants continue to loosen for air-conditioning applications, it can be expected that these refrigerants will first be allowed in low charge applications, such as small thru-wall and window air-conditioning units. As manufacturers begin to design systems based around these refrigerants, it is important to have a data base of experimentally validated fluid properties and correlations around which to design. Thus, the primary focus of the current investigation is to measure the void fraction for conditions suited to these small capacity air-conditioning systems.

1.2: Void Fraction

The void fraction, α, of a two-phase volume is defined as the geometric percentage of a two-phase fluid that is in the vapor phase, either on a linear, area, or volume basis. This is to not be confused with the homogenous quality, x, which is a thermodynamic, mass-based property defined as the percent mass of a two-phase fluid which is in the vapor state. Because the homogenous quality assumes homogenous flow, that is flow in which the liquid and vapor phases travel at the same velocity, it is not useful in determining geometric flow conditions as it ignores interfacial viscous and flow regime effects.

Void fraction prediction is important in system design for a number of reasons, the most obvious being charge inventory prediction. Being able to accurately predict void fraction during the design process reduces time required for charge optimization for system prototypes. Additionally, from an environmental

standpoint, by more accurately predicting the amount of refrigerant required to run a vapor compression system over a range of conditions, the volume of refrigerant receivers, which provide a buffer of liquid refrigerant during transient system operation, can be minimized. Thus, at the end of the system's life, in the event the refrigerant is not properly recovered and is released into the atmosphere, the greenhouse effect due to the release will be reduced for each system. This totals an overall substantial reduction is greenhouse gas emissions.

Accurate mass prediction for the purposes of charge minimization is especially important when designing systems for flammable refrigerants as the majority of refrigeration safety standards limit the charge of flammable refrigerant in an appliance. Specifically, ASHRAE Standard 15 [3] limits the charge of class A2L and A3 refrigerants to only 150 g.

In addition to charge prediction, void fraction has implications in two-phase heat transfer and frictional pressure loss. Because the void fraction is necessary to determine refrigerant velocity from the homogenous quality, many of the most commonly used two-phase pressure drop and pressure loss correlations utilize it as a variable. So, even though the methodology behind a particular correlation for either parameter may be sound, utilizing an incorrect void fraction correlation in the model can lead to skewed results.

The current investigation considers the volumetric void fraction, as opposed to the area or linear void fraction, as volumetric measurement method allows linear variations in the void fraction caused by non-homogenous flow effects to average out

over the length of the volume. This yields a more accurate average volumetric void fraction, defined as:

$$\alpha = \frac{V_G}{V_{tot}} \tag{1}$$

However, because an accurate method for directly determining the volumetric void fraction has not been developed, a derivation is necessary to determine void fraction in terms of measurable quantities. The total mass in a volume is written as:

$$m_{tot} = m_G + m_L = V_G * \rho_G + V_L * \rho_L \tag{2}$$

Also, the volume occupied by the vapor and liquid phases can be expressed as:

$$V_G = V_{tot} * \alpha \tag{3}$$

$$V_L = V_{tot} * (1 - \alpha) \tag{4}$$

Finally, if we define an average density for a volume a given time, assuming a constant distribution:

$$\rho_{avg} = m_{tot}/V_{tot} \tag{5}$$

Then, (2) can be re-written in terms of (3), (4) and (5) as:

$$V_{tot} * \rho_{avg} = V_{tot} * \alpha * \rho_G + V_{tot} * (1 - \alpha) * \rho_L \tag{6}$$

Finally, solving for the void fraction:

$$\alpha = \frac{\rho_L - \rho_{avg}}{\rho_L - \rho_G} \tag{7}$$

For a given refrigerant, the liquid and vapor densities can be determined from fluid properties. The measurement of the total volume is also a relatively simple exercise, with the method utilized in the current investigation being described in a

later section. The mass of refrigerant in the volume, however, is not as easily determined.

1.3: Mass Measurement Technique

The most commonly utilized procedure for direct charge determination, and the method used in the current investigation, is the Quick Closing Valves (QCV) method. The QCV method postulates that, if a charge of refrigerant flowing in a given volume can be instantaneously isolated from the rest of the system by means of two valves closing simultaneously at the inlet and outlet of the volume, the charge of stationary fluid in the closed volume is essentially a "snapshot" of the refrigerant flowing through the test section immediately prior to the valves being closed.

Once the refrigerant has been isolated, a method must be developed to determine the mass. Three methods are most commonly employed in literature: direct weight, separation-of-phases, or mass expansion.

The procedure of the direct weight method is to determine the mass of the refrigerant as the differential mass of the test volume with the trapped refrigerant less the weight of the empty test section:

$$m_{tot} = m_{ts,full} - m_{ts,empty} \tag{8}$$

The benefit of this method is its simplicity. However, because the mass of the test section utilized in the current investigation is several orders of magnitude greater than the predicted mass of refrigerant in the test section, this method was ultimately deemed infeasible due to the resulting high systematic error.

The separation-of-phases method has been used successfully in other experimental investigations, [4, 5, 6], and determines the refrigerant mass by

"draining" the liquid from the test section into a separate container until only vapor remains in the test volume. The total mass can then be determined as the differential mass in the new container plus the mass of vapor remaining in the test section, as determined from refrigerant properties:

$$m_{tot} = V_{ts} * \rho_{ts}(P,T) \; + \; (m_{container,full} - m_{container,empty}) \tag{9}$$

Though the calculated accuracy of this method is much greater than the direct weight method, it is best suited to higher temperatures tests. If any liquid remains in the test section, the void fraction measurement will be skewed significantly. Given the length of the test section used in the current investigation, it would be difficult to verify absolutely if any refrigerant remains in the test section. Also, the evaporator temperatures tested in the current investigation would make it more difficult to provide a receiver volume at a temperature sufficient low to ensure condensation into the volume. Finally, losses from connecting and disconnecting the receiver from the test volume can also cause immeasurable errors in the void fraction calculations.

Finally, the expansion method, developed by Erik Bjork [7] expands the two-phase refrigerant to a vapor state by releasing it into a container of known volume and sized to be several orders of magnitude larger than the test section. Once the expanded vapor has come to steady state, the pressure and temperature in the volume can be measured to determine the density in the expansion volume. Thus the mass of refrigerant in the test section can be calculated by:

$$m_{tot} = V_{ev} * \rho_{ev}(P,T) \tag{10}$$

Because this method does not require direct measurement of the volume's weight, there are no losses due to connecting and disconnecting the receiver volume,

as in the separation-of-phases method. Also, the accuracy of the method is comparable to the separation-of-phases method, and thus much greater than the direct weight measurement method. However, utilization of this method does require accurate measurement of the expansion volume to determine the refrigerant mass.

After considering the benefits and drawbacks of each method, the expansion method was chosen for the current investigation. The design of the expansion system and the mass measurement procedure are discussed in further sections.

1.4: Objectives

The objectives of the current investigation are three-fold:

- Design and fabricate a test facility to test the void fraction of fluids.
- Conduct an experimental investigation of the void fraction in adiabatic, horizontal tubes for refrigerants R134a, R290, and R1234yf over a range of flow conditions. Table 3 lists the test matrix for the current investigation. The saturation temperature of 7.2°C was chosen to conform with the AHRI Standard 540 [8] while the chosen mass flux corresponds to a capacity range of 0.75 – 1.50 kW.

Table 3: Test Matrix for Current Investigation

Refrigerant	T_{sat}	ID [mm]	G [kg/m^{2}s]	Quality
R134a	7.2°C	4.56, 2.99	150	0.1, 0.2, 0.3, 0.4, 0.5 0.6, 0.8
R290	7.2°C	4.56, 2.99	150	0.1, 0.2, 0.3, 0.4, 0.5 0.6, 0.8
R1234yf	7.2°C	4.56, 2.99	150	0.1, 0.2, 0.3, 0.4, 0.5 0.6, 0.8

- Compare the experimentally collected data to predictions made by twelve of the most commonly cited, explicit void fraction correlations (Table 4), and determine which of the models most accurately predicts void fraction.

Table 4: Investigated Void Fraction Correlations

Model	***Correlation***
Homogenous	Homogenous
X_{tt} Correlated	Lockhart-Martinelli **[9]**
	Baroczy **[10]**
Slip-Ratio Correlated	Zivi **[11]**
	Thom **[12]**
	Smith **[13]**
	Rigot **[14]**
Mass Flux Dependent	Premoli **[15]**
	Tandon **[16]**
	Steiner **[17]**
	Yashar **[5]**
	Harms-Groll **[18]**

Chapter 2: Literature Review

2.1: Homogenous Correlation

The homogenous correlation for void fraction is the simple analytical conversion from a mass to volume basis of the two phase flow:

$$\alpha = \frac{1}{1 + \frac{1-x}{x} * \frac{\rho_G}{\rho_L}} \tag{11}$$

This correlation makes the assumption that the liquid and vapor phases travel at the same velocity. Though this homogenous velocity assumption greatly simplifies analysis and yields a simple correlation, experimental observation indicates it is only accurate for a small range of flow conditions.

2.2: X_{tt} Correlated Models

X_{tt} correlated models utilize the Lockhart-Martinelli parameter for turbulent-turbulent flow (X_{tt}) as developed in [9]:

$$\mathrm{X_{tt}} = \frac{\mathrm{dP}}{dx_{\mathrm{G}}} \Big/ \frac{\mathrm{dP}}{dx_{\mathrm{L}}} = \left(\frac{1-\mathrm{x}}{\mathrm{x}}\right)^{0.9} * \left(\frac{\mu_L}{\mu_G}\right)^{0.1} * \left(\frac{\rho_G}{\rho_L}\right)^{0.5} \tag{12}$$

This parameter is defined as the ratio of the pressure gradient of vapor flowing in a tube to that of the pressure gradient of liquid flowing in a tube. The X_{tt} parameter accounts for some non-homogenous flow conditions due to frictional dissipation.

2.2.1: Lockhart-Martinelli Correlation

The first X_{tt} correlated model, and thus one of the first attempts to model the liquid and vapor phases as separate flow streams, was that of Lockhart-Martinelli [9].

The correlation was developed analytically as a function of the X_{tt} parameter and closed empirically using experimental data from previous researchers for air-water and air-oil mixtures.

$$\alpha = \frac{1}{1 + 0.28 * X_{tt}^{0.71}} \tag{13}$$

2.2.2: Baroczy Correlation

Baroczy [10], using data for air-water and mercury-nitrogen mixtures, also noted the correlation between liquid fraction, defined as $1 - \alpha$, and the Lockhart-Martinelli parameter. The authors utilized the relationship and added a dependence on the physical properties of the fluid outside of the X_{tt} parameter. The correlation was developed as tabulated data in table form, with the X_{tt} parameter on the x-axis and a property index, $P.I._2$, on the y-axis:

$$\text{P. I.}_2 = \left(\frac{\mu_L}{\mu_G}\right)^{0.5} \Big/ \frac{\rho_L}{\rho_G} \tag{14}$$

Table 5 presents the tabulated data for the liquid fraction correlation of Baroczy. For conditions not directly calculated in the chart, linear interpolation can be used to determine the liquid fraction:

Table 5: Tabulated Data for Baroczy [10]

	X_{tt}										
$P.I._2$	0.01	0.04	0.1	0.2	0.5	1	3	5	10	30	100
2e-5	0.000	0.000	0.000	0.001	0.009	0.068	0.17	0.22	0.30	0.47	0.71
1e-4	0.000	0.000	0.002	0.005	0.030	0.104	0.23	0.29	0.38	0.57	0.79
4e-4	0.000	0.002	0.007	0.018	0.066	0.140	0.28	0.35	0.45	0.67	0.85
1e-3	0.002	0.007	0.017	0.035	0.091	0.700	0.32	0.40	0.50	0.72	0.88
4e-3	0.004	0.017	0.037	0.065	0.134	0.222	0.39	0.48	0.58	0.80	0.92
1e-2	0.005	0.021	0.048	0.084	0.165	0.262	0.44	0.53	0.63	0.84	0.94
4e-2	0.0056	0.025	0.059	0.105	0.215	0.330	0.53	0.63	0.70	0.90	0.96
0.1	0.0058	0.027	0.064	0.117	0.242	0.380	0.60	0.70	0.78	0.92	0.98
1	0.0060	0.028	0.072	0.140	0.320	0.500	0.75	0.85	0.90	0.94	0.99

2.3: Slip-Ratio Correlated Models

As mentioned previously, an important consideration in the prediction of void fraction is the calculation of the separated flow condition, or the speed at which one phase moves relative to the other. As such, many models correlate void fraction as a function of a "slip-ratio" and typically follow a modified form of the homogenous equation:

$$\alpha = \frac{1}{1 + \frac{1-x}{x} * \frac{\rho_G}{\rho_L} * S} \tag{15}$$

where,

$S \equiv \frac{u_G}{u_L}$ and is calculated differently based on each correlation.

2.3.1: Zivi Correlation

The Zivi [11] correlation was developed as an analytical slip-ratio correlation assuming annular flow and based on the principle of minimum entropy production. The author made the assumption that energy dissipation through wall shear stress was negligible and that no liquid was entrained in the vapor annulus:

$$\mathrm{S} = \left(\frac{\rho_L}{\rho_G}\right)^{\frac{1}{3}} \tag{16}$$

The author compared his correlation to existing data for steam-water and found the correlation performed well. He observed that errors in the correlation caused by liquid entrainment had a more significant effect than errors due to wall shear effects, noting the assumption of zero entrainment as a possible shortcoming of the correlation.

2.3.2: Smith Correlation

Smith [13] developed his slip-ratio correlation for boiling water considering an annular flow model and closed the correlation empirically. The model assumes a liquid annulus with a core containing a mixture of vapor and entrained liquid and that the liquid and mixture have the same velocity head, i.e. $\rho_L * V_L^2 = \rho_m * V_m^2$. From analytical analysis, the slip-ratio then follows the form:

$$S = K + (1 - K) * \left(\frac{\frac{\rho_L}{\rho_G} + K * \left(\frac{1-x}{x}\right)}{1 + K * \left(\frac{1-x}{x}\right)} \right)^{0.5} \tag{17}$$

where,

$$K \equiv \frac{mass\ of\ liquid\ in\ mixture}{total\ mass\ of\ liquid}$$

The author compared the correlation to data for steam from previous experimental investigations to determine a correlation for K. Ultimately, he found that values of K between 0.3 and 0.5 suitably predicted most data, and, without a correlation for K apparent, determined that K = 0.4 provided the most accurate results for all data sets.

2.3.3: Rigot Correlation

Rigot [14], using experimentally collected data, found that a constant slip-ratio of S=2 correlated well for his application.

2.3.4: Ahren/Thom Correlation

Ahrens [19] used the steam-water data of Thom [12] to develop a correlation for the slip-ratio in the form of tabulated data in a table. Table 6 is a chart of the

tabulated data where $P.I._2$ is the property index in (14). For points not in the chart, linear interpolation between the nearest two points can be used to calculate the slip-ratio.

Table 6: Tabulated Data for Ahrens/Thom [12]

$P.I._2$	6.45	2.48	1.90	1.57	1.35	1.15	1.00
S	0.00116	0.01540	0.03750	0.08780	0.18700	0.49000	1.00000

2.4: Mass Flux Dependent Correlations

As the name implies, mass flux dependent models consider the effect of fluid mass flux, *G*, on void fraction, either by directly considering mass flux as a variable or by incorporating a dimensionless number which is a function of the mass flux, i.e. Reynolds number, Weber number, etc. Moreover, mass flux dependent correlations themselves have no defined "form" like the slip-ratio correlations and have been developed utilizing a number of methodologies.

2.4.1: Premoli Correlation

The Premoli [15] correlation was developed with the intent to minimize liquid density prediction error of two-phase refrigerant in nuclear reactors. The correlation follows the form of a slip-ratio correlation as in (15) with the slip-ratio correlated by using experimental data to analyze the effect of many dimensionless parameters on the slip-ratio. Ultimately the author determined that the liquid Reynolds number, Re_L, and the liquid Weber number, We_L, had the greatest influence on the slip-ratio.

$$S = 1 + F_1 * \left(\frac{y}{1 + F_2 * y} - F_2 * y\right)^{0.5} \quad (18)$$

where,

$$y = \frac{\beta}{1 - \beta} \quad (19)$$

$$F_1 = 1.578 * Re_L^{-0.19} * \left(\frac{\rho_L}{\rho_G}\right)^{0.22} \quad (20)$$

$$F_2 = 0.0273 * We_L Re_L^{-0.51} * \left(\frac{\rho_L}{\rho_G}\right)^{-0.08} \quad (21)$$

$$\beta = \frac{1}{1 + \frac{1 - x}{x} * \frac{\rho_G}{\rho_L}} \quad (22)$$

2.4.3: Tandon Correlation

Tandon et. al. [16] developed their model for void fraction by analytical analysis of annular flow in a pipe:

$$\alpha = 1 - 1.926 * \frac{Re_L^{-0.315}}{F(X_{tt})} + 0.993 * \frac{Re_L^{-0.63}}{F(X_{tt})^2} \quad for \;\; 50 < Re_L < 1125 \quad (23)$$

$$\alpha = 1 - 0.38 * \frac{Re_L^{-0.088}}{F(X_{tt})} + 0.0361 * \frac{Re_L^{-0.176}}{F(X_{tt})^2} \quad for \; Re_L > 1125 \quad (24)$$

where,

$$F(X_{tt}) = 0.15 * \left(\frac{1}{X_{tt}} + \frac{2.85}{X_{tt}^{0.476}}\right) \quad (25)$$

The correlation utilizes an approximation of film thickness as a function of the liquid Reynolds number developed by Traviss [20], and the shear stress at the wall is calculated using the method of Lockhart-Martinelli [9]. The authors compared their correlation along with existing correlations using experimental void fraction data for

steam. The conclusion was that their correlation predicted void fraction well, with only the Smith [13] correlation performing better.

2.4.4: Steiner Correlation

The Steiner [17] correlation follows the drift flux model of Zuber and Findley [21] which correlates void fraction as a function of the relative volumetric flow rate with respect to a reference velocity, $\overline{U}_{GU}$ and a correlation parameter, C_o:

$$\alpha = \frac{x}{\rho_G} * \left[C_o * \left(\frac{x}{\rho_G} + \frac{1-x}{\rho_L} \right) + \frac{\overline{U}_{GU}}{\dot{G}} \right]^{-1} \tag{26}$$

The author modified a previous correlation for vertical flow developed by Rouhani-Axelsson [22] to be used in horizontal applications, with his correlation parameters calculated as:

$$\overline{U}_{GU} = 1 + 0.2 * (1 - x) \tag{27}$$

$$C_0 = 1.18 * (1 - x) * \left[\frac{g * \sigma * (\rho_L - \rho_G)}{\rho_L^2} \right]^{0.25} \tag{28}$$

2.4.5: Yashar Correlation

The Yashar [5] correlation was developed based on experimental results collected by the author for refrigerants R134a and R410A at evaporating conditions and for a variety of flows. The authors noted that many existing correlations developed for annular flow fail to accurately predict void fraction outside of this regime. So, the authors fit a curve to their data:

$$\alpha = 0.4428 - 0.1987 * \beta + 0.658 * \beta^2 \tag{29}$$

where,

β is defined as the volumetric quality as calculated in (22).

The authors found that their correlation had an average deviation of 4% when compared to the experimental data but noted the fit was preliminary and could be improved with a larger data bank.

2.4.6: Harms-Groll Correlation

The Harms-Groll [18] correlation was developed in a manner similar to Tandon [16] by analytical analysis of annular flow in a pipe. However, the authors analytically developed their own model for liquid film thickness as a function of the liquid Reynolds number. In their analysis, the authors proposed two methods to close their model, an explicit approach following the work of Lockhart-Martinelli [9] and an implicit approach that requires a numerical solution. The explicit model can be written as:

$$\alpha = \left[1 - 10.06 Re_L^{-0.875}(1.74 + 0.104 Re_L^{0.5})^2 * \left(1.376 + \frac{7.242}{X_{tt}^{1.655}}\right)^{-0.5}\right]^2 \quad (30)$$

To verify the model, the authors compared their explicit and implicit analytical model with existing empirical models [16, 5] in conditions predicted to exhibit annular flow. Ultimately they noted the explicit model better agreed with the existing empirical models and, due to its ease of implementation, recommended it over the implicit model. As such, it is the model considered in the current investigation.

Chapter 3: Test Facility

3.1: Overview

The experimental facility constructed for this investigation is designed to measure the void fraction of pure refrigerants using a modified form of the QCV method of Bjork [7]. The system consists of two loops: a primary test loop thermally linked to an exterior two-stage vapor compression loop outfitted with an electronic Hot Gas Bypass (HGBP) valve. The test loop is a pumped loop, which allows for the testing of pure refrigerants without dilution by compressor oil. The vapor compression loop serves to both reject heat to the ambient and to modulate the saturation temperature within the test loop. Figure 1 presents a schematic of the test loop.

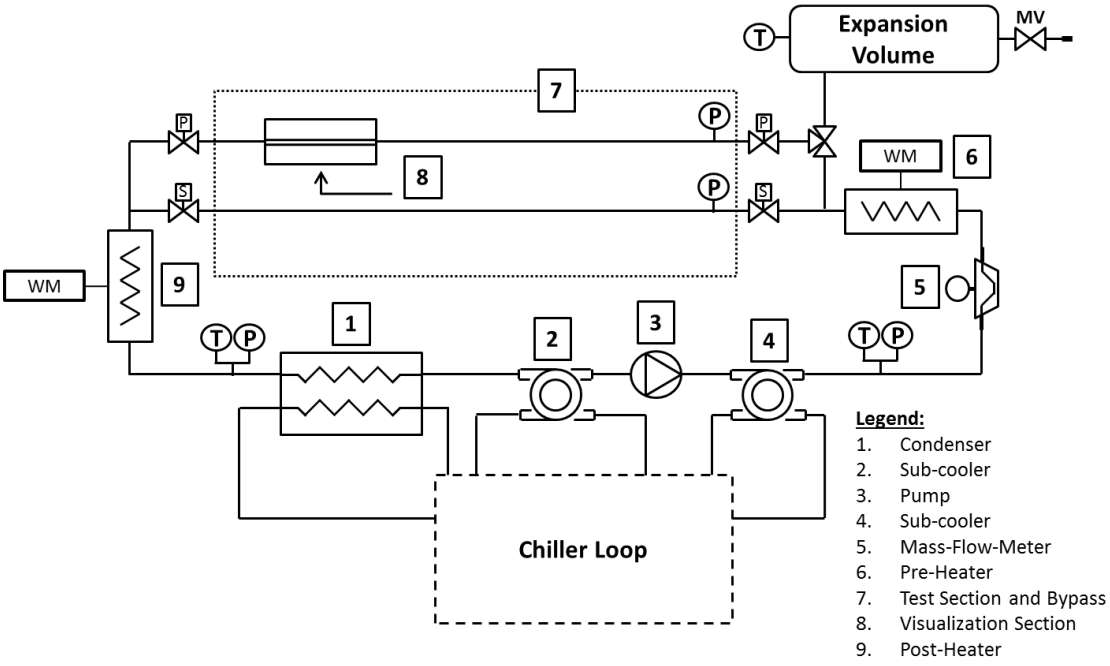

Figure 1: Test Loop Schematic

3.2: Test Loop

From Figure 1, the primary components of the test loop are: (1) a flat plate heat exchanger to condense superheated vapor to saturated liquid, (2) a sub-cooler to sub-cool the saturated liquid, (3) a pump to move the sub-cooled refrigerant, (4) a second sub-cooler to provide further sub-cooling, (5) a mass flow meter to measure the refrigerant mass flow, (6) a variable capacity, electric resistance heater outfitted with a watt meter to heat refrigerant to a specified quality, (7) the void fraction test section installed with (8) a visualization section, and (9) a second variable capacity heater and watt meter to superheat the refrigerant.

3.2.1: Controlled Variables

In the current investigation, three variables are controlled as part of the test matrix: the mass flow rate, quality, and saturation temperature of the refrigerant.

The mass flow rate is modulated with a Variable Frequency Drive (VFD) wired to a MicroPump GB-P35 gear pump. A PID controller maintains a constant mass flow rate based on the reading of the Coriolis-type mass-flow-meter.

The quality of the refrigerant entering the test section is determined mathematically. Liquid refrigerant leaves the sub-cooler and the enthalpy is determined from a temperature and pressure sensor. Heat is input to the system by means of the electric heater and measured with a watt-meter. The enthalpy of the refrigerant entering the test section is then determined according to (31).

$$h_{ts} = \frac{\dot{m}_{ref} * h_{ref} + \dot{Q}_{pre}}{\dot{m}_{ref}} \tag{31}$$

The calculated enthalpy is then used with the inlet test section pressure to provide two independent fluid properties at that point. The quality is determined from refrigerant property data using the commercially available RefProps software.

Finally, the inlet saturation temperature to the test section is controlled by electronically modulating a Sporlan SDR-230-S HGBP valve installed in the chiller. As the HGBP valve is opened, the evaporator pressure in the chiller loop increases, causing a similar increase in the condensing pressure on the test loop side of the flat plate heat exchanger. A steady value is maintained through the use of a PID controller tuned to control the valve position based on the saturation temperature measurement at the test section inlet.

3.2.2: Test Section

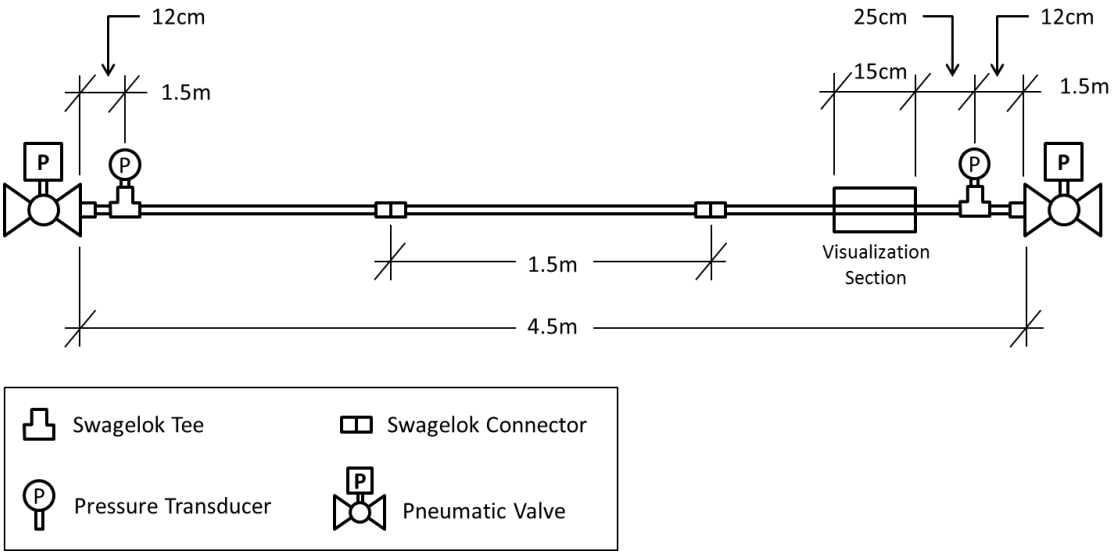

Figure 2: Test Section Schematic

In total, two test sections of inner diameter 4.56 mm and 2.99 mm were tested. Both test sections were approximately 4.5 m in length. The test sections are

constructed of multiple 1.52 m stainless steel tubes joined with Swagelok fittings to approximate a straight tube. A visualization section of similar inner diameter was installed near the outlet of the 1/4" test section. Figure 2 illustrates a schematic of the test sections and Figure 3 is the 1/4" test section installed in the system. Due to their length, the test sections had to be spanned across the environmental chamber at a height of approximately 2 meters. To support the test section and ensure that no bending occurred across the length, a beam comprised of two stainless steel T-beams was constructed to provide a means of support for the test sections.

Figure 3: 1/4" Test Section Installed in System

Because the tests were performed adiabatically, heat loss through the test section was an important consideration in the design of the system. The following steps were taken to minimize heat loss in the test section:

1) The test sections were insulated with an inner layer of Amor-flex pipe insulation (R = 2) and an outer layer of fiberglass pipe insulation (R = 4.4).
2) The entire test loop was constructed in an environmental chamber so that the ambient temperature around the test loop was maintained at the saturation temperature of the refrigerant in the test loop.

3.2.2.1: Pneumatic Valves

The QCV method utilized to measure the void fraction requires the installation of two fast acting valves at each end of the test section. For accurate determination of the void fraction, these valves must close sufficiently fast and in a synchronized manner to ensure no excess refrigerant is allowed in or out of the test section due to one valve closing before the other.

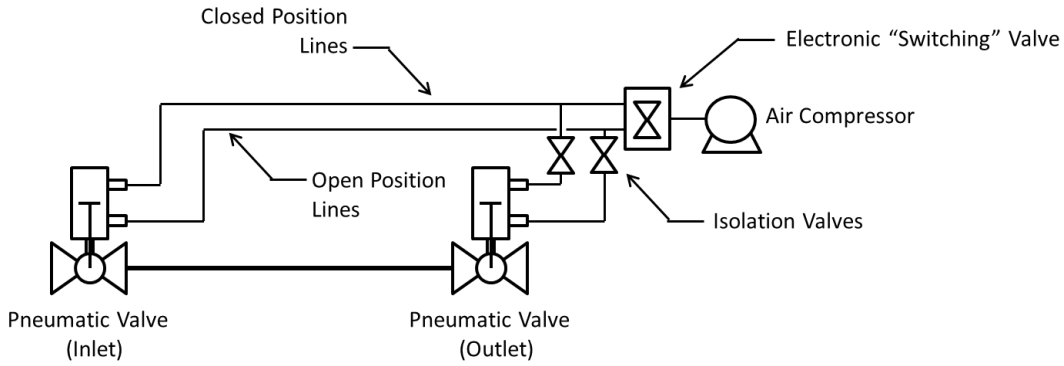

Figure 4: Pneumatic Valve System

Solenoid valves, the typical means by which to provide a sufficiently quick closing response would cause an immeasurable error in the adiabatic investigation due to the heat gain caused by the current in the coil. Manual ball valves connected with a linkage were considered but ultimately deemed unsatisfactory for this

investigation because deformation in the necessarily long linkage, approximately 4.5 meters, could cause an offset in closing time.

So, the test sections are closed on each end with an STC 2KD pneumatically activated valve controlled with compressed air at 100 psig supplied from a small air compressor (Figure 4). The pneumatic action causes no heat gain into the system, and the pneumatic lines were sized to be of equal length to ensure uniform static pressure loss to both valves, and thus a similar closing time.

3.2.2.2: Visualization Section

The visualization section used for flow regime observation was constructed according to Figure 5.

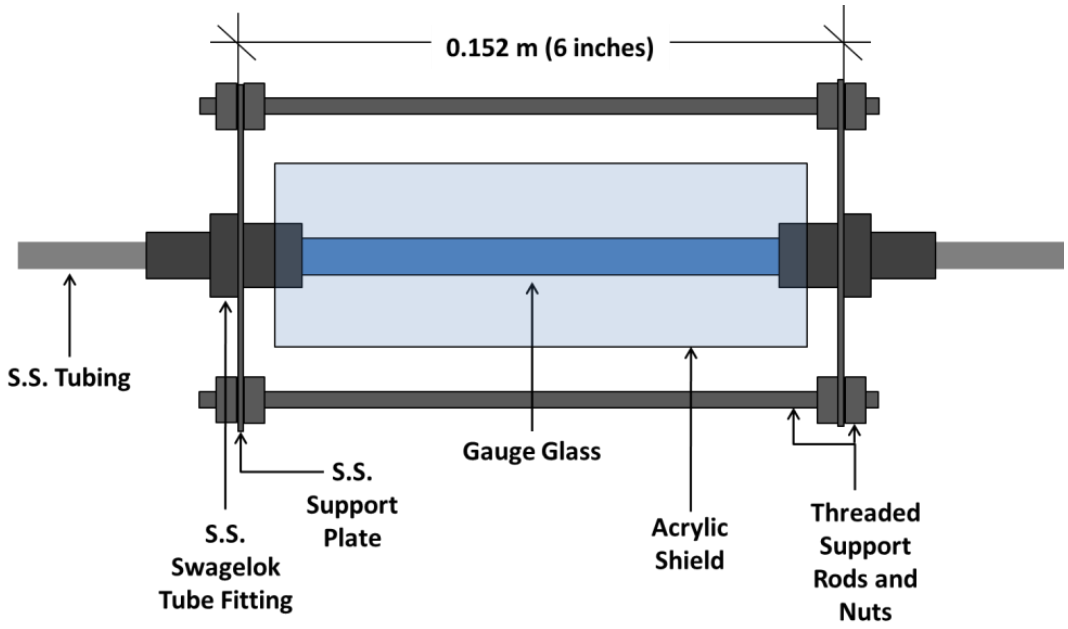

Figure 5: Construction of the Visualization Section

The glass itself is a 15cm (6 inch) length of commercially available gauge glass. The ID of the gauge glass was sized to approximately match the inner diameter of the tube being tested. A Swagelok coupler utilizing a Teflon ferrule provides

radial support to the gauge glass while two stainless steel plates held at a fixed distance with threaded rod provide axial support. The visualization section was installed near the outlet to the test section to allow sufficient length for inlet effects to dissipate.

3.2.2.3: Energy Balance

An energy balance is calculated for the test section to monitor heat loss. Heat input to the system is calculated as the sum of the pre-heater and post-heater additions. The heat transferred through the heat exchangers is calculated from the enthalpy measured at the inlet and outlet of the pre- and post-heaters, respectively. The heat loss is then determined according to (32):

$$\dot{Q}_{loss} = \dot{Q}_{pre} + \dot{Q}_{post} - \dot{m}_{ref} * (h_{pre,in} - h_{post,out}) \quad (32)$$

3.2.3: Expansion System

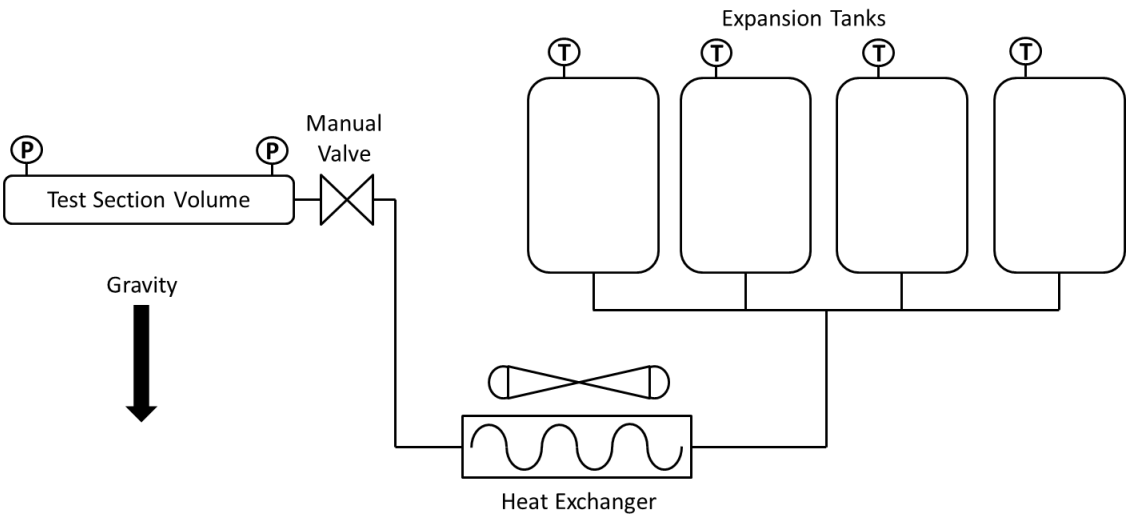

Figure 6: Schematic of the Expansion System

The expansion system utilized in the void fraction measurement was comprised of (1) a manual metering valve at the outlet of the test section serving as an expansion valve for the refrigerant, (2) a forced convection heat exchanger installed between the valve and the expansion volume, and (3) multiple refrigerant recovery tanks serving as the expansion volume of the system. Figure 6 illustrates a schematic of the system.

3.2.3.1: Expansion Volume

In designing the volume of the expansion system, it was required that the volume be large enough to ensure a superheated condition for the expanded vapor, yet not so large that the difference between the pressure corresponding to a void fraction of 0 and 1 was within the error of the measurement.

Figure 7: Expansion Tanks for Void Fraction Measurement

Initial estimates of the volumes of the test sections and refrigerant tanks were made and it was determined that a volume of 0.26 m^3 was sufficient for both test sections. So, two refrigerant tanks comprise the expansion system used in the current investigation (Figure 7).

3.2.3.2: Expansion Valve and Heat Exchanger

A primary concern in the design of the expansion system was the requirement that the refrigerant in the volume come to steady state, i.e. the ambient temperature of the environmental chamber, before calculation of the void fraction.

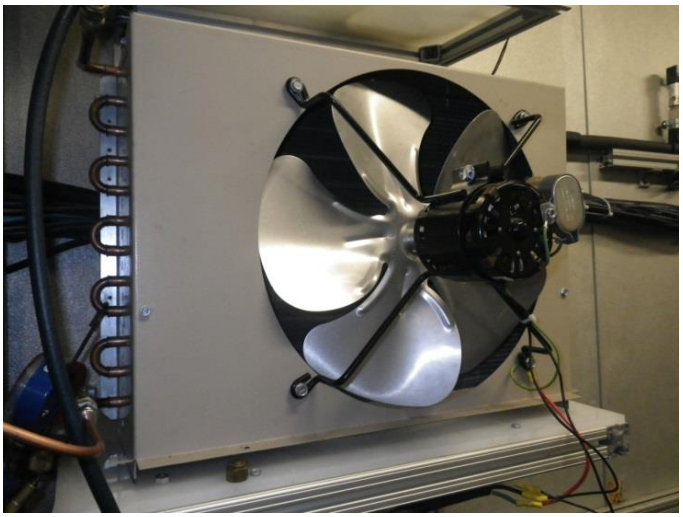

Figure 8: Heat Exchanger in Expansion System

Simply opening the test section to the expansion volume would cause a sudden drop in refrigerant temperature due to the boiling effect, and, with the primary means of heat transfer in the expansion volume being natural convection, the time required to come to steady state would be very long. To reduce the time to steady state, the metering valve at the outlet of the test section regulates the flow of refrigerant through the forced convection heat exchanger (Figure 8), reheating the expanded refrigerant to the ambient condition prior to entering the expansion tanks. To verify this method, surface thermocouples were installed at the inlet and outlet of the heat exchanger and temperature measurements were made with a hand-held thermocouple reader during shakedown testing. The measurements revealed that, except for a short time when the test section is initially opened to the expansion

volume, the heat exchanger is able to bring the system to an ambient condition prior to entering the expansion tanks, decreasing the required time to steady state.

3.3: Chiller Loop

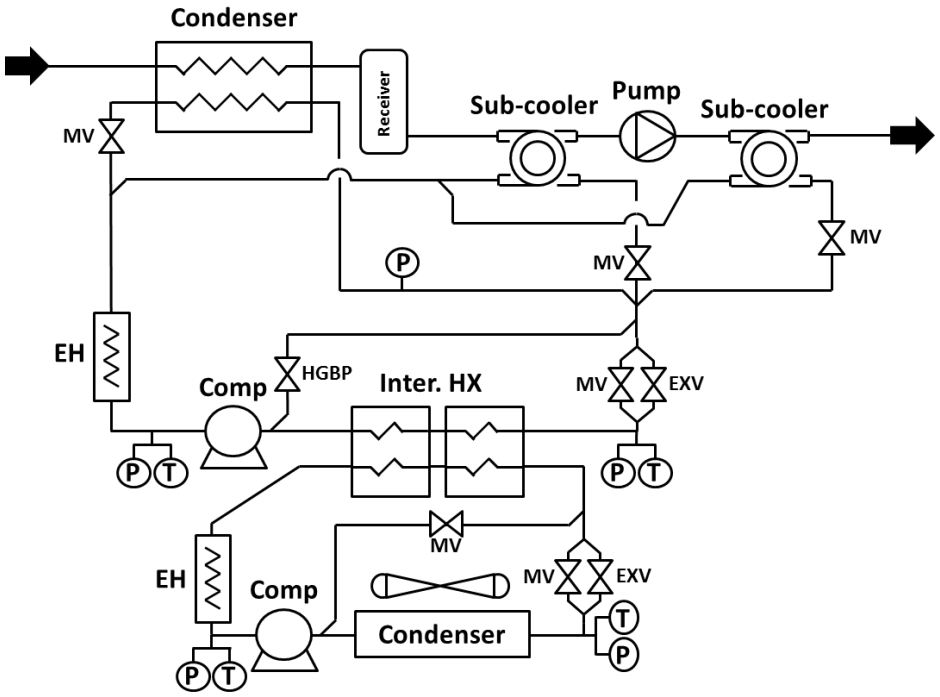

Figure 9: Chiller Loop Schematic

The chiller loop was designed as a two-stage vapor compression system to provide both a means of heat rejection for the test loop and control of the pressure levels at the test section inlet. Figure 9 illustrates a schematic of the system. The two stages allow for a large range of testing ability for future investigations, and the cascade provides a dampening effect against the instabilities caused by the air cooled condenser in the upper stage. This yields very steady results in the test section pressure level and highly accurate control of the saturation temperature.

3.3.1: Upper Stage

The upper stage of the chiller consists of a Tecumseh R22 compressor housed with an air-cooled, fin-and-tube heat exchanger which rejects heat to the ambient. A manual and electronic expansion valve provide course and fine control of the superheat in the compressor suction line, respectively, and two flat plate heat exchangers serve as the cascade between the two stages of the system. A manual needle valve serving as a HGBP valve provides course control of the pressure levels in the test loop.

3.3.2: Lower Stage

The lower stage consists of a Danfoss R404A compressor, and, like the upper stage, a manual and electronic expansion valve. A step-motor electronic bypass valve is used to provide fine control of the pressure in the test loop. To provide the most reactive control of the test section pressure, this stage was designed with two evaporator pressure levels to allow for separation of the condensing and sub-cooling processes in the test loop. On the chiller side, liquid refrigerant from the cascade heat exchanger is first expanded in the EEV. Part of this refrigerant is fed to the flat-plate heat exchanger in the test loop, condensing the refrigerant in the test loop to a saturated state and providing the control for the test system pressure. The refrigerant not sent to the condenser is expanded further through manual valves and fed through two tube-in-tube heat exchangers to provide the necessary sub-cooling at both the receiver and pump outlets. The manual valves are used both to control the amount of sub-cooling and as a means of evaporator pressure level control in the lower stage.

Finally, to ensure that the pressure level in the test section is controlled by the evaporator temperature in the lower stage of the chiller loop and not by the superheat temperature out of the heat exchanger, an electric resistance heater is installed in the suction line of this stage to provide additional capacity and force a two-phase condition in the flat-plate and tube-in-tube heat exchangers.

3.4: Instrumentation

For the current investigation, the measurements made can be classified into two categories: the non-critical measurements made only to monitor the operation of the system and the critical measurements used in data analysis. These critical measurements are the variables used to calculated quality, saturation temperature, mass flow rate, energy balance, and void fraction. For the non-critical measurements, sensors with a standard accuracy were utilized. However, for the critical measurements sensors with a high accuracy were utilized.

3.4.1: Pressure Measurement

Three models of pressure transducers were utilized in the current investigation. Performance data for each model is presented in Table 7.

Table 7: Pressure Transducer Performance Data

Model	Range	Accuracy
Setra 280E	**0-1724 kPa**	**±1.90 kPa**
Wika S-10	**0-1724 kPa**	**±4.31 kPa**
Omegadyne MMA150	**0-1034 kPa**	**±0.31 kPa**

The lower accuracy Setra and Wika pressure transducers were utilized for the non-critical measurements. For the critical pressure measurements at the test section

inlet and outlet, it was determined that the higher accuracy Omegadyne pressure transducers were required to maintain an acceptable accuracy in the measurements.

3.4.2: Temperature Measurement

For the majority of the temperature measurements in the chiller and test loop, in-stream and surface mounted T-type thermocouples were utilized (Figure 10).

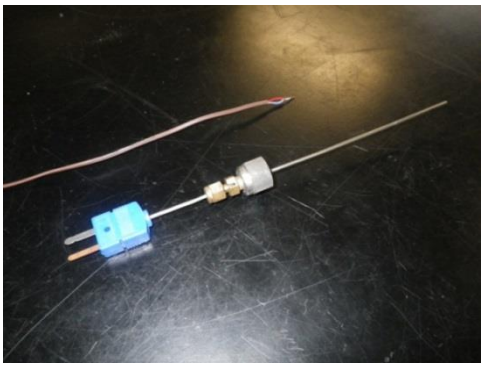

Figure 10: T-type Thermocouples

The accuracy of these measurements was assumed to be the manufacturer's accuracy of ±0.5°C and ±1.0°C for the in-stream and surface thermocouples, respectively. However, in order to improve the accuracy of critical measurements, the temperature measurements at the inlet of the pre-heater and outlet of the post-heater were made with Resistance Temperature Detectors (RTD's) manufactured by Omega with a rated accuracy of ±0.15°C (Figure 11).

Figure 11: Resistance Temperature Detector (RTD)

After calibration in with a temperature bath, the accuracy of the RTD's was taken as the manufacturers rating.

3.4.3: Mass Flow Measurement

The mass flow meter installed in the test loop is a Micro-Motion CMFS010 with a rated accuracy of 0.1 g/s. After calibration of the device, the accuracy was taken as the manufacturers rating.

3.4.4: Power Measurement

Two watt-meters manufactured by Ohio-Semitronics (Figure 12) were used to measure energy input to the pre- and post-heaters. The manufacturer's accuracy for each is 0.2% of the reading.

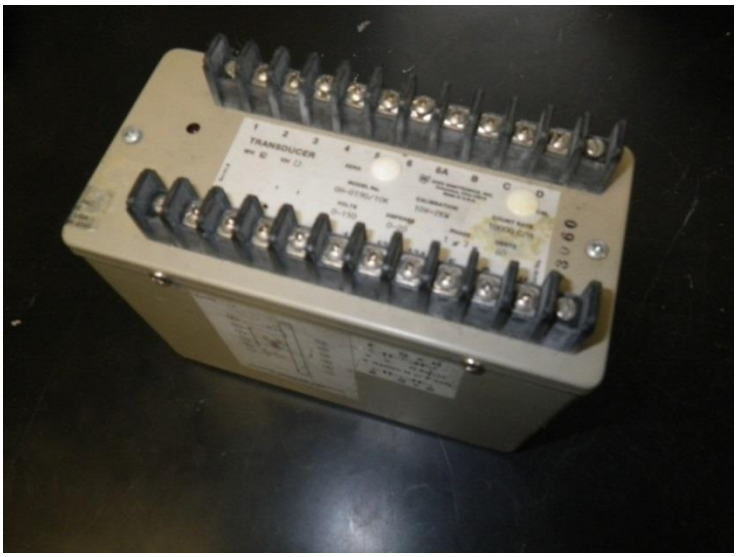

Figure 12: Watt Meter

3.5: Data Acquisition System

All sensors and controlled devices were connected to a bank of Field Point modules manufactured by National Instruments and installed near the test system. These modules allow for remote collection of data and remove the necessity to run a large number of connections directly to the data acquisition computer, reducing error in the measurement from voltage drop through long signal wires.

Data collection, analysis, and system control were accomplished with a Virtual Interface (VI) programmed using the commercially available LabView software integrated with a refrigerant properties routine, RefProps.

3.6: Uncertainty Analysis

To provide for the highest degree of certainty in each measurement, the total error in each measurement made is defined as the summation of the systematic and random error:

$$u_{tot} = u_{sys} + u_{rand} \tag{33}$$

For all measurements, to account for error caused by unsteady flow, the random error was taken as the standard deviation in the measurement.

$$u_{rand} = \sqrt{\frac{\sum(x_n - \bar{x})^2}{n-1}} \tag{34}$$

where,

u_{rand} is the total random error of the calculated measurement

x_n is the measurement made at time step, *n*

$\bar{x}$ is the average measurement over all time steps

For the directly measured variables, the systematic error was taken as the manufactures' rating as discussed above. The systematic uncertainty of the calculated variables in the experiment was accomplished using the Pythagorean Summation of Errors method:

$$u_{sys} = \sqrt{\left(u_{x_1} * \frac{\partial f}{\partial x_1}\right)^2 + \left(u_{x_2} * \frac{\partial f}{\partial x_2}\right)^2 + \cdots + \left(u_{x_n} * \frac{\partial f}{\partial x_n}\right)^2} \quad (35)$$

where,

u_{sys} is the total systematic error of the calculated measurement

u_{x_n} is the systematic error of the directly measured variable

$\frac{\partial f}{\partial x_n}$ is the partial derivate of the calculated measurement, *f*,

Table 8 lists the systematic uncertainty for the critical variables:

Table 8: Systematic Uncertainties for Critical Variables

Variable	Observed Range	Systematic Error
Quality, *x*	**10 - 80%**	**0.1%**
Saturation Temperature, T_{sat}	**7.2°C**	**0.02°C**
Mass Flow Rate	**1.0 – 2.5 g/s**	**0.1-0.25 g/s**
Void Fraction	**60 - 95%**	**0.3-0.9%**

It should be noted that there exists a repeatability error in the void fraction measurement, especially for flow regimes with non-uniform cross-section, due to differences in the area void fraction along the length of the test section. However, by sizing the length of the test section to be several orders of magnitude greater than the test section inner-diameter, it is assumed that these errors average out over the length of the test section. Repeatability testing performed during system shakedown supports this supposition.

Chapter 4: Testing Procedures

4.1: Volume Measurement Procedure

In order to implement the mass measurement technique of Bjork [7], the volumes of the test section and expansion volume must be determined. The volume of the expansion system is first determined. A recovery tank charged with refrigerant is weighed on a scale with a systematic error of 2.2 g. The expansion volume, which has previously been evacuated using a vacuum pump, is then charged with refrigerant from this tank such that a superheated state exists in the volume. The refrigerant tank is then weighed again to determine the differential mass. The refrigerant in the tank is allowed to come to steady state. The pressure and temperature in the tanks is then recorded. The volume of the expansion system is then determined according to:

$$V_{ev} = \frac{(m_1 - m_2)}{\rho_{ev}(T_{ev}, P_{ev})} \tag{36}$$

Table 9 is a sample calculation for the volume measurement. This procedure was performed three times at different pressures to verify the repeatability of the measurement. The average was taken as the volume of the expansion volume.

Table 9: Sample Expansion Volume Calculation

	Measurement	Systematic Error
m_1	**11.44 [kg]**	**0.0022 [kg]**
m_2	**10.78 [kg]**	**0.0022 [kg]**
T_{ev}	**22.7 [C]**	**0.35 [C]**
P_{ev}	**333.3 [kPa]**	**0.22 [kPa]**
ρ_{ts}	**14.91 [kg/m^3]**	**0.02 [kg/m^3]**
V_{ev}	**0.0439 [m^3]**	**1.42x10^{-4} [m^3]**

To determine the volume of the test section, the test system is charged and brought to steady state at a low mass flow rate with sub-cooled liquid flowing through the test section. The steady state pressure in the test section is taken as the average of the readings of the test section inlet and outlet pressure sensors. The temperature of the refrigerant is taken as the reading of a surface mounted thermocouple installed near the inlet to the test section.

Once steady state flow has been achieved, the test section is bypassed and the refrigerant trapped in the test section is expanded into the expansion volume, which has previously been evacuated. Once the refrigerant in the expansion system has come to steady state, the pressure and temperature is recorded. The volume of the test section is then determined by:

$$V_{ts} = \frac{\mathrm{V_{ev}} * \rho_{ev}(T_{ev}, P_{ev})}{\rho_{ts}(T_{ts}, P_{ts})} \tag{37}$$

Table 10 is a sample calculation for the test section volume measurement. Like the expansion volume, this procedure was performed three times, and the average was taken as the volume for each test section.

Table 10: Sample Test Section Volume Calculation

	Measurement	Systematic Error
V_{ev}	**0.04393 [m^3]**	**1.06x10^{-4} [m^3]**
T_{ts}	**-15.35 [C]**	**1.00 [C]**
P_{ts}	**228.3 [kPa]**	**0.21 [kPa]**
ρ_{ts}	**1344 [kg/m^3]**	**3.11 [kg/m^3]**
T_{ev}	**-6.935 [C]**	**0.35 [C]**
P_{ev}	**73.18 [kPa]**	**0.21 [kPa]**
ρ_{ev}	**73.18 [kg/m^3]**	**0.01 [kg/m^3]**
V_{ts}	**1.12x10^{-4} [m^3]**	**0.54x10^{-6} [m^3]**

4.2: Void Fraction Measurement Procedure

The void fraction measurement procedure is illustrated in Figure 13. Prior to startup of the system, a vacuum pump is connected to the expansion volume to bring it a deep vacuum, and the fan on the air-cooled heat exchanger is turned on to bring the thermal mass of the heat exchanger to the temperature of the environmental chamber.

1. Once the refrigerant flowing through the test section is at a steady state, data is recorded for 15 minutes. Though the only time increments of importance are those immediately leading up to the isolation of the test section, this 15 minute time length ensures that any system transients, such as the thermal mass in the electric heater, have had sufficient time to dissipate.
2. At the end of the 15 minutes, a relay simultaneously closes the two pneumatic valves in the test section and opens two solenoid valves in the bypass line.
3. The three way valve in the test loop is switched and the refrigerant trapped between the valve and the bypass is evacuated through the expansion volume.
4. Once the expansion volume is once again to a sufficiently deep vacuum, the pneumatic lines to the test section outlet valve are isolated and the inlet pneumatic valve is opened to release refrigerant to the expansion volume.

A sufficiently long time is waited to allow the refrigerant in the expansion volume to come to steady state, verified by the pressure and temperature measurements. Once steady state has been achieved, data for the void fraction is recorded. Finally, the process is reversed to open the test section back to the test loop and the expansion volume is evacuated for the next test point.

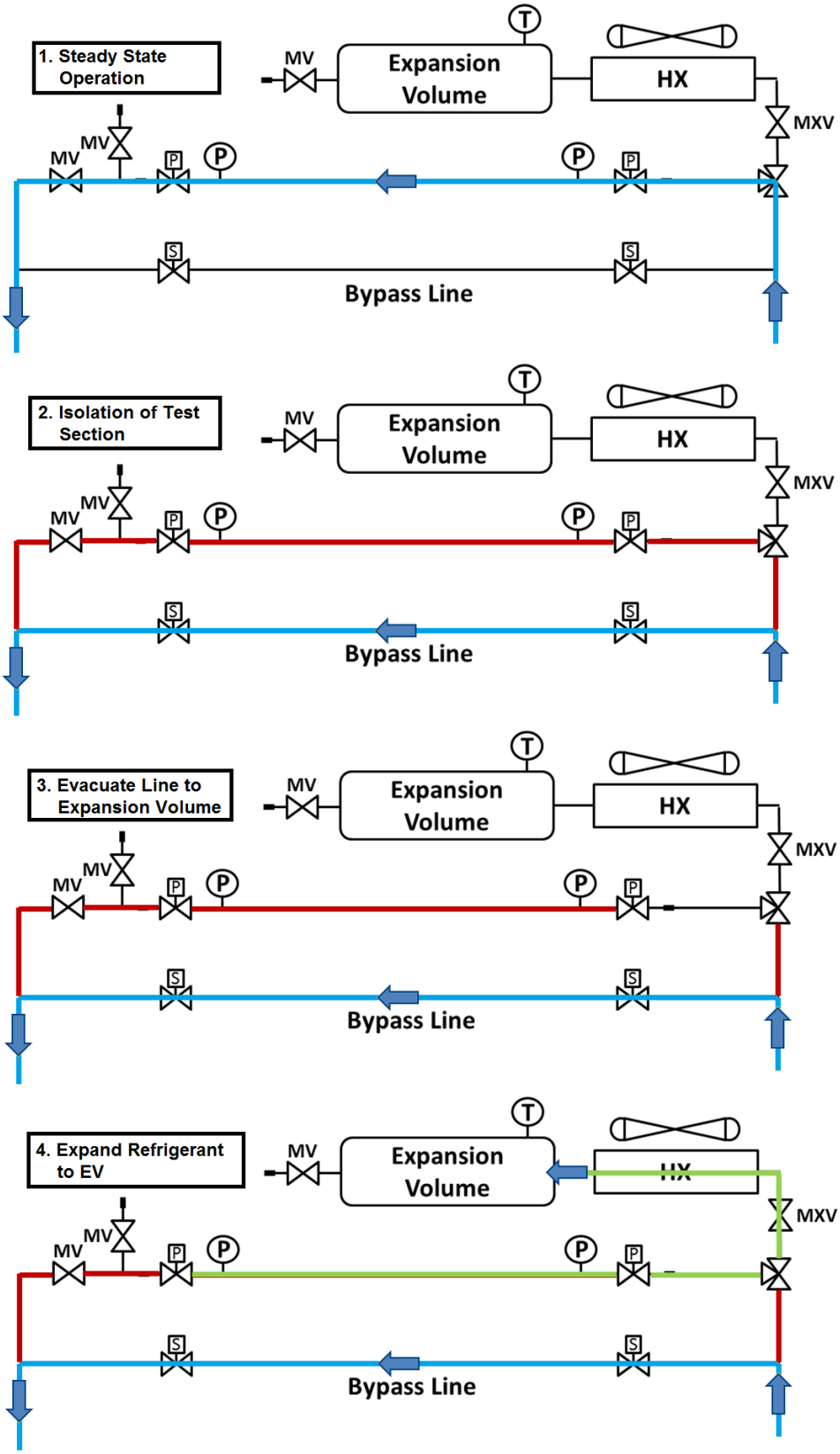

Figure 13: Void Fraction Measurement Procedure

Chapter 5: Results and Discussion

5.1: Flow Visualization

Flow visualization was performed for points in the 1/4" OD test section to determine the transition characteristics of each refrigerant relative to the other two. Figure 14 presents photographs taken during testing of select data points which illustrate the transition characteristics of the three refrigerants. For clarity, the interfacial boundary in each picture has been highlighted.

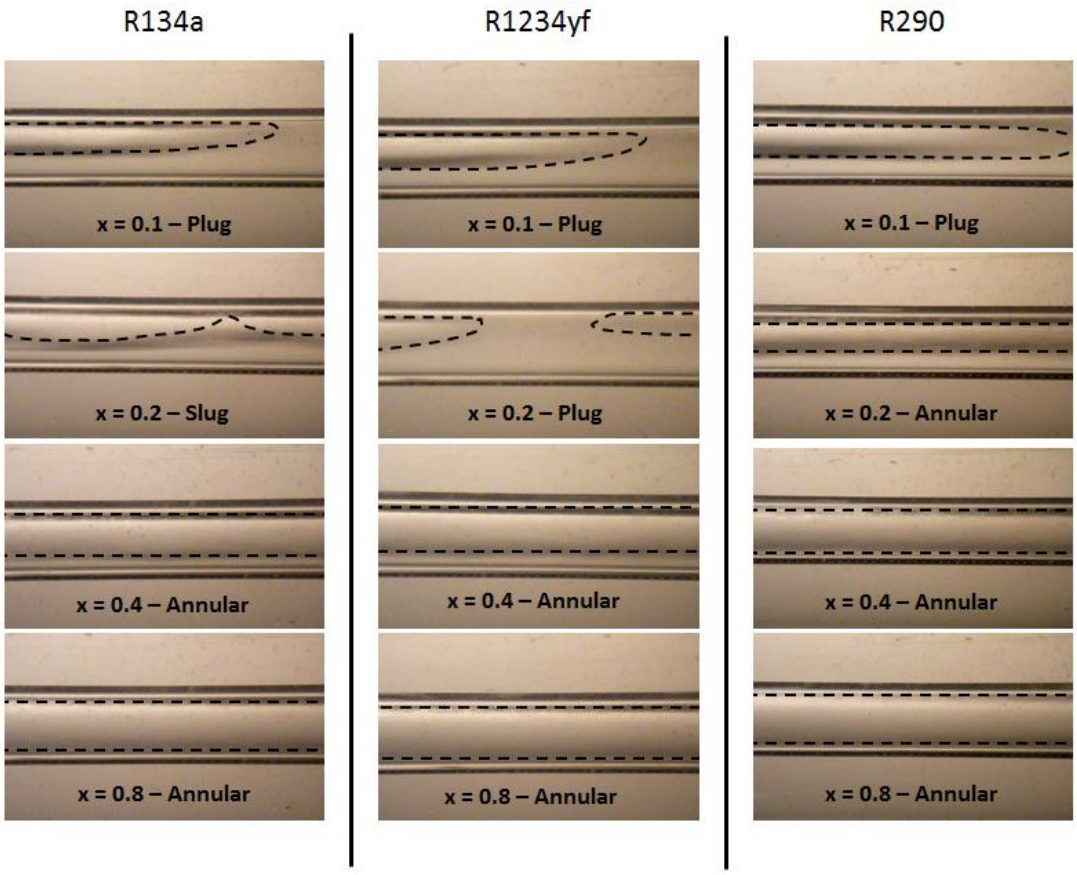

Figure 14: Flow Regimes for T_{sat} = 7.2°C, G = 150 kg/m^{2}s, ID = 4.56 mm

From Figure 14, R1234yf transitions from regime to regime at a slower rate than that of R134a. At a x = 0.2, R134a has begun to exhibit the turbulent "wavy"

behavior of slug flow, while R1234yf is still exhibiting the laminar plug flow, resembling elongated bubbles flowing through the tube. Similarly, while R134a has formed a complete annulus by x = 0.3, annular flow for R1234yf was not observed until x = 0.4.

R290 in contrast, exhibits much more turbulent flow characteristics at low qualities than the other two refrigerants and transitions to annular flow faster than R134a. The top of the tube was observed to be fully wetted by x = 0.2.

Typically, the rate of transition from regime-to-regime is driven primarily by the vapor velocity, calculated as:

$$u_G = \frac{\dot{m} * x}{\rho_G} * \frac{1}{A_{cs} * \alpha} \tag{38}$$

Figure 15 plots the vapor velocities for each refrigerant in the 1/4" test section, using the void fraction data from the current investigation.

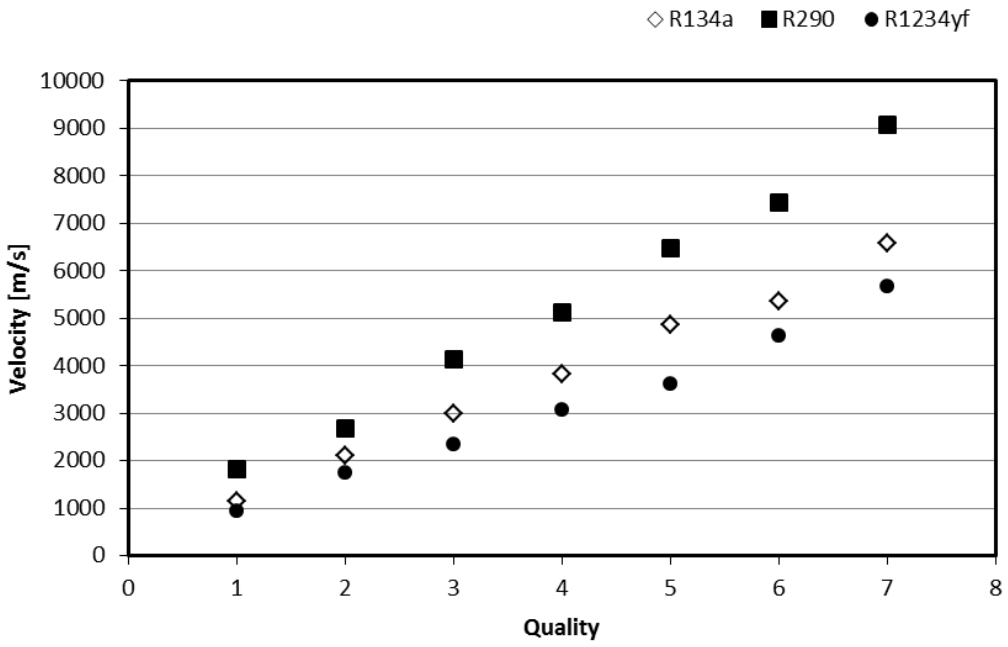

Figure 15: Vapor Velocities for the 1/4" Test Section

The trends illustrated in Figure 15 support the supposition that transition rate can be correlated to vapor velocity. R290, which exhibited faster, more turbulent transition characteristics, has the highest velocity vapor; while R1234yf, which was slower in transition, has the lowest vapor velocity of the three refrigerants. Table 11 lists all flow observations made for all tests:

Table 11: Flow Regime Observations

x	R134a	R1234yf	R290
0.1	Plug	Plug	Plug
0.2	Slug	Plug	Annular
0.3	Annular	Slug	Annular
0.4	Annular	Annular	Annular
0.5	Annular	Annular	Annular
0.6	Annular	Annular	Annular
0.8	Annular	Annular	Annular

Though, it should be noted that due to the low resolution of the current test matrix, it is difficult to make definite observations regarding exact flow regime trends and transition points.

5.2: Void Fraction Data

Experimental measurements of void fraction were made according to the test matrix in Table 3 with the goal of determining the differences, if any exist, among the void fraction trends of R134a, R290, and R1234yf. Data for each experiment is tabulated in Appendix A. The project looked specifically at differences in void fraction due to the (1) fluid properties and (2) the physical geometry of the flow channel, with R134a as a baseline.

5.2.1: Refrigerant Comparison

Figure 16 and Figure 17 illustrate the void fraction trends for R134a and R290 in the 3/16” and 1/4” test section, respectively.

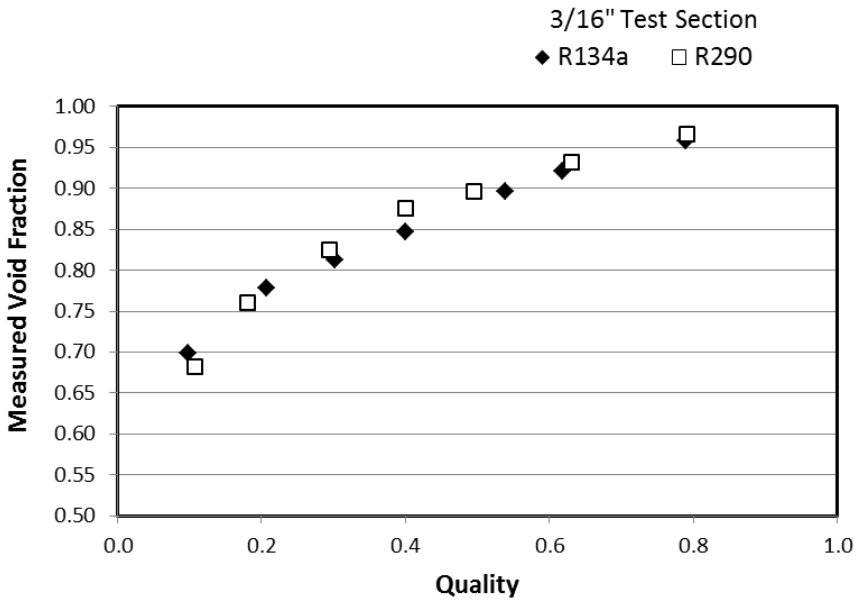

Figure 16: Void Fraction vs. Quality for R134a and R290 in a 3/16" Tube

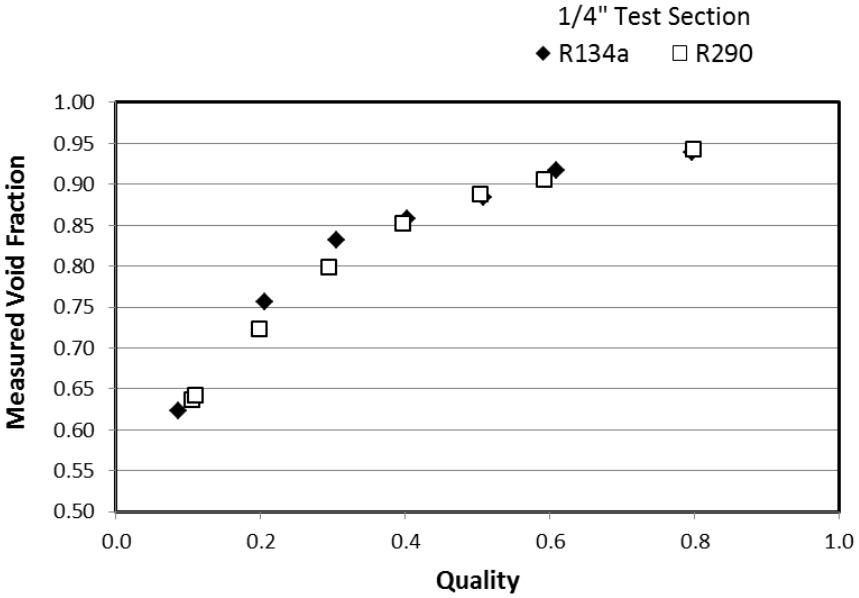

Figure 17: Void Fraction vs. Quality for R134a and R290 in a 1/4" Tube

It should be noted that for all graphs of void fraction versus quality, the charts are plotted from a void fraction of 0.5 to 1.0 to improve resolution. In reality, as the quality decreases below 0.1, the void fraction drops quickly to 0. From the above graphs, it is evident that, for both test sections, the void fraction curve for R290 compared to that of R134a does not deviate significantly. For the majority of the points, the difference is within the combined systematic error of the measurement. In the 1/4" test section, it appears that, for lower qualities the void fraction of R290 begins to trend below that of R134a, and for many of the points in the 3/16" test section, R290 appears to trend above R134a.

Figure 18 illustrates the void fraction trends for R134a and R1234yf in the 3/16" test section.

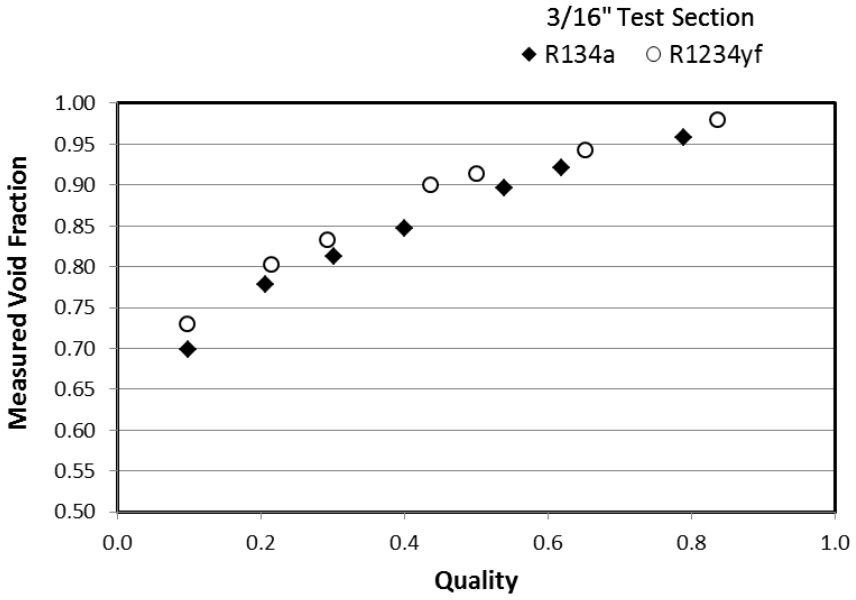

Figure 18: Void Fraction vs. Quality for R134a and R1234yf in a 3/16" Tube

The void fraction of R1234yf in the 3/16" test section consistently trends higher than that of R134a. As all of the differences are outside the combined

systematic error of the measurement, this trend can most likely be attributed to interfacial viscous dissipation due to differences in the fluid properties, specifically the density and viscosity ratios. A useful metric to test this supposition is the X_{tt} parameter, defined by (12).

Figure 19 is a plot of the X_{tt} parameter for the R134a and R1234yf for data points in 3/16" test section (the data plotted in Figure 18).

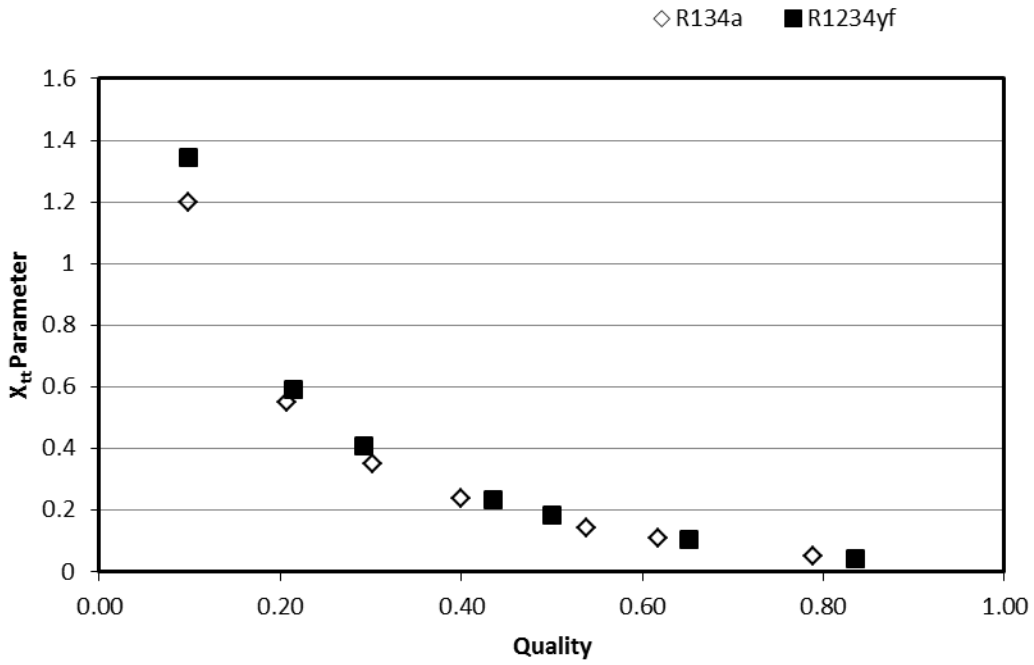

Figure 19: X_{tt} for a 3/16" tube for R134a and R1234yf

From the above plot, the X_{tt} parameter for R1234yf trends above R134a. This means that the ratio of the vapor single phase pressure gradient to the liquid single phase pressure gradient is greater for R1234yf compared to the same metric for R134a. This would lead to greater viscous dissipation, and thus a higher void fraction. In fact, as will be discussed later, void fraction correlations that make use of the X_{tt} factor tend to more accurately predict the void fraction for R1234yf compared

to the other refrigerants, indicating that viscous forces are more dominant in this refrigerant in small diameter applications.

Figure 20 illustrates the void fraction trends for R134a and R1234yf in the 1/4” test section.

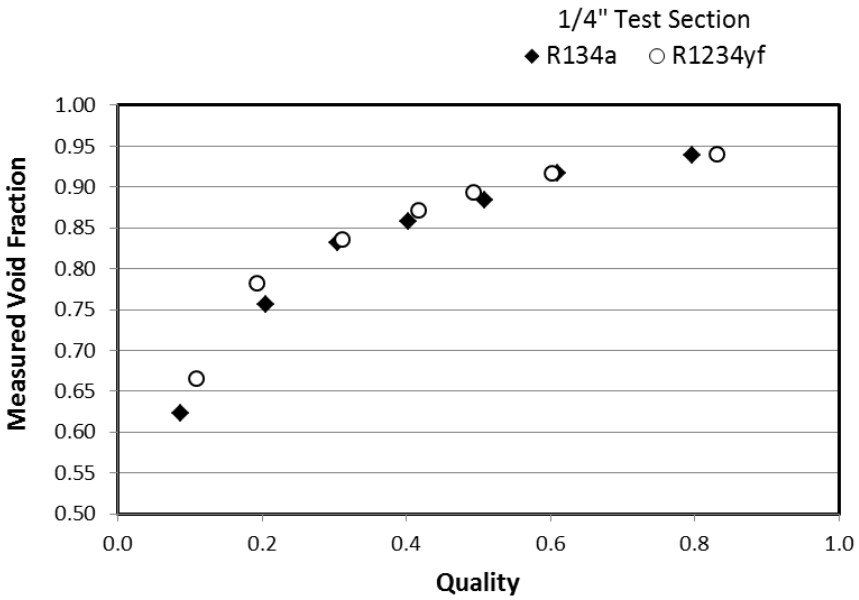

Figure 20: Void Fraction vs. Quality for R134a and R1234yf in a 1/4" Tube

Compared to the distinct trend in Figure 18, the differences between R134a and R1234yf in the 1/4” test section are not as evident. Though it appears that the void fraction for R1234yf trends slightly above R134a for most points, once again, many of the measurements are within the systematic error of the void fraction measurement. This fact can also be attributed to the frictional dissipation effects being less dominant in the larger tube.

5.2.2: Effect of Tube Diameter

It would also useful to understand the effect that tube diameter has on void fraction and fluid flow. Figure 21, Figure 22, and Figure 23 are a visual comparison

of the difference in void fraction between the 3/16” and 1/4” test sections for R134a, R1234yf, and R290, respectively.

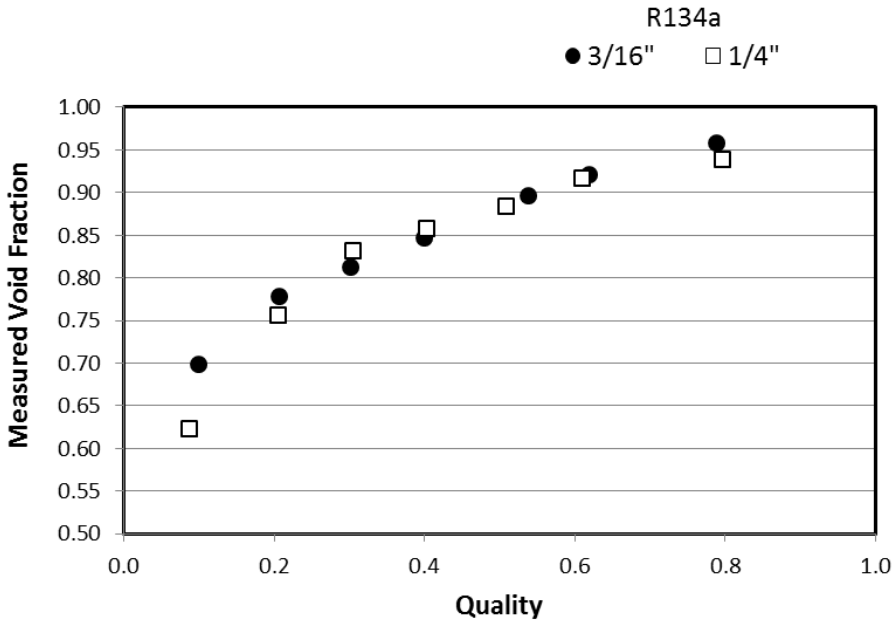

Figure 21: Void Fraction vs. Quality in the 3/16" and 1/4" Test Sections for R134a

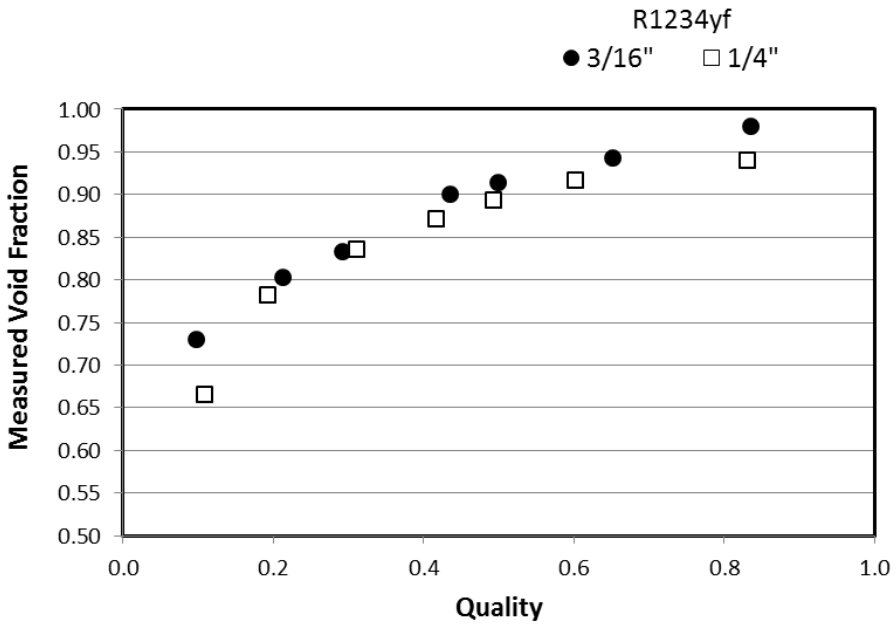

Figure 22: Void Fraction vs. Quality in 3/16" and 1/4" Test Sections for R1234yf

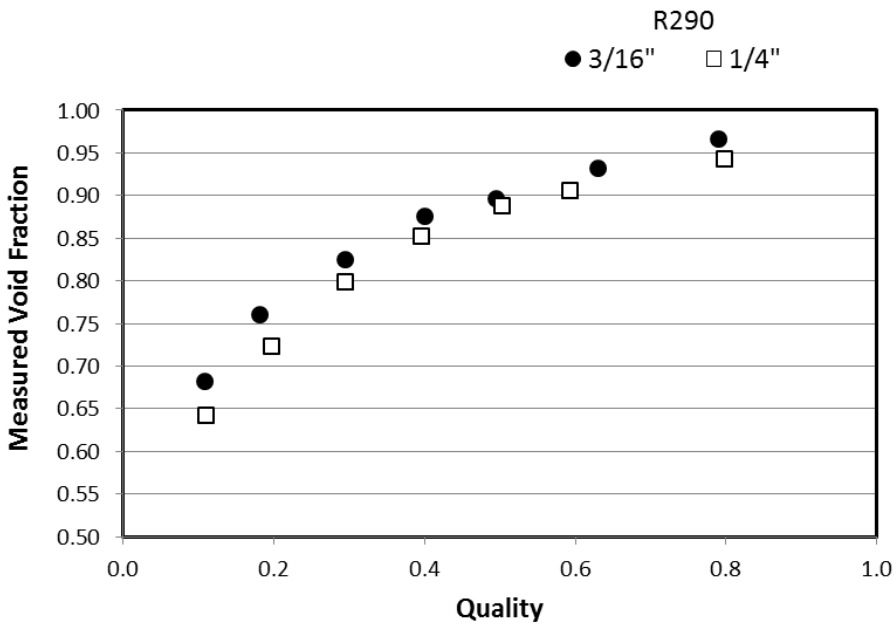

Figure 23: Void Fraction vs. Quality in 3/16" and 1/4" Test Sections for R290

For all three refrigerants, the void fraction in the 3/16" inch tube is greater than in the 1/4" tube to varying degrees. By inspection, difference is lowest for R134a in Figure 21 with many points overlapping between the two test sections. For R290 and R1234yf, the trend is more distinct. This could once again be explained by the fact that viscous dissipation is more dominant for smaller tube diameters and that the X_{tt} parameter for R290 and R1234yf is higher than that of R134a for the current data set.

5.3: Correlation Predictions

Following completion of the experimental data collection, the results were compared to the twelve correlations discussed in the literature review. The following plots compare the predicted void fraction to the measured void fraction:

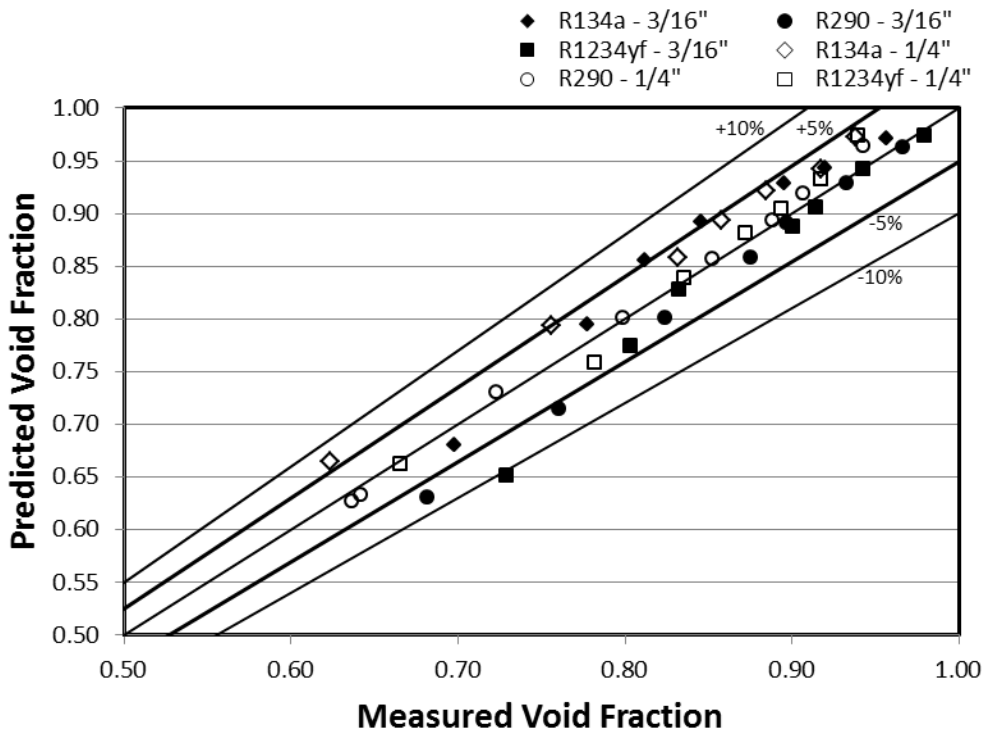

Figure 24: Performance of the Baroczy void fraction correlation

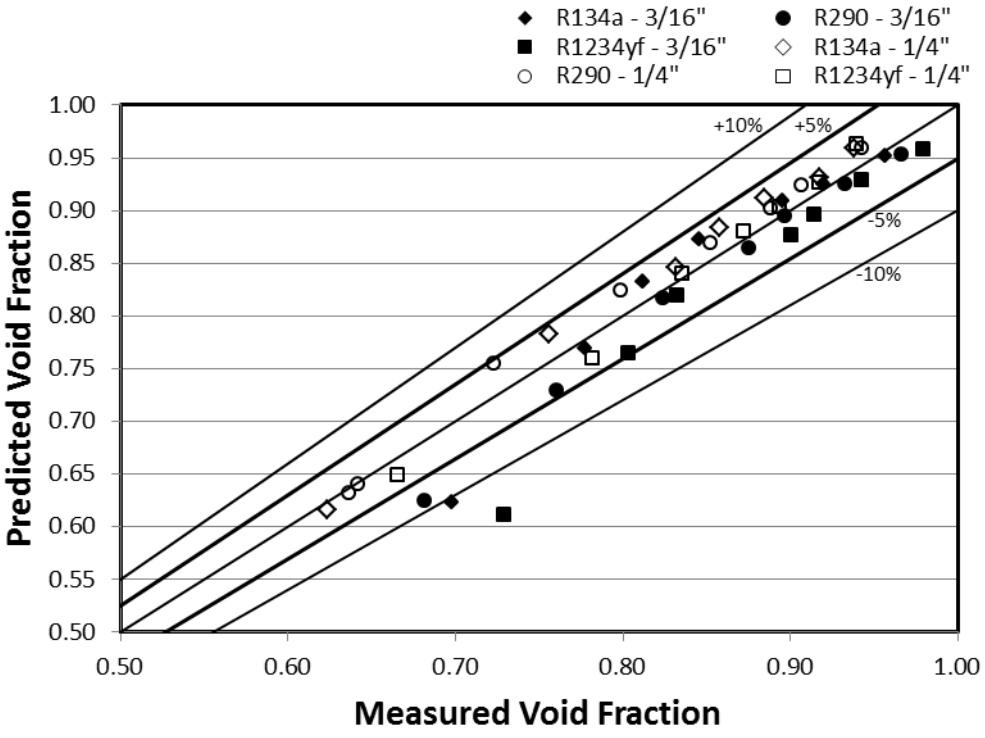

Figure 25: Performance of the Harms-Groll void fraction correlation

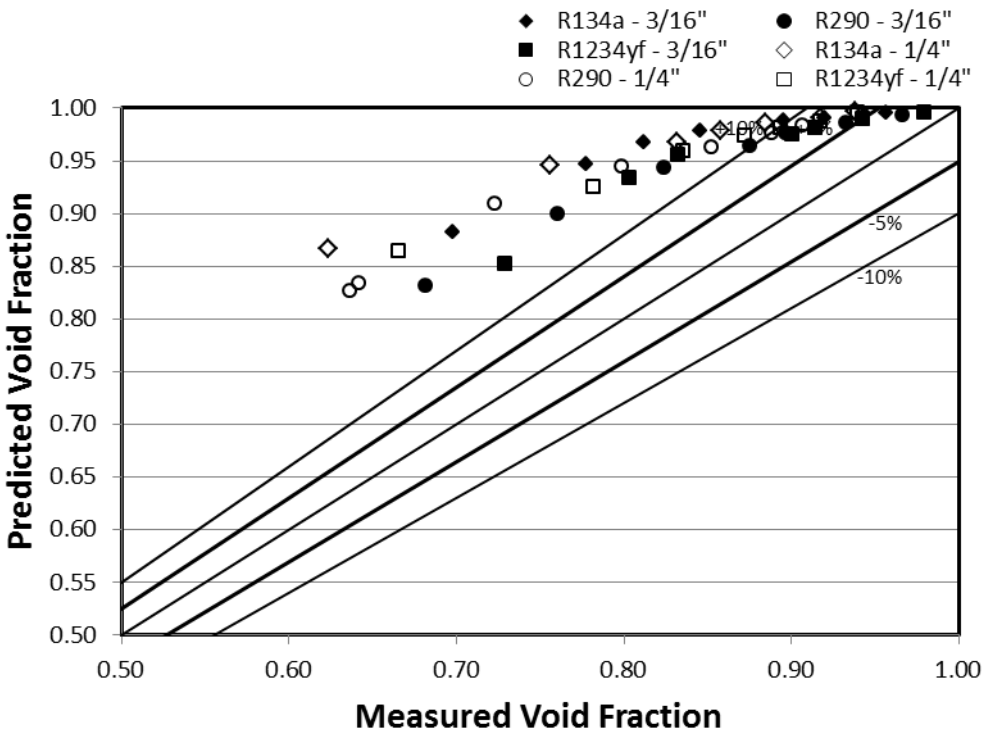

Figure 26: Performance of the Homogenous void fraction correlation

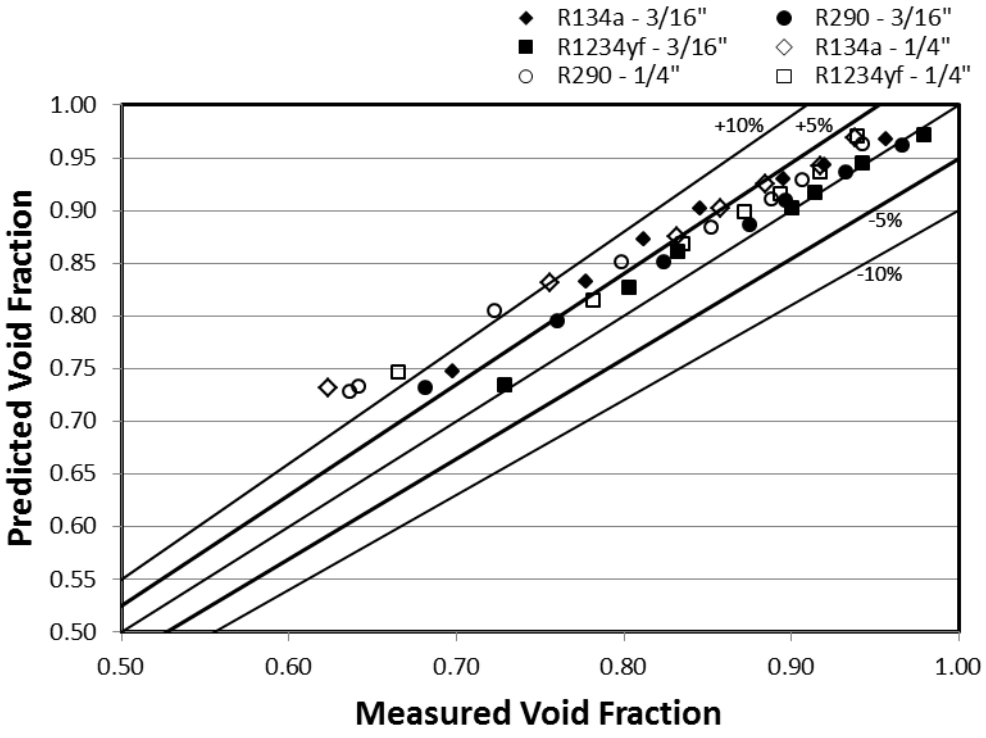

Figure 27: Performance of the Lockhart-Martinelli void fraction correlation

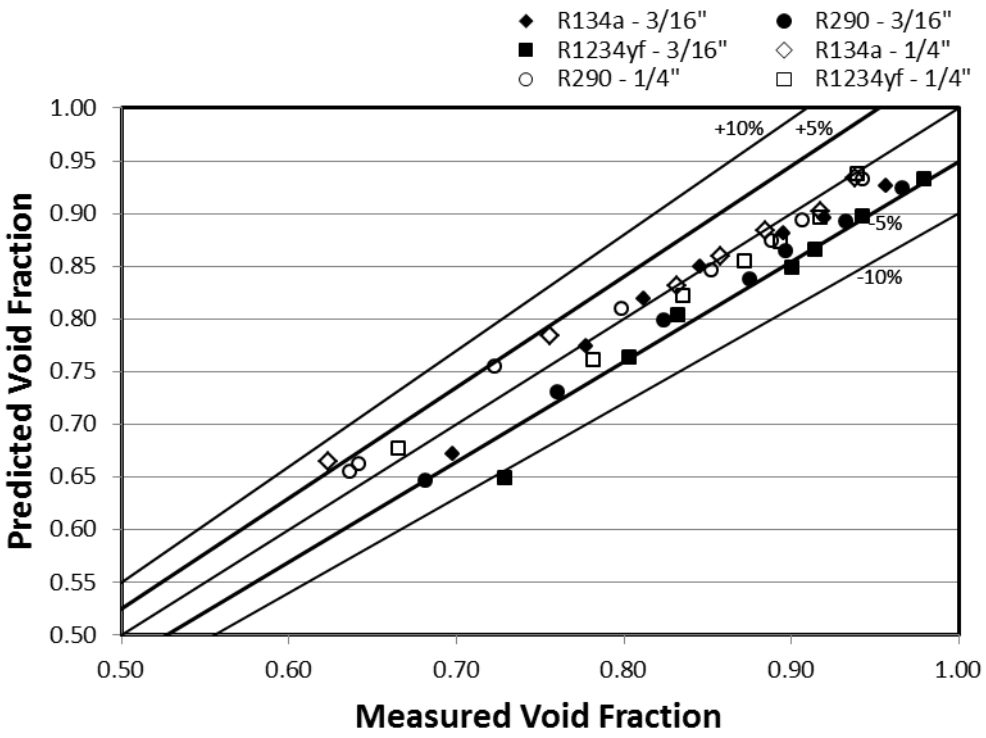

Figure 28: Performance of the Premoli void fraction correlation

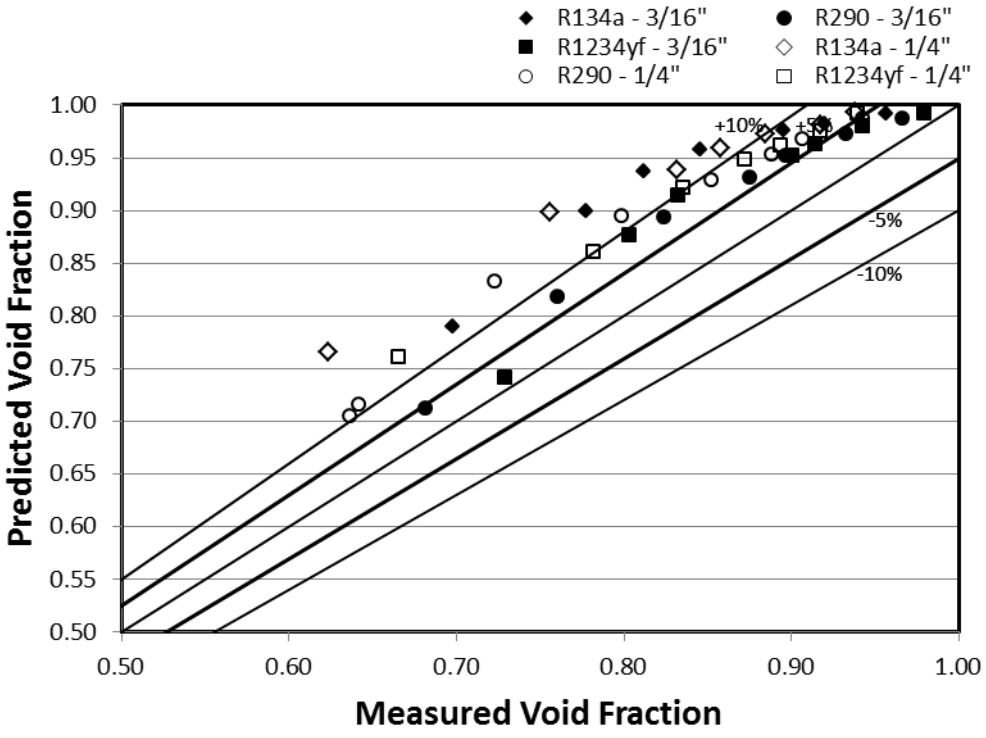

Figure 29: Performance of the Rigot void fraction correlation

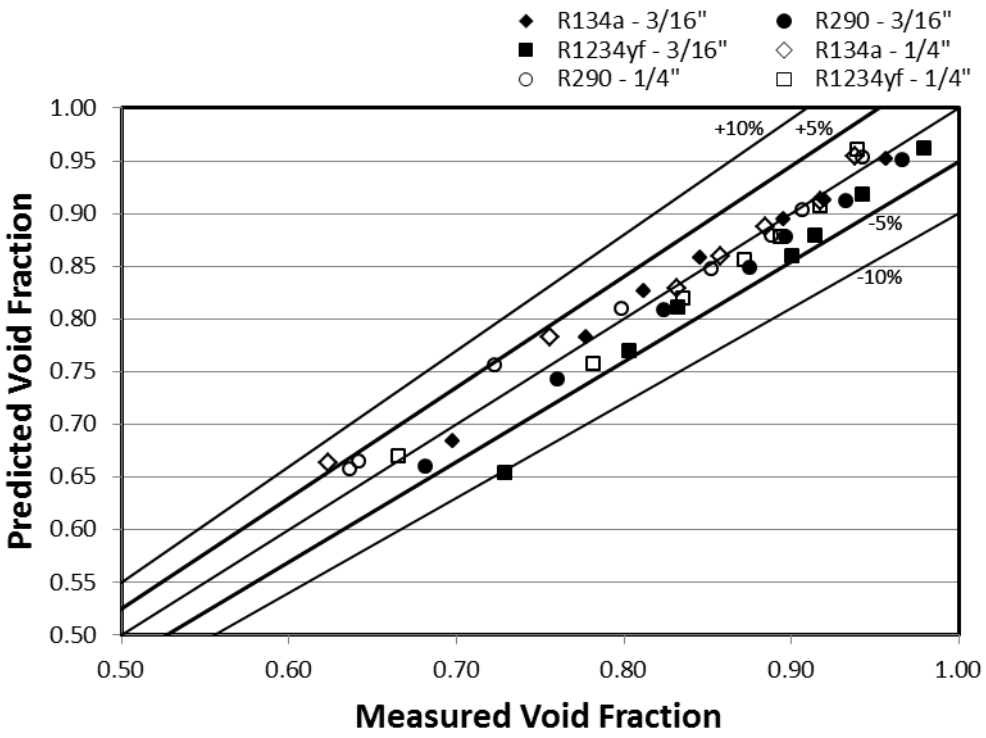

Figure 30: Performance of the Steiner void fraction correlation

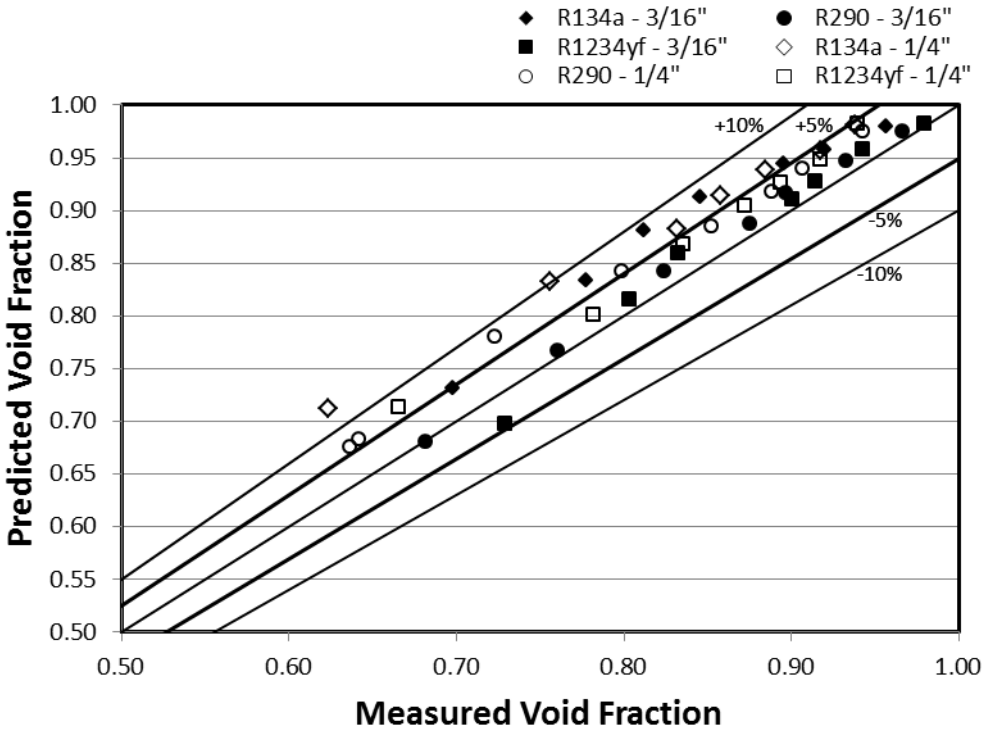

Figure 31: Performance of the Smith void fraction correlation

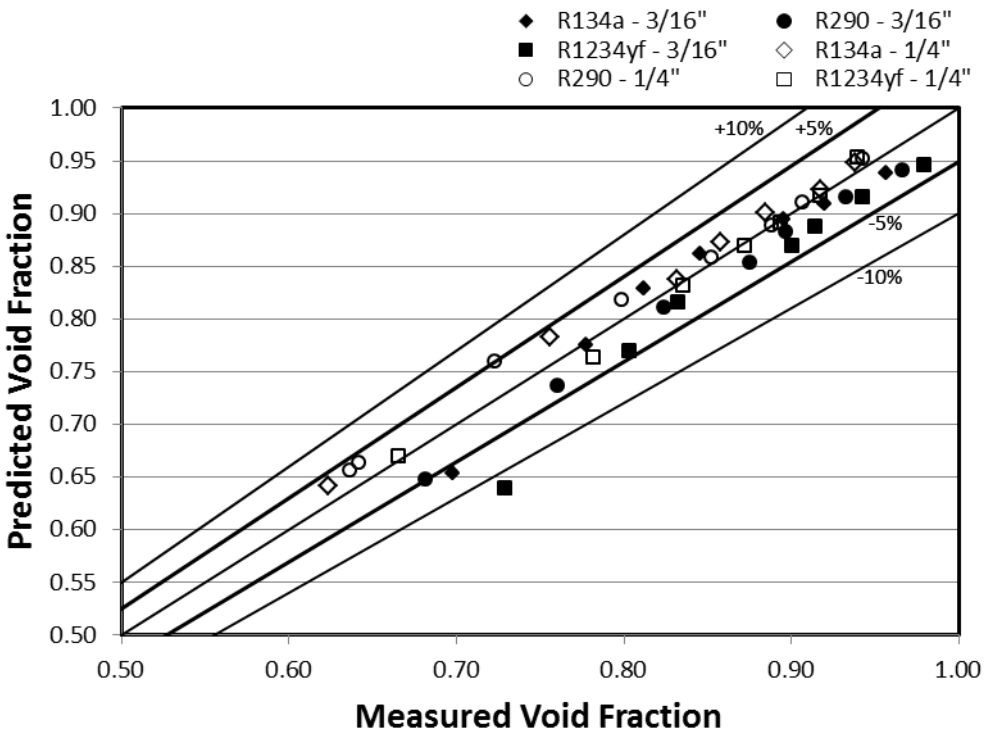

Figure 32: Performance of the Tandon void fraction correlation

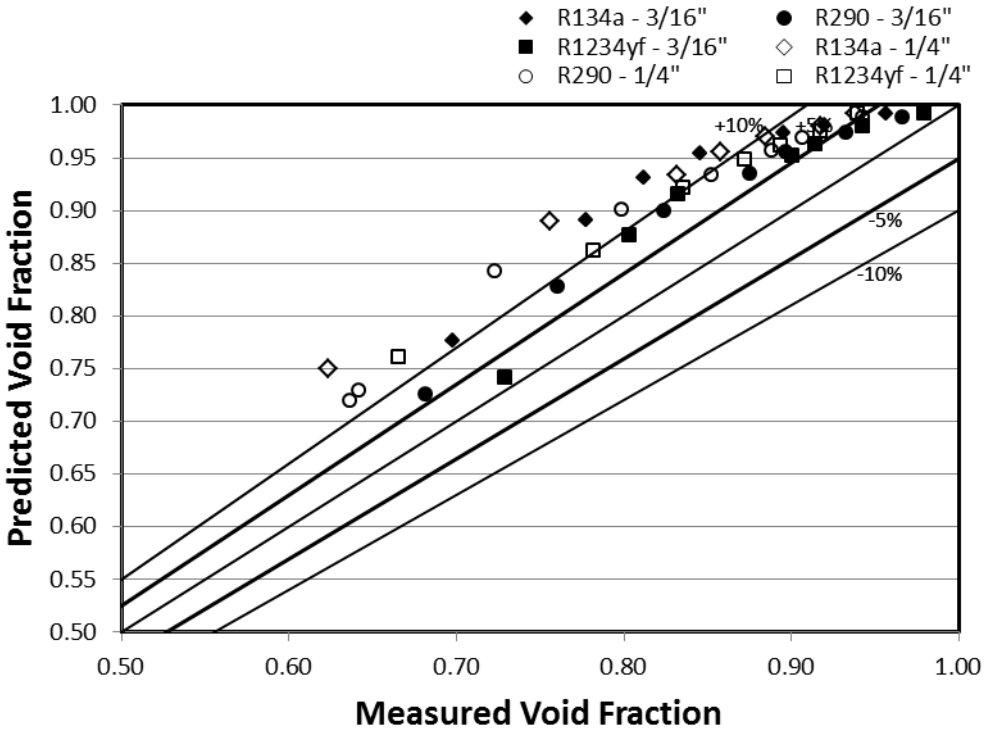

Figure 33: Performance of the Thom void fraction correlation

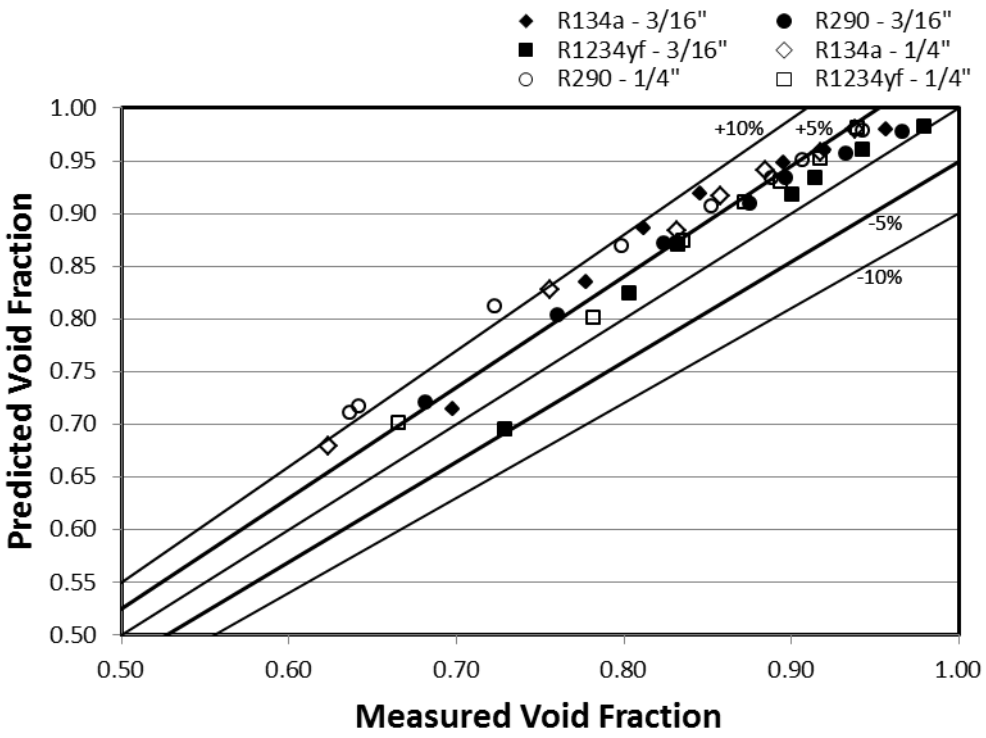

Figure 34: Performance of the Yashar void fraction correlation

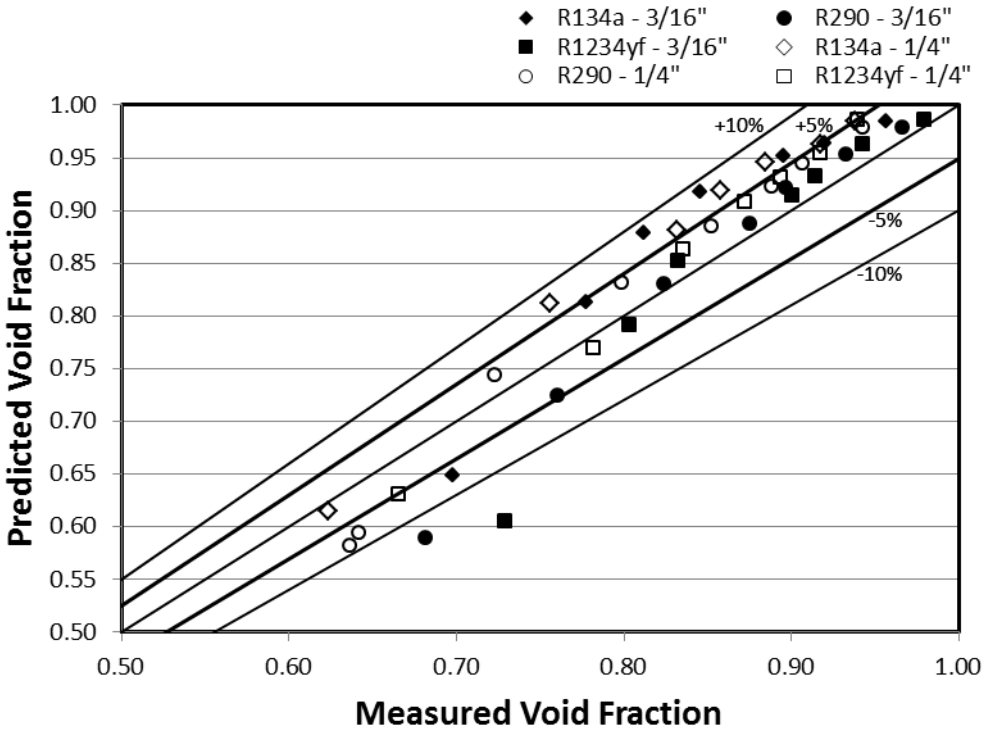

Figure 35: Performance of the Zivi void fraction correlation

5.3.1: Correlation Predictions for all Refrigerants and Diameters

From the above figures it is possible to determine, by visual inspection, how accurately the correlations are able to predict the void fraction. In all the above charts, the two lines furthest from the center indicate a 10% error in the prediction. The two lines nearest to the center indicate a 5% error in the prediction, and the center line indicates an exact prediction. Plots with only one refrigerant per chart are included in Appendices B, C, and D. For a more quantitative statistical analysis, the absolute mean deviation for all data points was calculated as:

$$e_a = \frac{1}{N} * \sum \left| \alpha_{exp} - \alpha_{pred} \right| \tag{39}$$

Table 12 lists the statistical performance for all twelve correlations considering all 42 data points. The table lists the absolute mean deviation as well as the percentage of the points which were predicted to within a 10% and 5% error.

Table 12: Statistical Performance of Void Fraction Correlations

VF Model	*Mean Deviation*	*% of pts within 10%*	*% of pts within 5%*
Baroczy	0.021	97.62%	83.33%
Harms-Groll	0.021	95.24%	92.86%
Homogenous	0.110	40.48%	9.52%
Lockhart-Martinelli	0.034	88.10%	69.05%
Premoli	0.024	97.62%	85.71%
Rigot	0.072	66.67%	19.05%
Steiner	0.018	97.62%	95.24%
Smith	0.034	95.24%	69.05%
Tandon	0.018	97.62%	90.48%
Thom	0.072	66.67%	16.67%
Yashar	0.042	95.24%	57.14%
Zivi	0.037	95.24%	69.05%

From the above table, the Steiner and Tandon correlations had the lowest mean deviation. The Steiner and Harms-Groll correlations were able to predict the highest percentage of the data points to within 5% accuracy. Overall, the Steiner correlation was able to predict the highest percentage of points to within 5% accuracy with the lowest mean deviation.

5.3.2: Correlation Predictions by Diameter

Table 13 lists the performance for all twelve correlations by tube diameter.

Table 13: Statistical Performance of Correlations Separated by Tube Diameter

VF Model	3/16" OD			1/4" OD		
	e_a	< 10%	< 5%	e_a	<10%	< 5%
Baroczy	0.023	95%	76%	0.019	100%	90%
Harms-Groll	0.025	90%	86%	0.017	100%	100%
Homogenous	0.099	43%	19%	0.122	38%	0%
Lockhart-Martinelli	0.024	100%	76%	0.044	76%	62%
Premoli	0.033	95%	76%	0.015	100%	95%
Rigot	0.060	81%	33%	0.083	52%	5%
Steiner	0.021	95%	95%	0.014	100%	95%
Smith	0.025	100%	81%	0.044	90%	57%
Tandon	0.025	95%	86%	0.011	100%	95%
Thom	0.061	81%	29%	0.083	52%	5%
Yashar	0.034	100%	67%	0.049	90%	48%
Zivi	0.037	90%	71%	0.038	100%	67%

Considering the data for the 1/4" OD test section, only the Harms-Groll correlation was able to predict all points to within 5% accuracy, though several predicted all data points to within 10%. Of these that predicted to within 10%, the Tandon correlation had the lowest mean deviation of 0.011 with a prediction percentage of 95%.

Predictions made for the 3/16" OD data were the least accurate of all data sets considered, with no one correlation able to predict all data points to within 5% accuracy and only the Lockhart-Martinelli and Smith correlations able to predict to within 10%. This data set also had the highest mean deviation of all the data sets with the lowest being the Steiner correlation which predicted with a mean deviation of 0.21, compared to the lowest mean of 0.18 when all data points are considered.

As effects due to viscous dissipation increase with decreasing tube diameter, it is apparent that the correlations developed for larger diameter applications begin to skew for lower diameters as they do not put sufficient weight on the viscous effects.

5.3.3: Correlation Predictions by Refrigerant

Table 14 lists the statistical performance for all twelve correlations, separated by refrigerant.

Table 14: Statistical Performance of Correlations Separated by Refrigerant

VF Model	R134a			R290			R1234yf		
	e_a	< 10%	< 5%	e_a	<10%	< 5%	e_a	< 10%	< 5%
Baroczy	0.031	100%	100%	0.015	100%	93%	0.017	100%	93%
Harms-Groll	0.021	100%	93%	0.018	100%	93%	0.024	93%	93%
Homogenous	0.126	36%	7%	0.108	50%	7%	0.097	50%	14%
Lockhart-Martinelli	0.047	93%	64%	0.033	100%	79%	0.022	100%	93%
Premoli	0.015	100%	100%	0.025	100%	100%	0.032	100%	86%
Rigot	0.095	50%	7%	0.061	93%	29%	0.059	100%	29%
Steiner	0.011	100%	100%	0.017	100%	100%	0.026	100%	93%
Smith	0.053	100%	43%	0.025	100%	93%	0.025	100%	100%
Tandon	0.015	100%	100%	0.018	100%	100%	0.022	100%	93%
Thom	0.089	57%	7%	0.067	86%	29%	0.059	100%	29%
Yashar	0.051	100%	36%	0.046	100%	71%	0.028	100%	100%
Zivi	0.048	100%	50%	0.032	100%	93%	0.032	93%	93%

For R134a, the Premoli, Steiner, and Tandon correlations were able to accurately predict the void fraction to within 5% for all points, also with the lowest mean deviation of all twelve correlations. This indicates that these three correlations exhibit a large number of points grouped at the centerline of the plots above.

For R290, Premoli, Steiner, and Tandon are again able to predict all points to within 5% accuracy. Of those three, the Steiner and Tandon correlations have the lowest mean deviation. Though, the lowest mean deviation for R290 is significantly higher R134a, indicating that, though the points are generally centered around the no-error line, there is more scattering of the points, especially for the lower quality measurements.

For both these fluids, the void fraction is predicted most accurately by mass-flux dependent, semi-empirically developed correlations. Because semi-empirical correlations are developed using analytical models, they tend to have a greater applicability than purely empirical models, which tend to only be accurate for the data for which they were developed. Also, because semi-empirical models are closed using empirical data, they have an advantage over purely analytical models due to the fact that most of these mathematically based models can't account for all the intricacies of fluid flow and have inherent errors due to simplifying assumptions. Thus, they need empirical factors to "fit" the correlation to real world data.

In contrast to R290 and R134a, the correlation with the lowest mean deviation for R1234yf is the Baroczy correlation, one of the X_{tt} correlated models considered in the investigation. The Baroczy correlation has significantly more scattering than

other correlations, but is more centered along the 0% error line. The correlation is able to predict 93% of the data points to within 5% accuracy.

It should be noted that, in contrast to R134a and R290, R1234yf is most accurately predicted by an X_{tt} correlated model. This is possibly due to viscous dissipation being more dominant with R1234yf for these conditions, as evidenced by Figure 19. This would make the X_{tt} parameter a more reliable predictor of the void fraction for this refrigerant. Another explanation for the difference in performance between R1234yf and the other two refrigerants is that the semi-empirically derived correlations that most accurately predict the void fraction for R134a and R290 did not perform as well for R1234yf because it is a novel fluid. As semi-empirical equations have a component that is fit to existing data, and because data for R134a and R290 has been in literature for decades, these correlations were developed for these fluids. R1234yf, in contrast, is a newer refrigerant. Fluid data is not yet readily available. Thus, the empirical coefficients of these correlations do not account for R1234yf. So, it would be expected that the most accurate correlation for R1234yf would be less accurate than that of R134a or R290.

5.3.4: Correlation Performance and Charge Prediction

In summary, the Steiner correlation would be recommended for general use at the conditions tested. When considering data by refrigerant, for the refrigerants R134a and R290, the Steiner correlation was also best able to predict the void fraction. In contrast, for R1234yf the Baroczy correlation best predicted the data. Figure 36, Figure 37, Figure 38 plot R134a, R290, and R1234yf with their best performing correlation, respectively, in the ¼" test section.

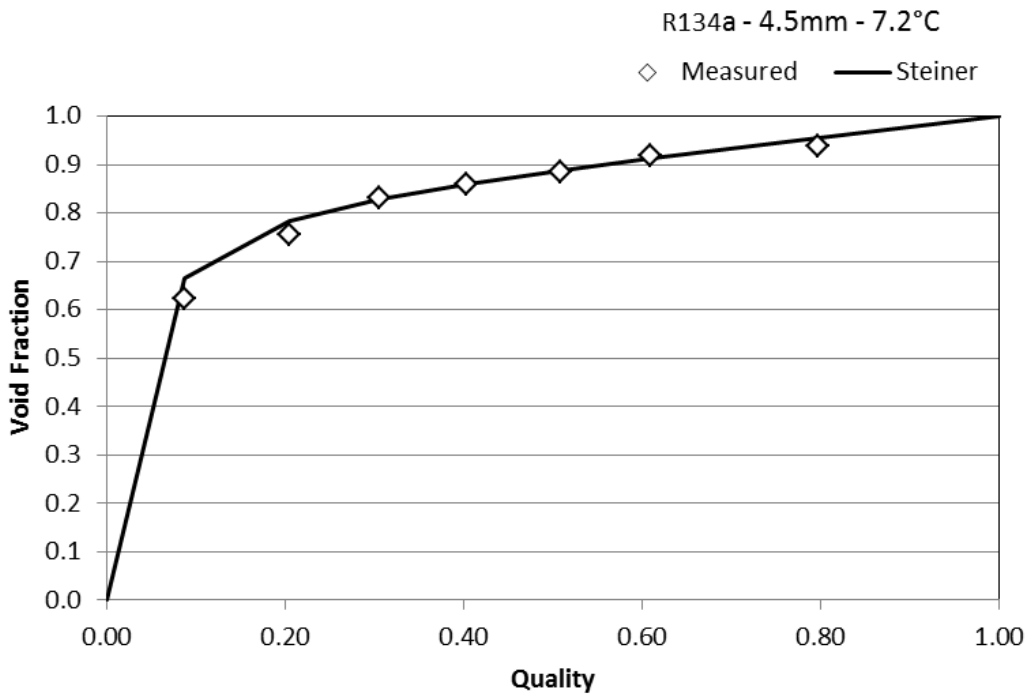

Figure 36: Performance of R134a plotted with the Steiner correlation

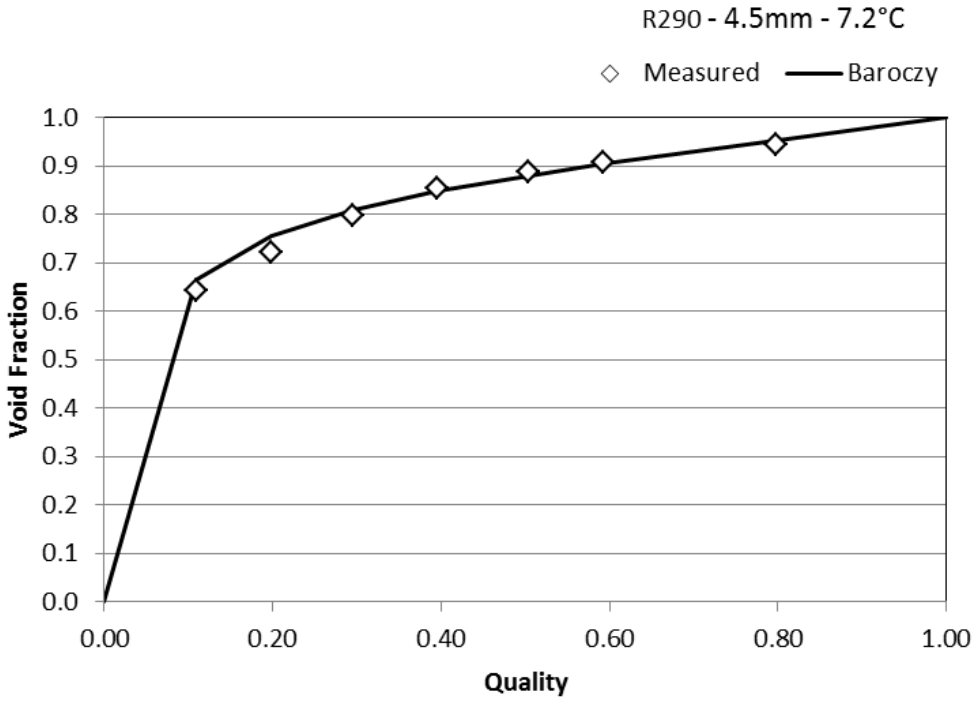

Figure 37: Performance of R290 plotted with the Steiner correlation

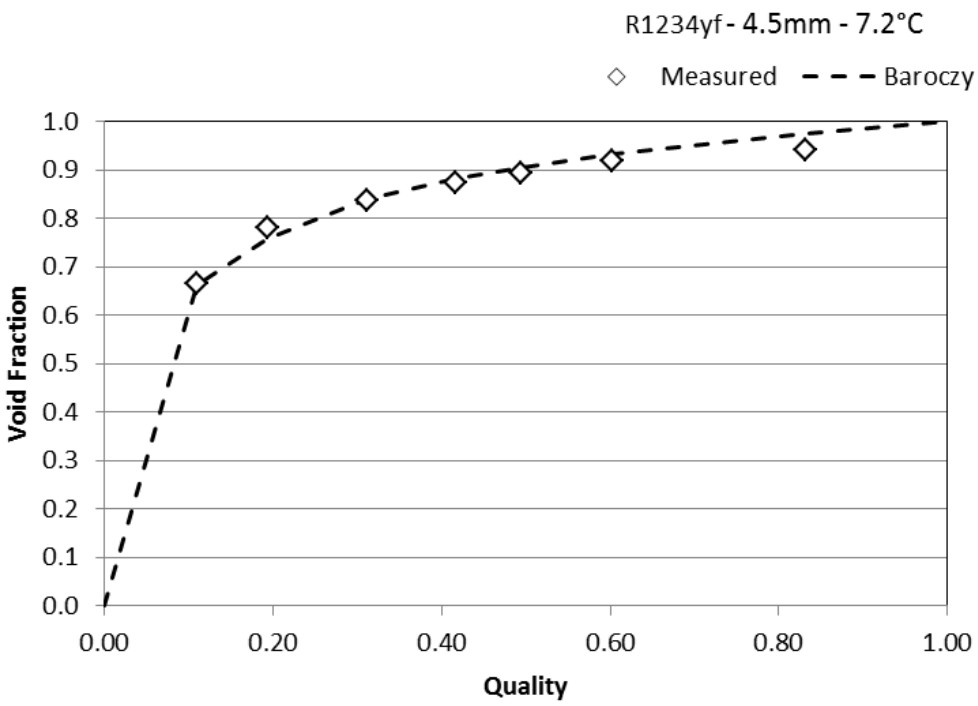

Figure 38: Performance of R1234yf plotted with the Baroczy correlation

From the above plots, general agreement with the data is achieve with each correlation. From Figure 38, it is obvious that R1234yf is the least accurately predicted for reasons discussed above. However, the increased accuracy at the lower qualities due to the higher void fraction measurements offsets the error at the higher quality points.

Since the primary utilization of the void fraction is in charge inventory prediction. It would be interesting to use these recommended correlations to predict a required refrigerant charge relative to R134a for each of the two low GWP refrigerants. As discussed previously, charge minimization is especially important when designing with flammable refrigerants as safety standards limit their use in most applications.

A simple simulation using (6) for evaporating refrigerant was performed in Excel to determine the required charge in an evaporating tube similar in dimension to the ¼" test section in the current investigation. It should be noted from the equation that the total mass can be calculated as $m_{tot} = V_{tot} * \rho_{avg}$ Figure 39 illustrates the simulated test section with the input variables noted.

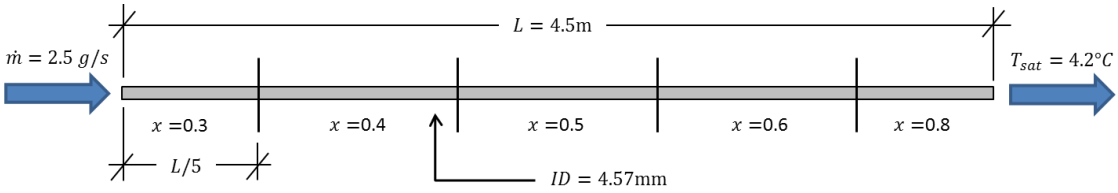

Figure 39: Illustration of charge prediction model

Table 15 lists the results of the charge prediction exercise for each refrigerant calculated by its best predicting correlation. The percent difference in required charge for R290 and R1234yf relative to R134a has also been calculated

Table 15: Results of Charge Prediction Exercise

Refrigerant	R134a	R290	R1234yf
Required Charge	13.12 g	6.04 g	12.40 g
% Change	--	-54.01%	-5.54%

For each of the low GWP refrigerants, a reduction in required charge is observed. Considering the restrictions placed on the utilization of flammable refrigerants, a reduction in charge for both refrigerants makes them more viable candidates for use in future appliance design. For R290, the required charge is greatly reduced relative to R134a due to the much lower liquid density of propane at the modeled condition. R1234yf, which has a similar liquid density compared to R134a, has only a 5.54% reduction in required charge.

Finally, as noted previously, utilizing an accurate void fraction correlation is important in system design. Table 16 is the result of the simulation described above calculated using both the Baroczy and Steiner correlations for 1234yf.

Table 16: Charge Prediction for 1234yf for Two Correlations

Baroczy	Steiner	% Change
12.40 g	12.91 g	3.97%

Simply by utilizing a different void fraction correlation, the predicted charge increased by 0.51 g, or 3.97%. Though this may seem a negligible amount, extrapolation of this difference to the volume of a vapor compression system could yield significant differences in charge prediction, affecting both the performance of the system and the overall environmental impact.

Chapter 6: Conclusions

A test facility was constructed to evaluate the volumetric void fraction for two low GWP refrigerants and R134a. Experimental tests were performed at low mass fluxes and with a saturation temperature of 7.2°C. The facility is a pumped loop designed to deliver pure, steady state refrigerant at a constant mass flux, quality, and saturation temperature to a test section of approximately 4.5 meters in length. Two test sections with outer diameters of 1/4" and 3/16", corresponding to inner diameters of 4.56 mm and 2.99 mm, respectively, were tested. The void fraction was measured using a QCV, mass expansion method developed by [7]. An uncertainty analysis of the void fraction measurement was performed and it was found that the systematic error in the measurement ranged from 0.3% to 0.9% depending on the tube diameter and flow condition.

Flow visualization was also performed in the 1/4" test section to determine flow regime and transition characteristics for each of the refrigerants. All three refrigerants exhibited the plug/slug/annular transition pattern typical of medium pressure refrigerants. It was found that R290 transitioned through the flow regimes faster than R134a, which transitioned faster than R1234yf. Using fluid properties and void fraction measurements made during the current investigation, the vapor velocity was determined for each of these data points and the transition rate was found to correlate with the vapor velocity.

There was no discernible difference in the void fraction trends of R134a and R290. However, R1234yf exhibited a higher void fraction than R134a for both test section diameters, with the difference being greater in the 3/16" test section. It was

postulated this trend was the result of increased viscous dissipation in the fluid as the ratio of vapor frictional pressure loss to liquid frictional pressure loss was higher than that of R134a, which would yield a higher void fraction.

The experimental void fraction measurements were compared to predictions of void fraction by twelve explicit correlations commonly cited in literature. Table 17 presents the recommended correlation for each refrigerant, and Table 18 presents the recommended correlation for each tube diameter. It should be noted that these recommendations are made based only on the correlations investigated.

Table 17: Correlation Recommendation by Refrigerant

Refrigerant	Correlation Recommendation
R134a	**Steiner, Tandon**
R290	**Steiner, Tandon**
R1234yf	**Baroczy**

Table 18: Correlation Recommendation by Tube Diameter

Tube OD	Correlation Recommendation
1/4"	**Harms-Groll, Tandon**
3/16”	**Steiner**

When considering all data points, the Steiner correlation predicted more points to within 5% accuracy with the lowest absolute mean deviation.

When considering data by test section diameter, the Harms-Groll correlation predicted all points with the 1/4” test section data to within 5% while the Tandon correlation had the lowest mean deviation. For the 3/16” test section, no correlation predicted all data points to within 5% and all correlations had a relatively poor mean deviation, indicating that the increased viscous dissipation of the small diameter tube

was not properly accounted for in the investigated correlations. Of all twelve correlations, the Steiner correlation performed the best for the 3/16" tube.

When considering data by refrigerant, the Steiner, and Tandon correlations most accurately predicted the void fraction for R134a and R290, also with the lowest mean deviation. The common characteristic of these correlations is that they were developed using semi-empirical methods. In contrast to the other two fluids, the most accurate prediction of void fraction for R1234yf was made by the Baroczy correlation. It was postulated that, as viscous forces seem to be more dominant for this refrigerant, an X_{tt} correlated model would more accurately predict the void fraction over other models, as the X_{tt} parameter is a measure of frictional pressure loss.

Finally, a simple charge inventory prediction was performed for each of the three refrigerants using their respective correlation. The volume modeled was similar to the ¼" test section utilized in the current investigation. A reduction in required charge relative to R134a was found for both the low GWP refrigerants, with the reduction for R290 found to be large due to the lower liquid density at the tested conditions. The implications of using different void fraction models was then investigated using the same model. By predicting the void fraction for R1234yf using the Steiner correlation, a 4% increase in predicted charge was observed relative to the charge predicted by the Baroczy correlation.

Chapter 7: Future Work

The breadth of the data set collected in the current investigation is admittedly limited, with conclusions made applicable only to the small range of conditions tested. Before any universal conclusions can be made regarding void fraction trends for either of these low GWP refrigerants, an expanded test matrix should be developed and tested considering a wider range of mass fluxes, capacities, and channel geometries.

Beyond expanding the test matrix, there exist other low GWP alternatives to R134a for which publically available fluid property data is limited. The current investigation considered only R290 and R1234yf, as they simple replacements. Though, because of their flammability, implementation as a standard refrigerant is likely a few years away. However, mixtures of R134a and R1234yf have been demonstrated to exhibit environmental friendly characteristics with a greatly reduced flammability. Further investigation of these mixtures, as well as other refrigerants, should be pursued.

Even beyond void fraction measurement, frictional pressure loss and the convective heat transfer coefficient are equally important fluid characteristics which will need investigation before comprehensive modeling of systems utilizing these fluids can be realized and could be pursued using the current system.

Finally, it was noted that the void fraction for R1234yf trended above the other two refrigerants considered in this investigation; and of the three refrigerants tested, R1234yf was most poorly predicted. Development of an improved correlation for this novel refrigerant should be considered in future studies.

Appendix A: Tabulated Void Fraction Data

Table 19: Tabulated Data for R134a

Refrigerant	Tube ID	Quality	T_{sat} [°C]	G [kg/m^{2}s]	Void Fraction
R134a	2.99 mm	0.10	7.25	149.32	0.6987
		0.21	7.52	148.12	0.7783
		0.30	7.43	149.62	0.8128
		0.40	7.25	149.37	0.8465
		0.54	7.08	148.56	0.8964
		0.62	7.55	148.69	0.9205
		0.79	7.34	148.12	0.9575
	4.56 mm	0.09	7.22	152.60	0.6233
		0.21	7.44	152.86	0.7557
		0.30	7.00	152.98	0.8319
		0.40	7.08	151.17	0.8580
		0.51	7.13	152.97	0.8845
		0.61	7.34	152.96	0.9172
		0.80	7.06	153.19	0.9383

Table 20: Tabulated Data for R290

Refrigerant	Tube ID	Quality	T_{sat} [°C]	G [kg/m^{2}s]	Void Fraction
R290	2.99 mm	0.11	7.13	145.55	0.6815
		0.18	7.21	143.27	0.7606
		0.29	7.58	149.49	0.8243
		0.40	7.29	143.45	0.8753
		0.50	7.18	149.04	0.8966
		0.63	7.15	139.75	0.9325
		0.79	7.12	141.06	0.9662
	4.56 mm	0.11	7.13	150.71	0.6417
		0.20	7.44	152.58	0.7227
		0.29	7.47	151.24	0.7987
		0.40	7.69	152.46	0.8523
		0.50	7.41	153.24	0.8886
		0.59	7.19	152.72	0.9066
		0.80	7.38	152.32	0.9432

Table 21: Tabulated Data for R1234yf

Refrigerant	Tube ID	Quality	T_{sat} [°C]	G [kg/m^{2}s]	Void Fraction
R1234yf	2.99 mm	0.10	6.73	151.20	0.7295
		0.21	7.08	145.83	0.8034
		0.29	7.27	148.28	0.8328
		0.44	7.58	142.17	0.9005
		0.50	7.46	147.92	0.9144
		0.65	7.02	147.72	0.9429
		0.84	7.40	149.05	0.9797
	4.56 mm	0.11	7.18	151.40	0.6655
		0.19	7.21	152.77	0.7818
		0.31	7.04	152.66	0.8359
		0.42	7.58	152.78	0.8721
		0.49	7.19	152.12	0.8939
		0.60	7.05	153.20	0.9172
		0.83	7.41	152.62	0.9396

Appendix B: Correlation Performance – R134a

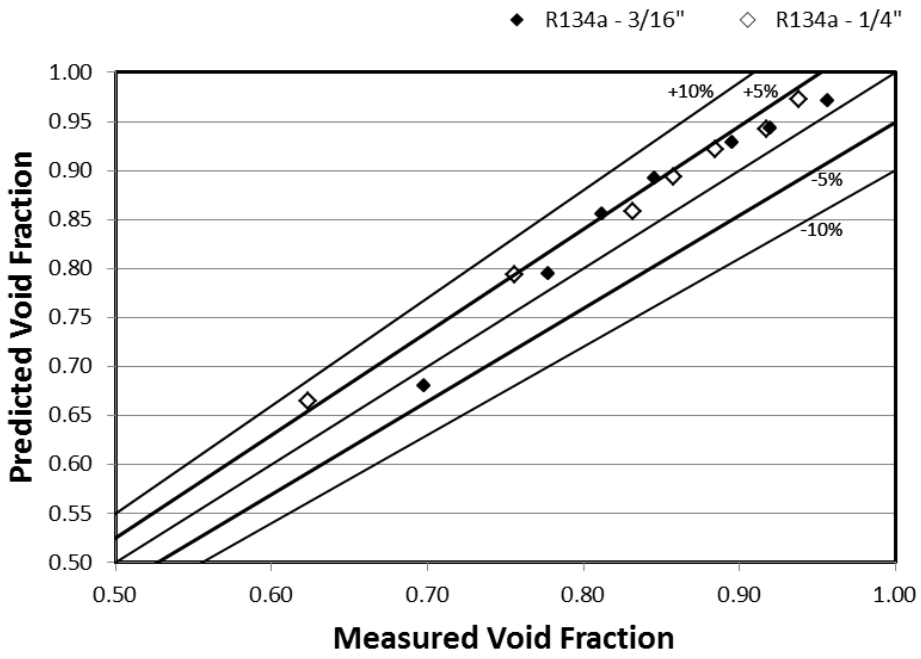

Figure 40: Performance of the Baroczy correlation – R134a

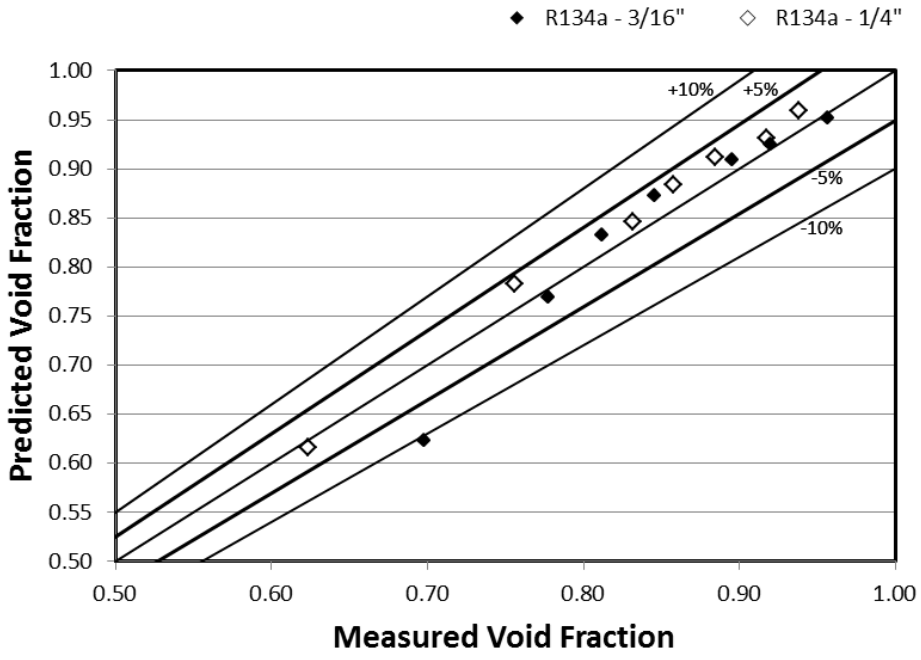

Figure 41: Performance of the Harms-Groll correlation – R134a

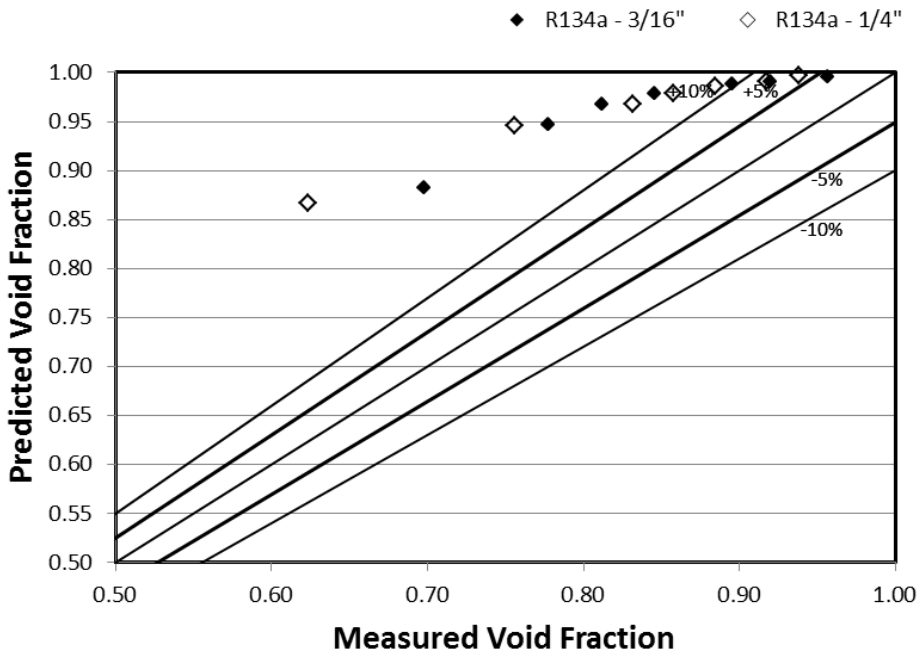

Figure 42: Performance of the Homogenous correlation – R134a

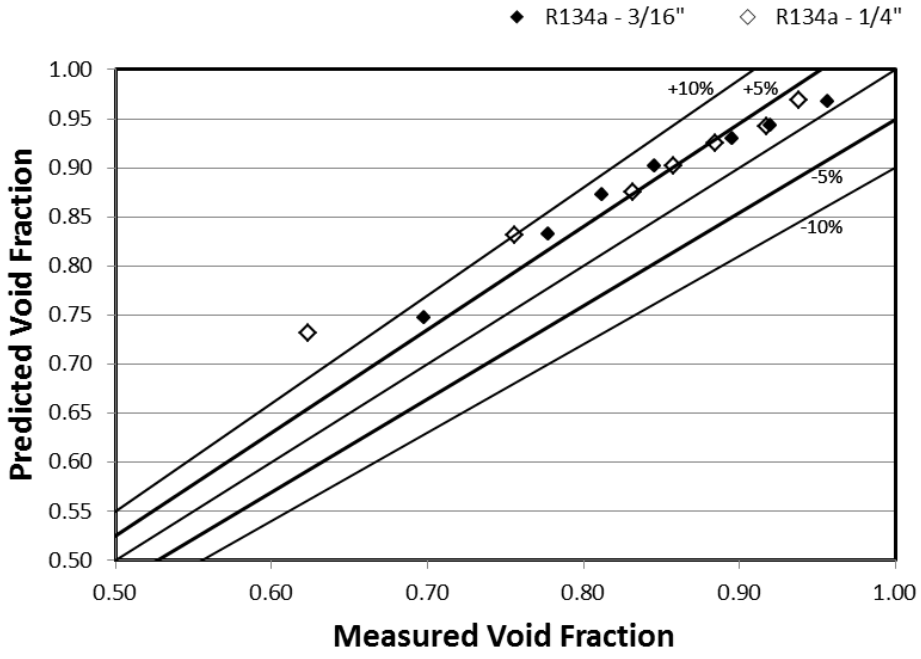

Figure 43: Performance of the Lockhart-Martinelli correlation – R134a

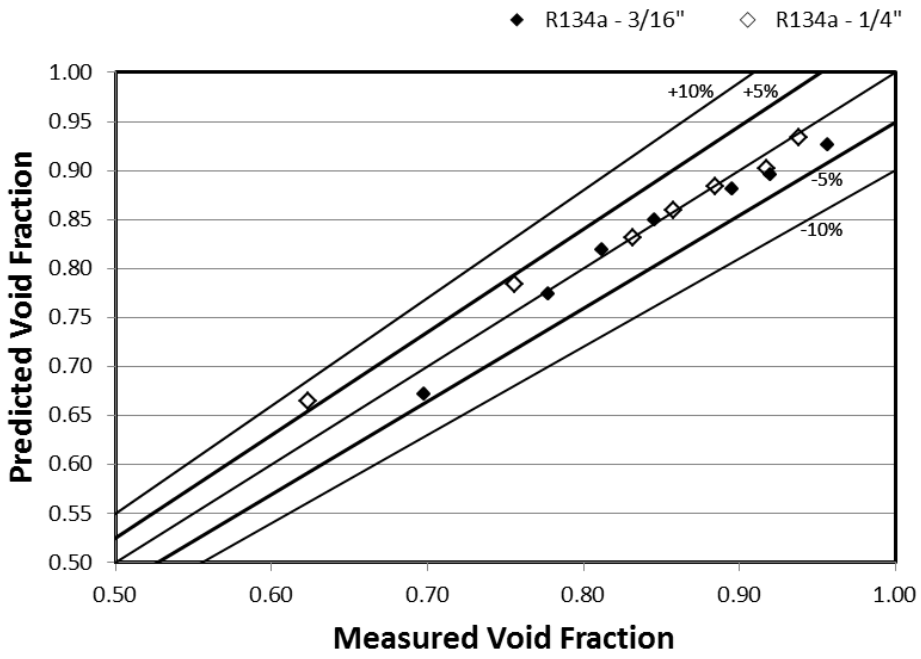

Figure 44: Performance of the Premoli correlation – R134a

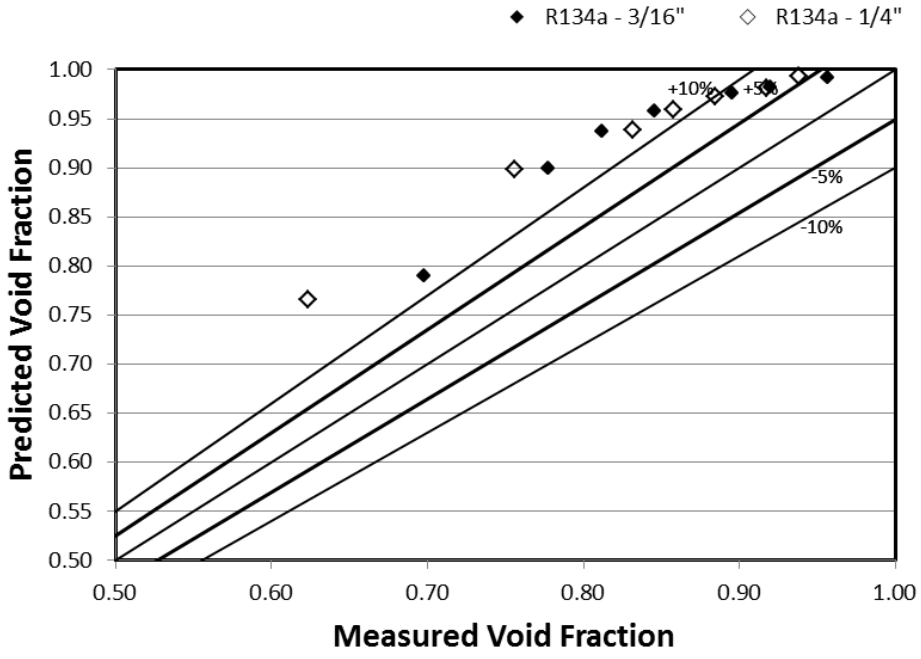

Figure 45: Performance of the Rigot correlation – R134a

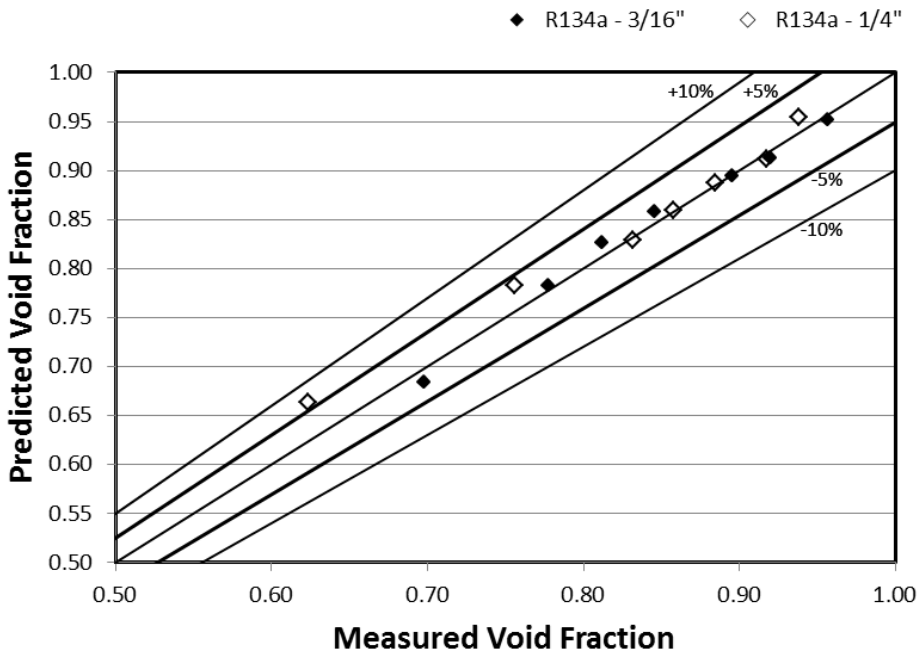

Figure 46: Performance of the Steiner correlation – R134a

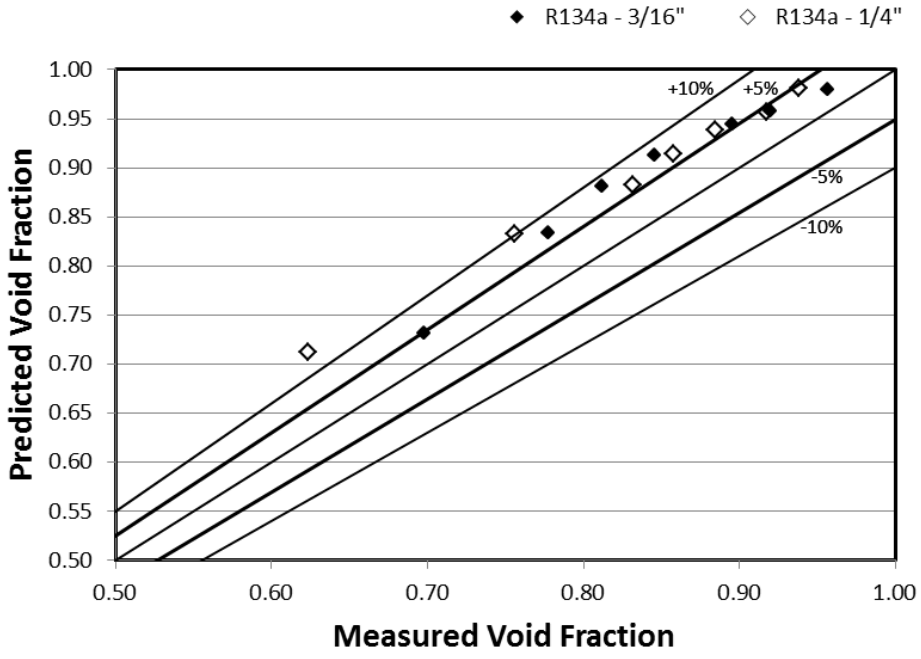

Figure 47: Performance of the Smith correlation – R134a

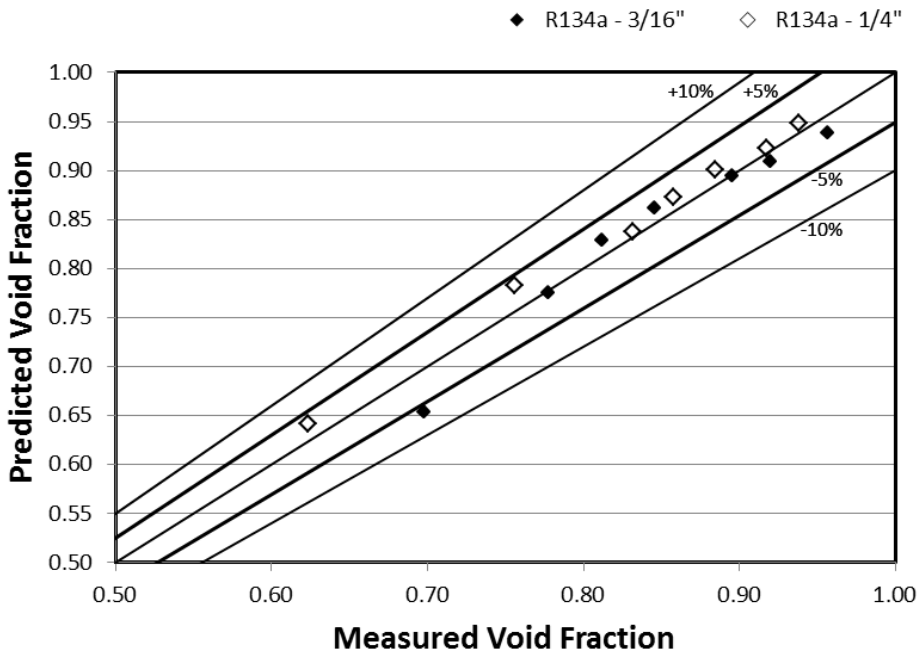

Figure 48: Performance of the Tandon correlation – R134a

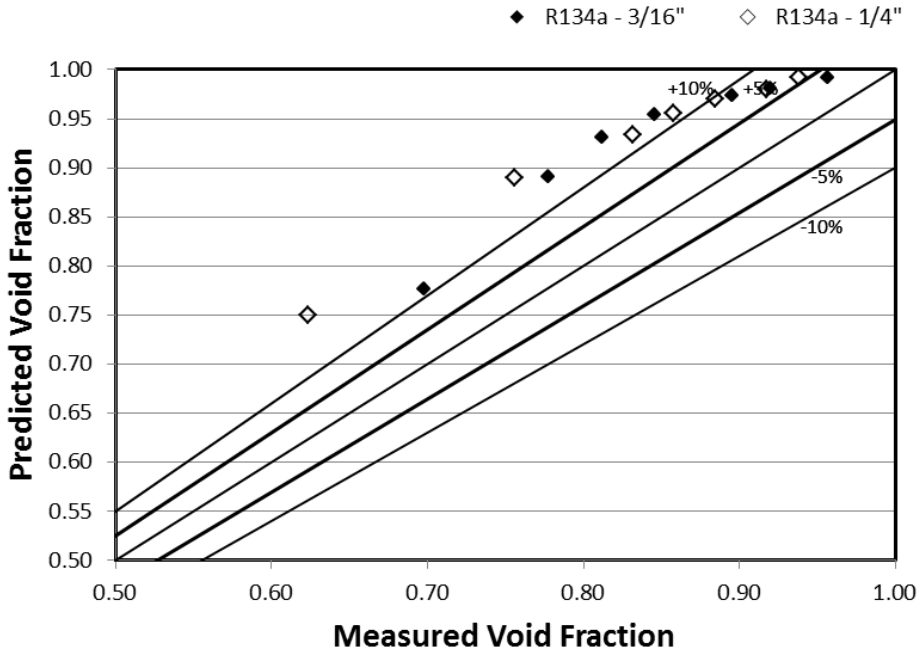

Figure 49: Performance of the Ahrens/Thom correlation – R134a

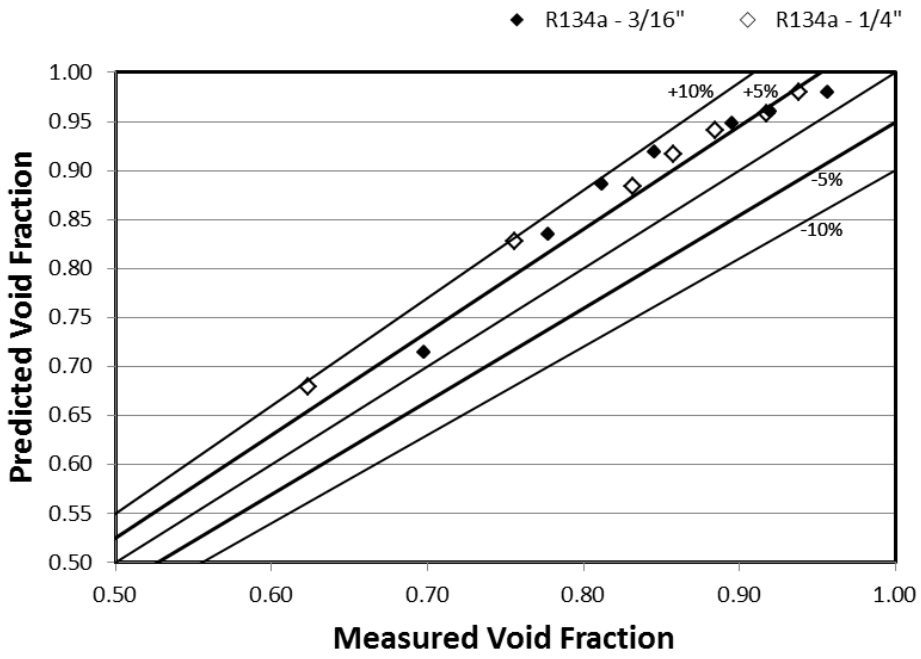

Figure 50: Performance of the Yashar correlation – R134a

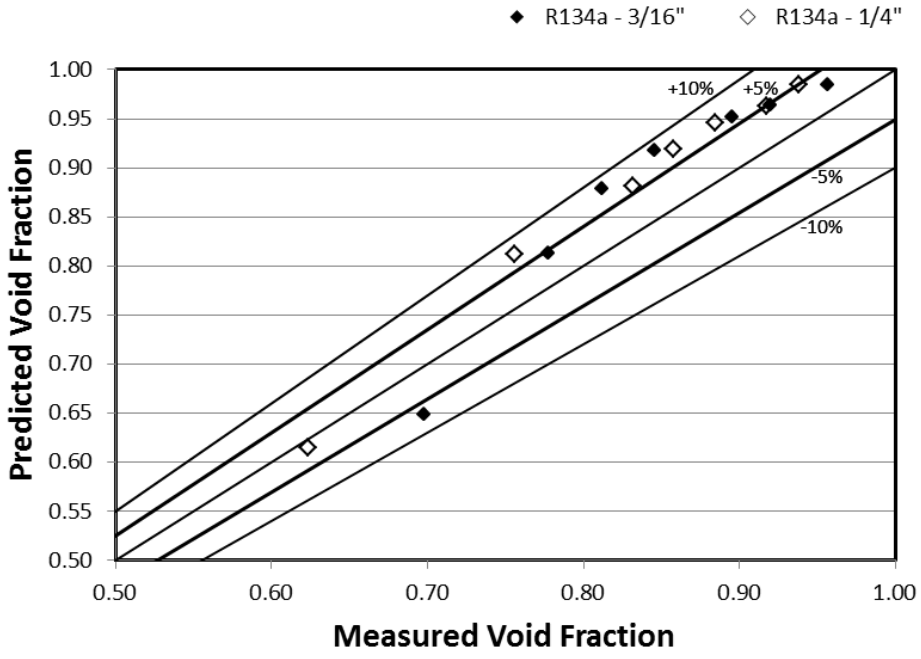

Figure 51: Performance of the Zivi correlation – R134a

Appendix C: Correlation Performance – R290

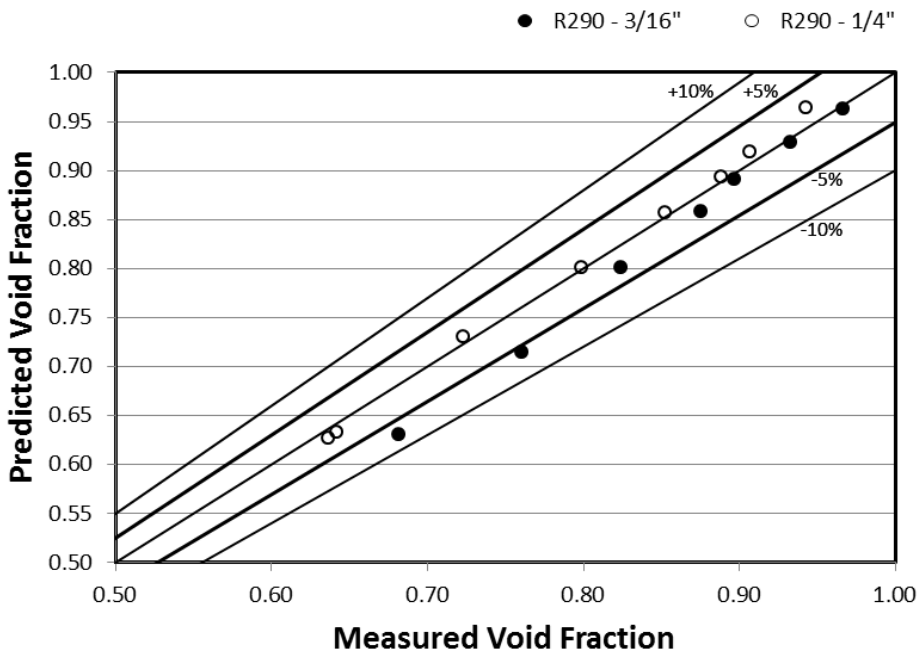

Figure 52: Performance of the Baroczy correlation – R290

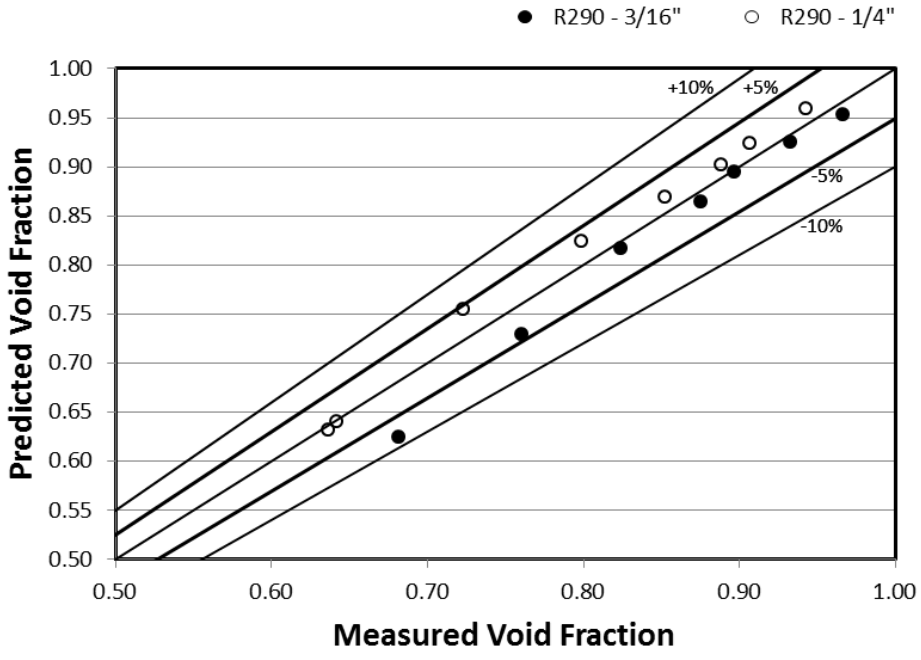

Figure 53: Performance of the Harms-Groll correlation – R290

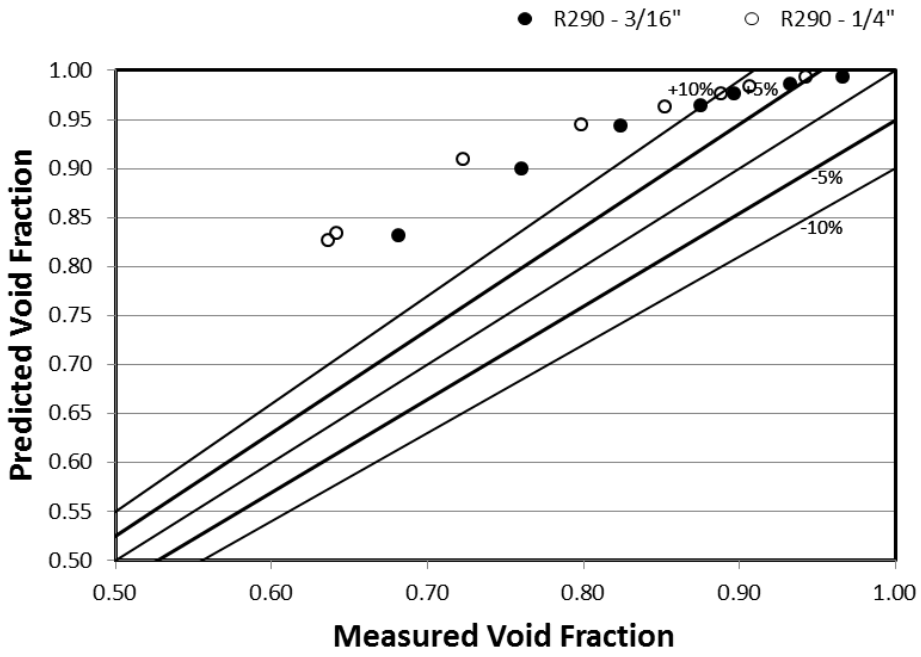

Figure 54: Performance of the Homogenous correlation – R290

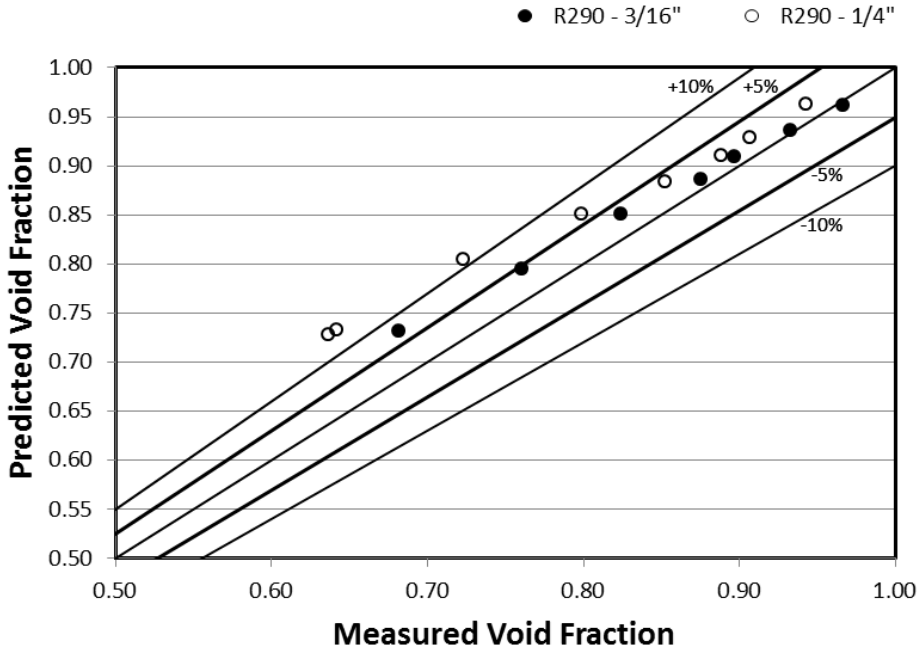

Figure 55: Performance of the Lockhart-Martinelli correlation – R290

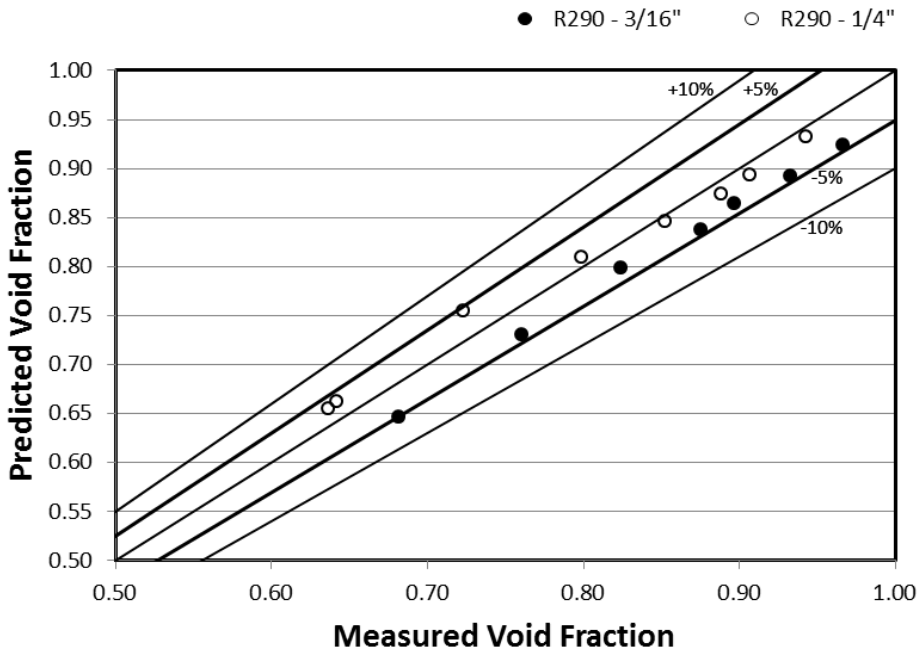

Figure 56: Performance of the Premoli correlation – R290

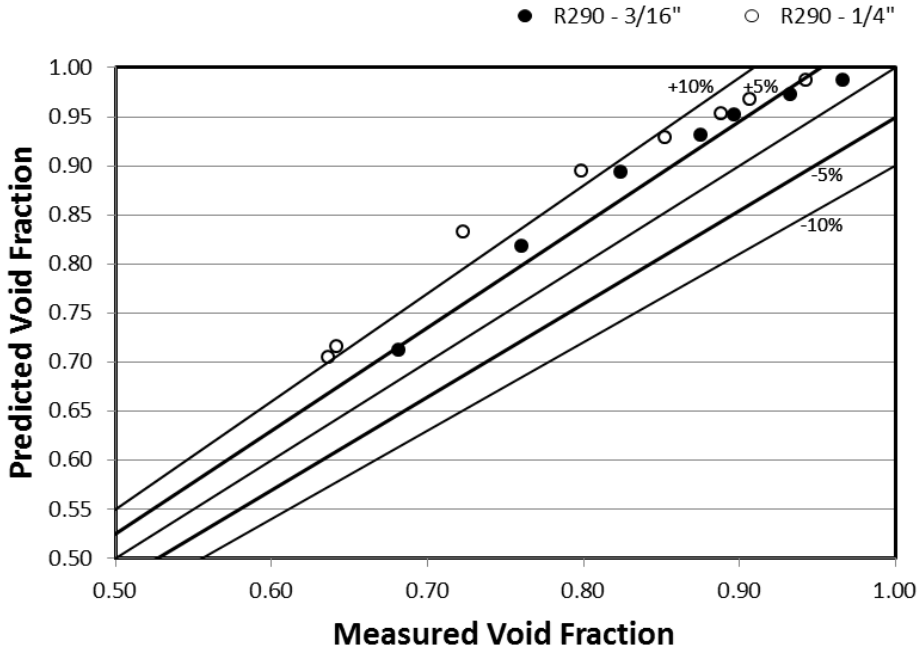

Figure 57: Performance of the Rigot correlation – R290

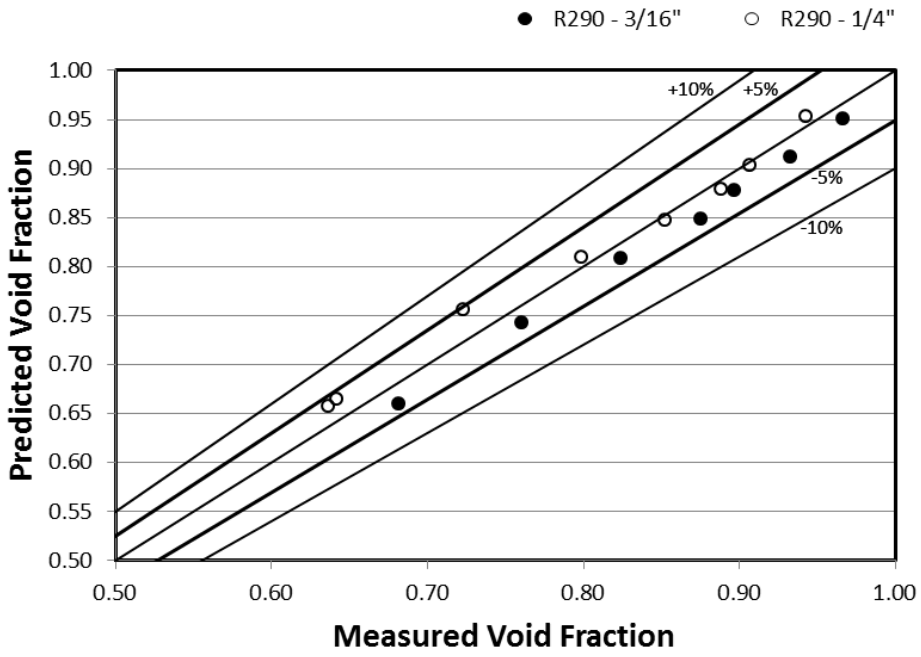

Figure 58: Performance of the Steiner correlation – R290

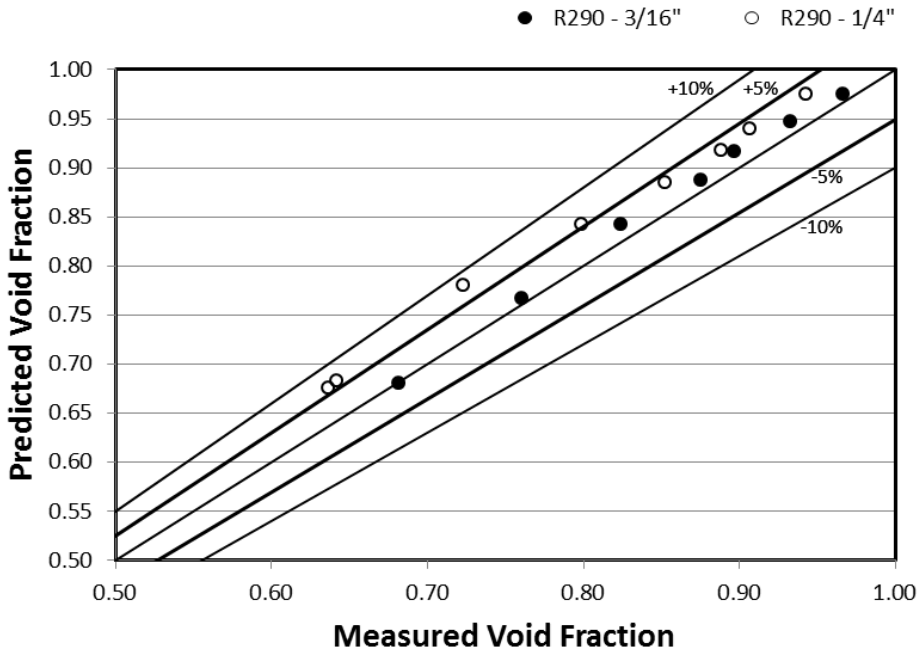

Figure 59: Performance of the Smith correlation – R290

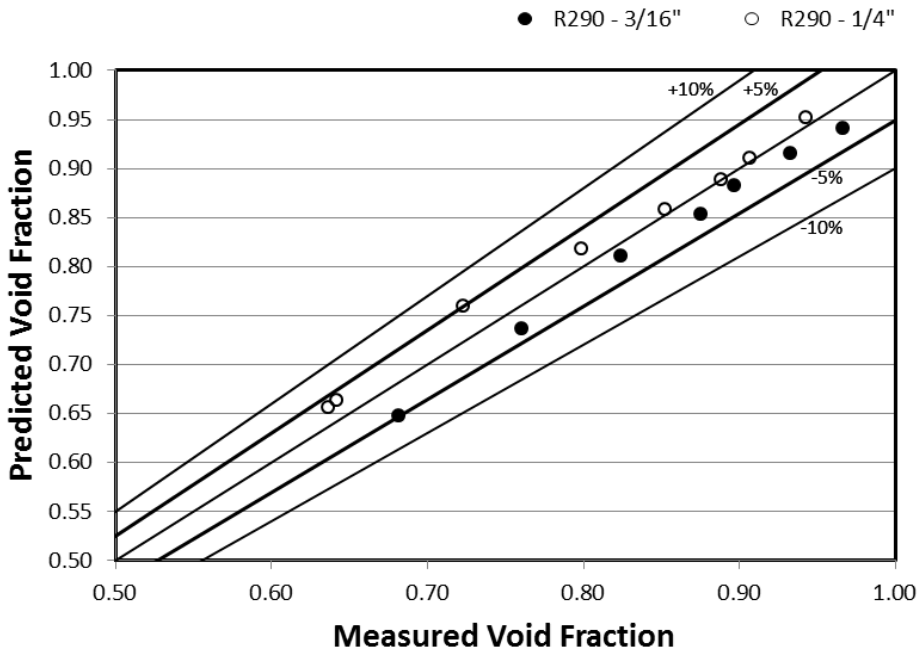

Figure 60: Performance of the Tandon correlation – R290

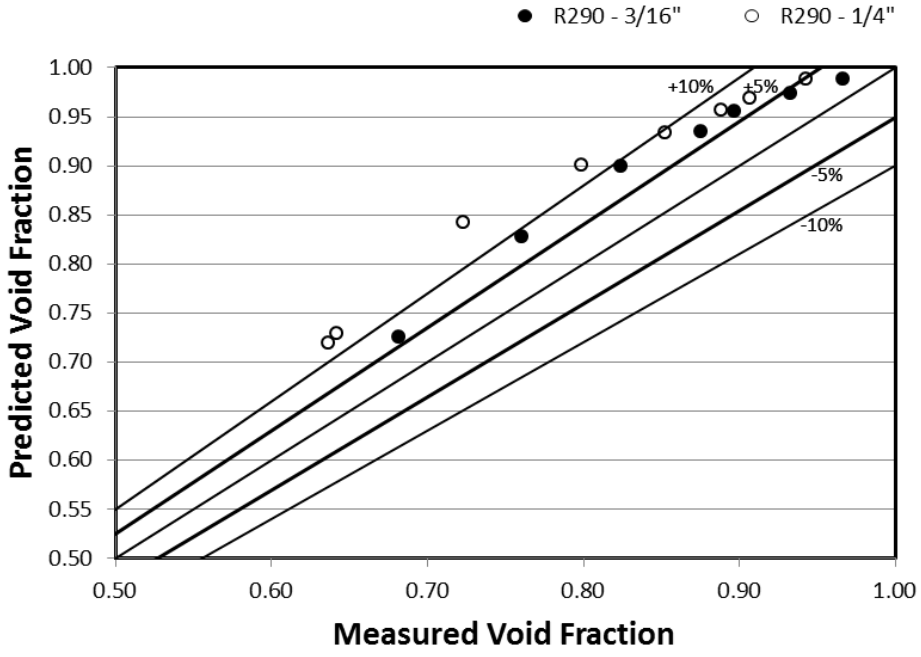

Figure 61: Performance of the Thom correlation – R290

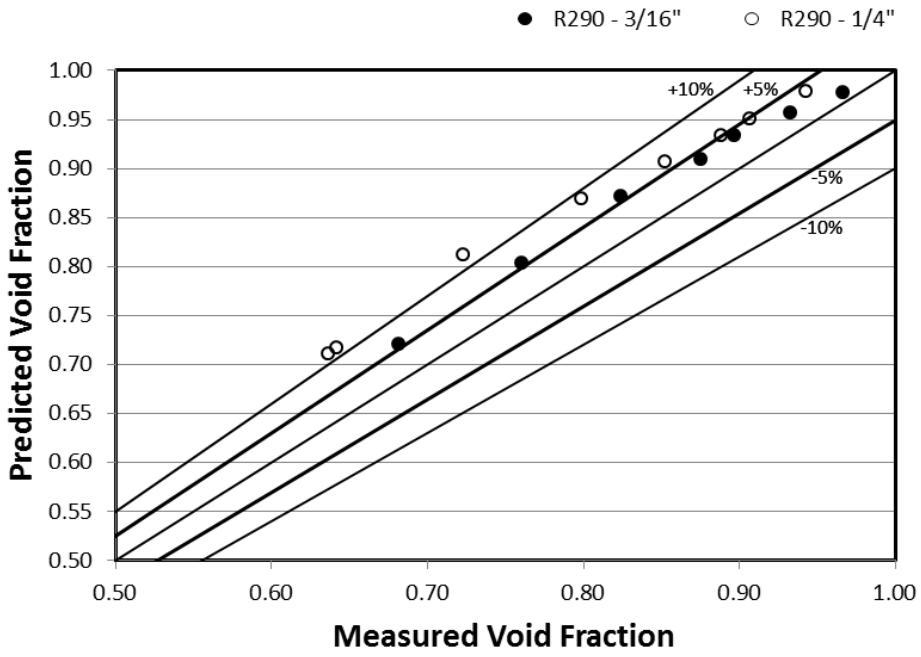

Figure 62: Performance of the Yashar correlation – R290

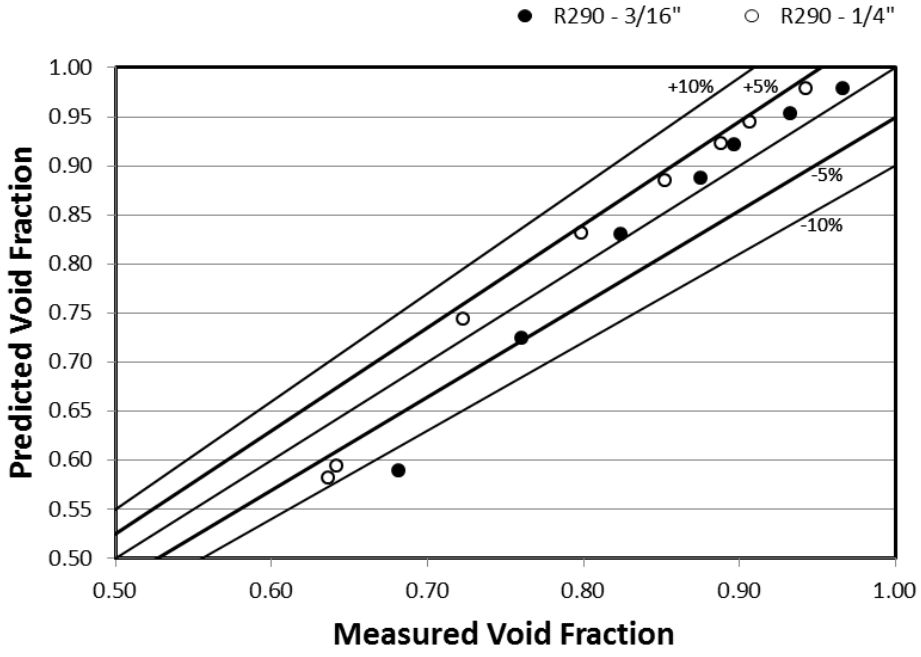

Figure 63: Performance of the Zivi correlation – R290

Appendix D: Correlation Performance – R1234yf

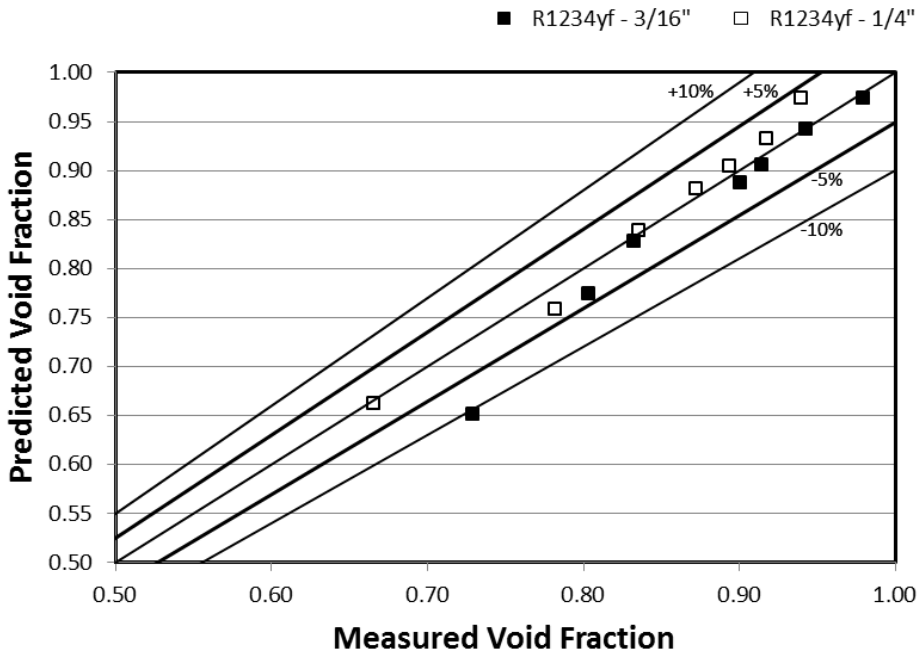

Figure 64: Performance of the Baroczy correlation – R1234yf

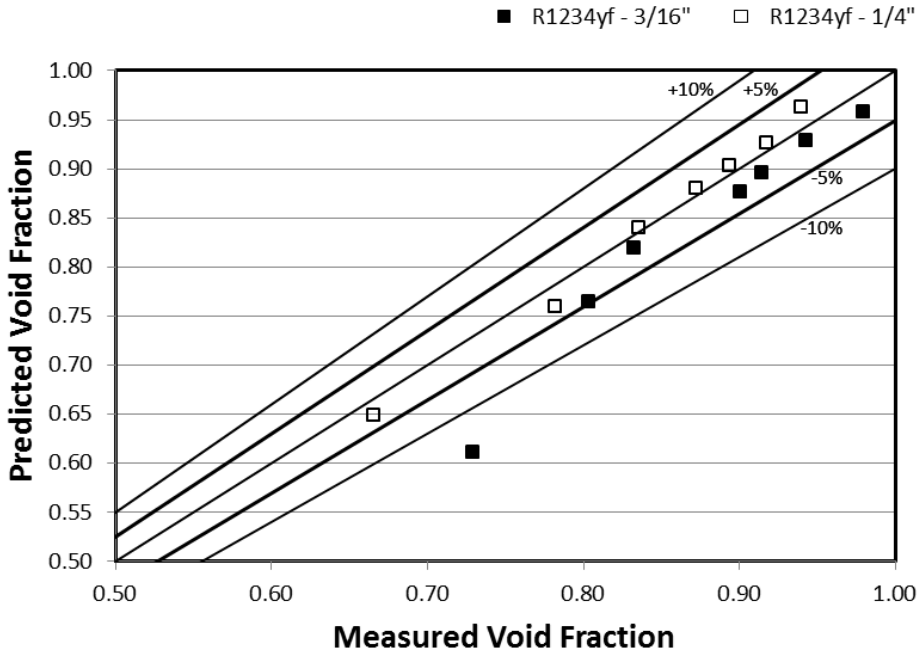

Figure 65: Performance of the Harms-Groll correlation – R1234yf

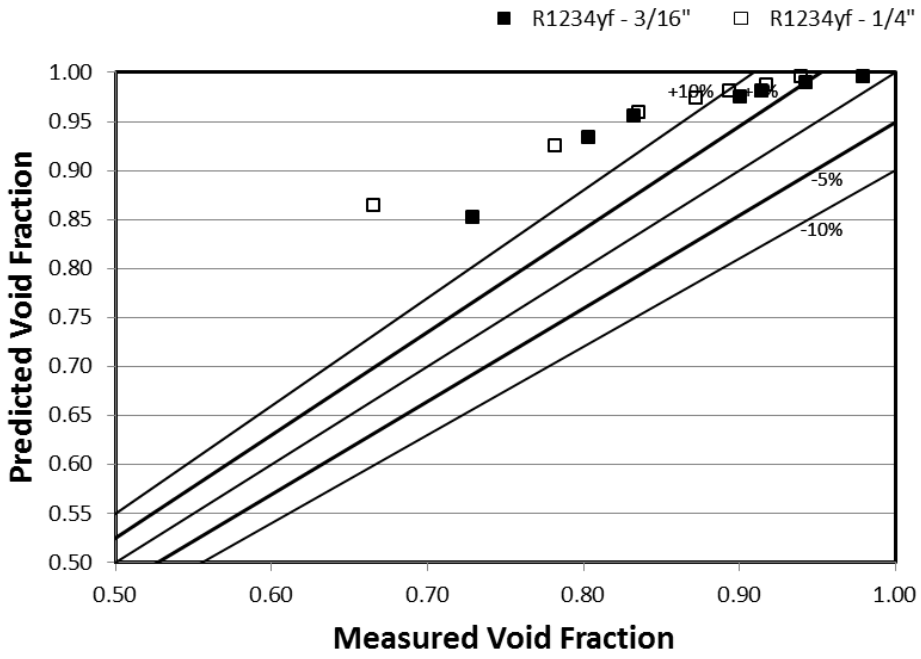

Figure 66: Performance of the Homogenous correlation – R1234yf

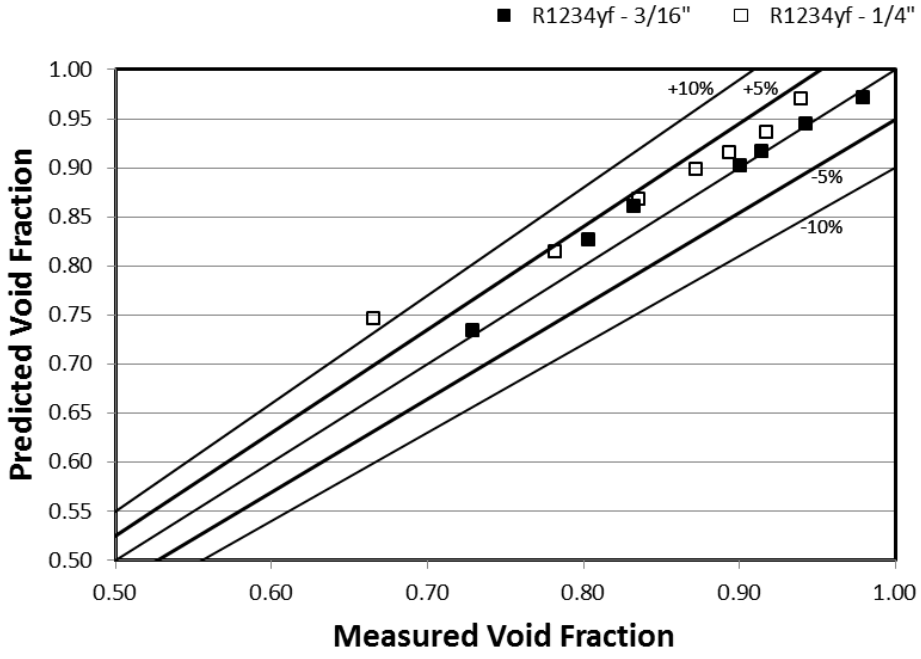

Figure 67: Performance of the Lockhart-Martinelli correlation – R1234yf

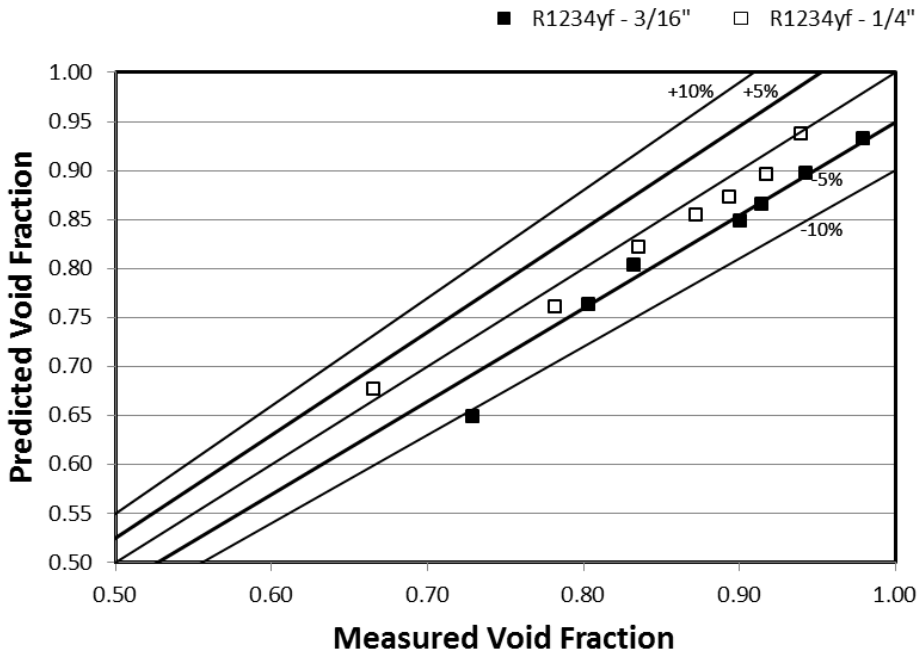

Figure 68: Performance of the Premoli correlation – R1234yf

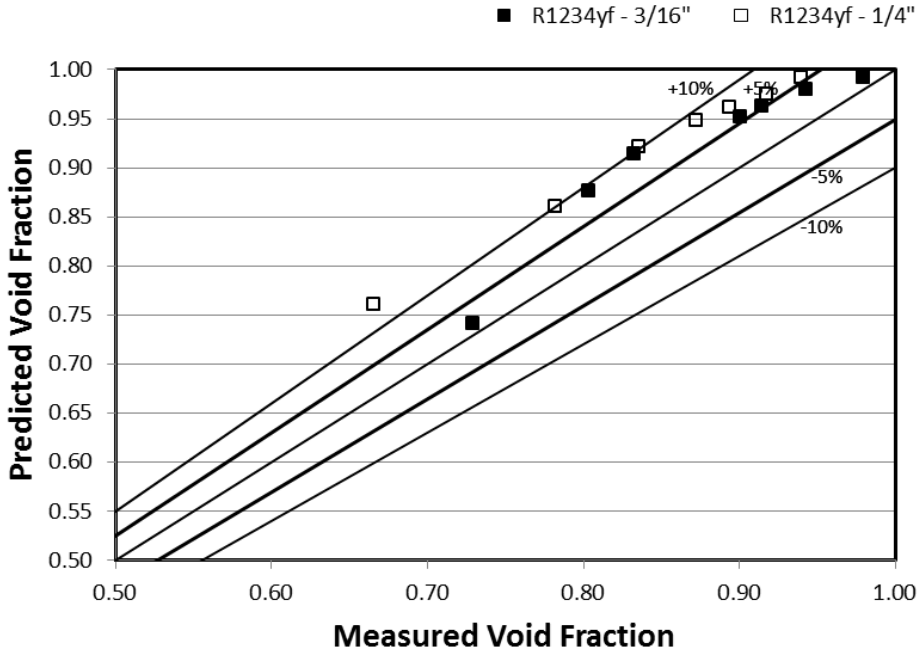

Figure 69: Performance of the Rigot correlation – R1234yf

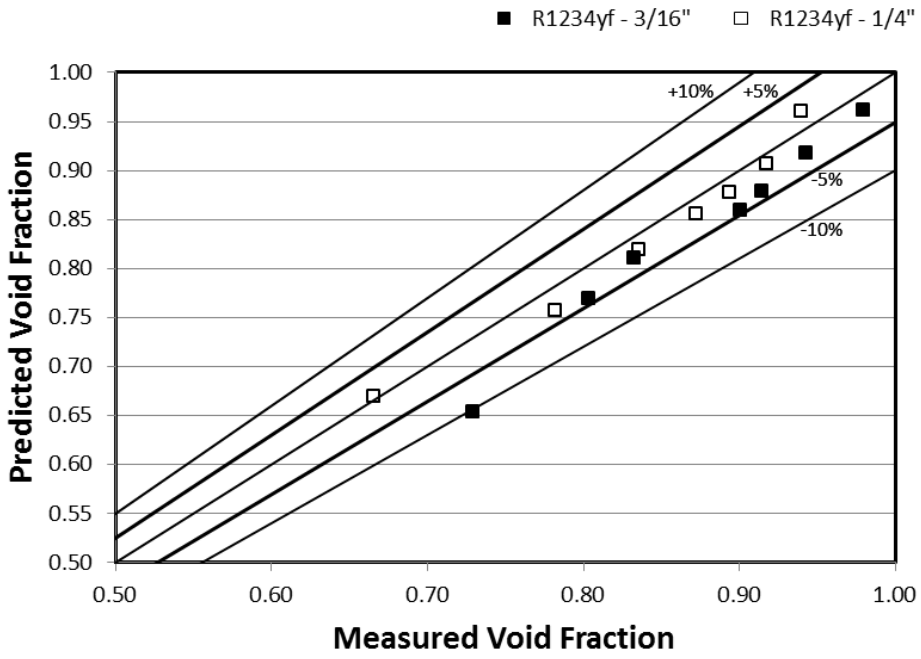

Figure 70: Performance of the Steiner correlation – R1234yf

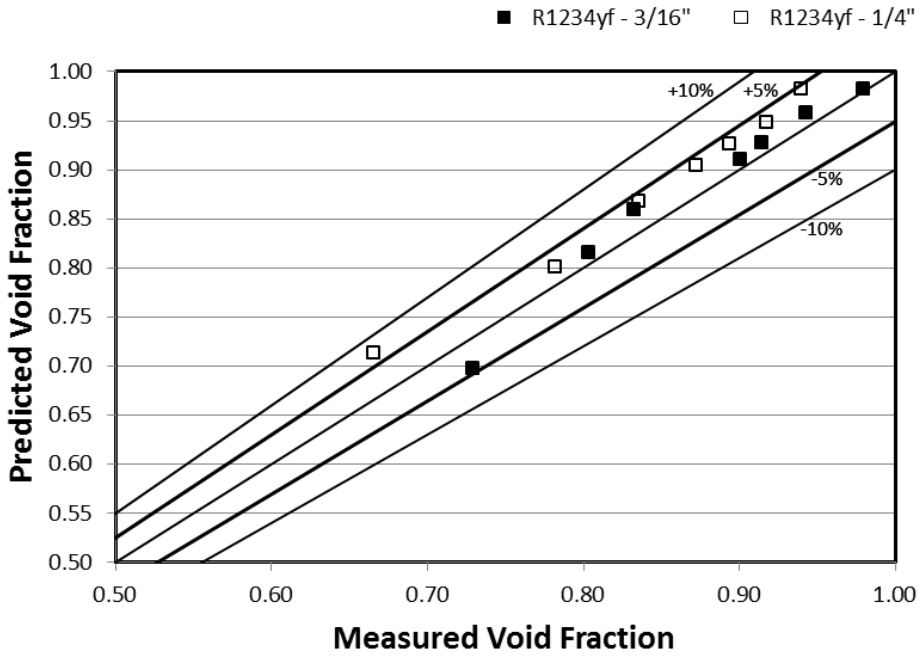

Figure 71: Performance of the Smith correlation – R1234yf

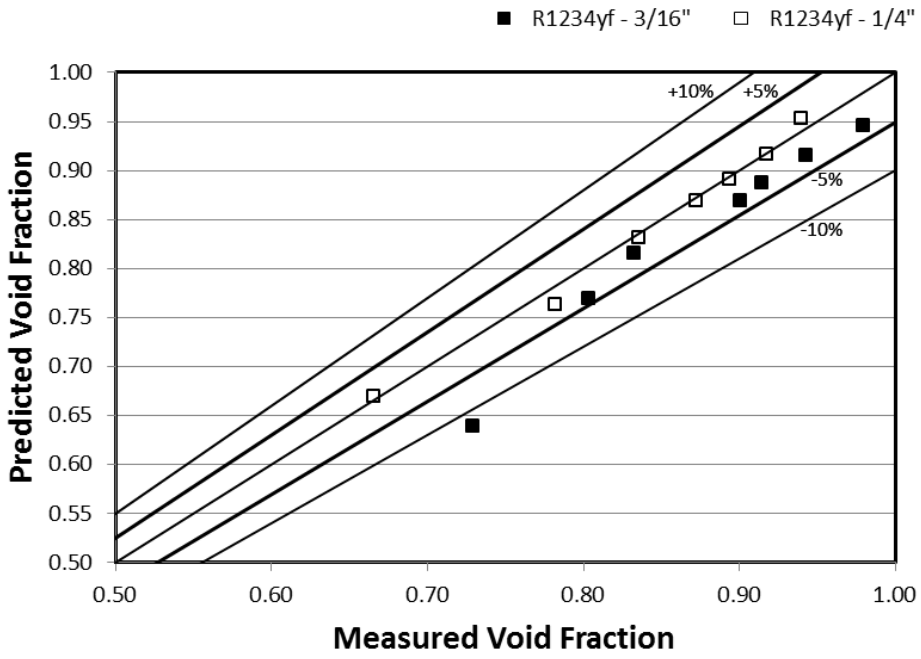

Figure 72: Performance of the Tandon correlation – R1234yf

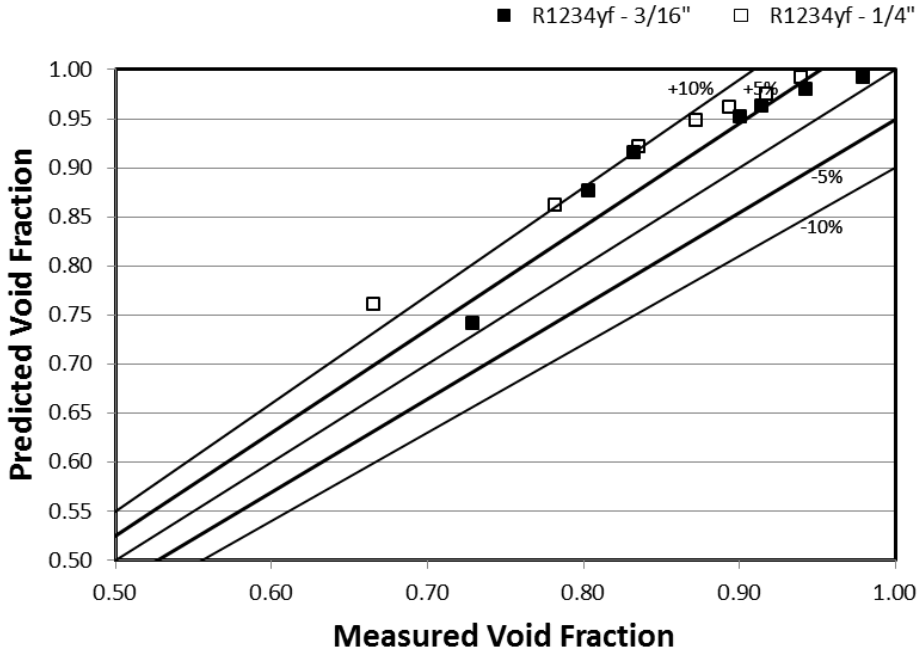

Figure 73: Performance of the Thom correlation – R1234yf

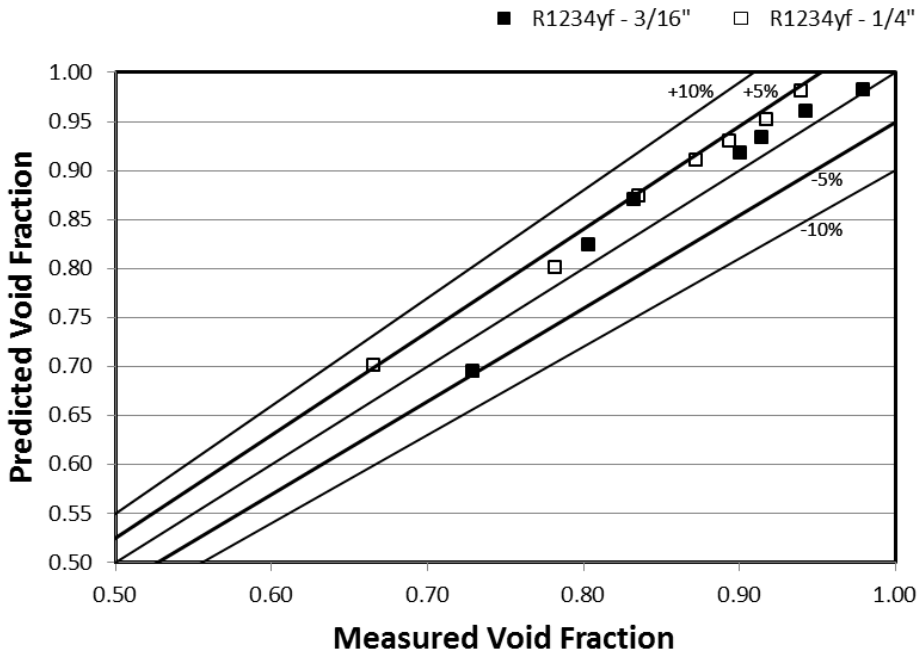

Figure 74: Performance of the Yashar correlation – R1234yf

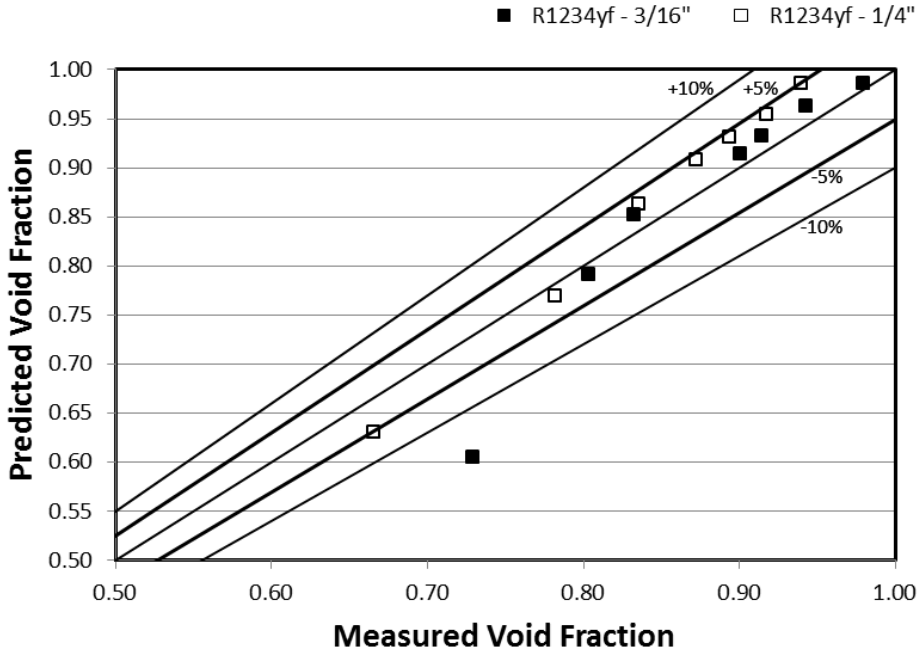

Figure 75: Performance of the Zivi correlation – R1234yf

References

[1] ASHRAE, "Standard 34-2007 - Designation and Safety Classification of Refrigerants," American Society of Heating Refrigeration and Air-Conditioning Engineers (ASHRAE), Atlanta, GA, 2007.

[2] U.S. Environmental Protection Agency, "Protection of Stratospheric Ozone: Listing of Substitues for Ozone-Depleting Substances - Hydrocarbon Refrigerants," *U.S. Federal Register*, pp. 78832-78858, 20 December 2011.

[3] ASHRAE, "Standard 15-2007 - Safety Standard for Refrigeration Systems," American Society of Heating Refrigeration and Air-Conditioning Engineers (ASHRAE), Atlanta, GA, 2007.

[4] M. J. Wilson, T. A. Newell and J. C. Chato, "Experimetnal Investigation of Void Fraction During Horizontal Flow in Larger Diameter Refrigerant Applications," Air Conditioning and Refrigeration Center, University of Illinois, Urbana, IL, 1997.

[5] D. A. Yashar, T. A. Newell and J. C. Chato, "Experimental investigation of void fraction during horizontal flow in smaller diameter refrigeration applications," Air Conditioning and Refrigeration Center, University of Illinois, Urbana, IL, 1998.

[6] D. M. Graham, T. A. Newell and J. C. Chato, "Experimental Investigation of Void Fraction During Refrigerant Condensation," Air Conditioning and Refrigeration Center, University of Illinois, Urbana, IL, 1997.

[7] E. Bjork, "A simple technique for refrigerant mass measurement," *Applied*

Thermal Engineering, vol. 25, no. 8-9, pp. 1115-1125, 2005.

[8] AHRI, "Standard 540-2004 - Standard for performance rating of positive displacement refrigerant compressors and compressor units," Air-Conditioning, Heating and Refrigeration Institute, Arlington, VA, 2004.

[9] R. Lockhart and R. Martinelli, "Proposed correlation of data for isothermal two-phase, two-component flow in pipes," *Chem. Eng. Prog.*, vol. 45, no. 1, pp. 39-48, 1949.

[10] C. Baroczy, "Correlation of liquid fraction in two-phase flow with application to liquid metals," *Chemical Engineering Progress Symposium Series*, vol. 62, no. 64, pp. 223-249, 1966.

[11] S. Zivi, "Estimation of steady-state void fraction by means of the principle of minimum entropy production," *J. Heat Transfer*, vol. 84, pp. 247-252, 1964.

[12] J. R. S. Thom, "Prediction of pressure drop during forced circulation boiling of water," *Intl. J. of Heat and Mass Trans.*, vol. 28, no. 1, pp. 191-198, 1985.

[13] S. L. Smith, "Void fractions in two-phase flow: A correlation based upon an equal velocity head model," *Proc. Instn. Mech. Engrs.*, vol. 184, no. 36, pp. 647-664, 1969.

[14] G. Rigot, "Fluid Capacity of an evaporator in direct expansion," *Chaud-Froid-Plomberie*, no. 328, pp. 133-144, 1973.

[15] A. Premoli, "A dimensional correlation for evaluating two-phase mixture density," *La Termotecnica*, vol. 25, no. 1, pp. 17-26, 1971.

[16] T. N. Tandon, H. K. Varma and C. P. Gupta, "A void fraction model for annular

two-phase flow," *Intl. J. Heat Mass Trans.*, vol. 28, no. 1, pp. 191-198, 1985.

[17] D. Steiner, "Heat transfer to boiling saturated liquids," in *VDI-Warmeatles (VDI Heat Atlas)*, Dusseldorf, Germany, VDI-Gesellschaft Verfahrenstechnik und Chemieingenieurwesen, 1993.

[18] T. M. Harms, D. Li, E. A. Groll and J. E. Braun, "A void fraction model for annular flow in horizontal tubes," *Intl. J. of Heat and Mass Trans.*, vol. 46, no. 21, pp. 4051-4057, 2003.

[19] F. Ahrens, "Heat pump modeling, simulation and design," in *Heat Pump Fundamentals. Proceedings of the NATO Advanced Study Institute on Heat Pump Fundamentals*, Espinho, Spain, Martinus Nijhoff Publishers, 1980.

[20] D. P. Travis, W. M. Rohsenow and A. B. Baron, "Forced convection condensation inside tubes: A heat transfer equation for condenser design," *ASHRAE Transactions*, vol. 79, no. 1, pp. 157-165, 1973.

[21] N. Zuber and J. A. Findlay, "Average volumetric concentration in two-phase flow systems," *J. Heat Transfer*, vol. 87, pp. 435-68, 1965.

[22] Z. Rouhani and E. Axelsson, "Calculation of void volume fraction in the subcooled and quality boiling regions," *Intl. J. of Heat and Mass Trans.*, vol. 13, no. 2, pp. 383-393, 1970.

[23] G. Hughmark, "Holdup in gas-liquid flow," *Chem. Engr. Progr.*, vol. 58, no. 4, pp. 62-65, 1962.

[24] S. Bankoff, "A variable density single-fluid model for two-phase flow with particular reference to steam-water flow," *Trans. ASME, J. Heat Trans.*, vol. 82,

pp. 265-272, 1960.

[25] C. Rice, "The effect of void fraction correlation and heat flux assumption on refrigerant charge inventory predictions," *ASHRAE Transactions*, vol. 93, no. 1, pp. 341-367, 1987.